NORTH-WEST UNIVERSITY
YUNIBESITI YA BOKONE-BOPHIRIMA
NOORDWES-UNIVERSITEIT

PRELIMINARY DESIGN OF A SELF-LAUNCHING SYSTEM FOR THE JS-1 GLIDER

Y.A.M. Nogoud

Dissertation submitted in partial fulfilment of the requirement for the degree
Master of Engineering
at the Potchefstroom Campus of the North-West University

Supervisor: Mr. A.S. Jonker

November 2009

ABSTRACT

In this project a preliminary design of a self-launching system for the JS1 sailplane was attempted. The design was done according to CS-22 airworthiness requirements for sailplanes, which governs sailplane design. The basic design process consists of the engine selection for the system, aerodynamic design of a propeller, modeling of a retraction system mechanism with the frame and prediction of the performance of the JS1 with the system.

The engine selected was the 39kW SOLO 2625-01 engine, which will give a climb rate of 4.26 m/s at an all up weight of 600 kg. The propeller was designed using the minimum induced loss propeller design technique. A requirement for the self launching was that it should be fully retractable allowing an unaltered aerodynamic shape when retracted. The maximum retract and extract speed is 140 km/h. A spreadsheet model was developed to calculate the retraction forces and to allow parametric optimization of the retract mechanism.
There was severe geometrical constrains on the system as there is only limited space available in the fuselage of the glider.

When all specifications and constraints were taken into account it was possible to design a self launching system that will fit in the glider and meet the specifications. Further work will allow the preliminary design to be worked into a detailed system suitable for prototype manufacture.

ACKNOWLEDGEMENTS

I would like to first thank God (Allah), without whom I can do nothing.

Gratefulness goes to my father, mother, brothers, sisters, wife and daughter for their continuous support and encouragement through this study. I would like to thank all my friends for motivation when I needed it most. A special thanks to Mr. Johan Bosman and Mr. Pietman Jordaan.

Finally, my biggest thanks go to my supervisor, Attie Jonker, whose positive, informed, and encouraging nature has been an inspiration throughout.

TABLE OF CONTENTS

LIST OF FIGURES

LIST OF TABLES

NOMENCLATURE

A	Area	[m^2]
A	Cross sectional area	[mm^2]
AF	Activity factor	[-]
A_m	Mean area	[mm^2]
AR	Aspect ratio	[-]
B	Number of blades	[-]
B	Belt width	[mm]
b	width	[mm]
C_{Do}	Zero lift drag	[-]
C_f	Skin friction drag coefficient	[-]
C_{fw}	Turbulent flat plate friction coefficient	[-]
C_L	Lift coefficient	[-]
C_P	Power coefficient	[-]
C_T	Thrust coefficient	[-]
D	Drag	[N]
D	Propeller diameter	[m]
D_p	Pulley pitch diameter	[mm]
E	Elastic modules	[GPa]
F_1	Force in forced belt	[N]
F_2	Force in unloaded belt	[N]
FF	Form factor	[-]
F_{gyro}	Gyroscopic force	[N]
F_o	Initial force	[N]
F_r	Radial force	[N]
F_u	Effective force	[N]
g	Gravity constant	[m/s^2]
h	Height	[mm]
hp	Hours power	
I	Moment of inertia	[mm^4]
J	Advance ratio	[-]
L	Lift	[N]
L	Length of rod	[mm]
L'	Aerofoil thickness location parameter	[-]

M	Moment	[N.m]
M_{gyro}	Gyroscopic moment	[N.m]
M_{max}	Maximum bending moment	[N.m]
n	Rotational speed	[rpm]
n	Load factor	[-]
P_A	Power available	[Kw]
P_{bru}	Allowable ultimate load for shear-bearing	[MPa]
P_{cr}	Critical force	N
P_{tru}	Allowable ultimate load for transverse	[MPa]
P_{tu}	Allowable ultimate load for tension	[MPa]
Q	Propeller torque	[N.m]
q	Dynamic pressure	[N/m^2]
q	Shear flow	[N/m]
Q	Interference factor	[-]
R	Turn radius	[m]
r	Radius of gyration	[mm]
R/C	Rate of climb	[m/s]
Re	Reynolds number	[-]
R_{LS}	Lift surface correction factor	[-]
R_{wf}	Pylon- fuselage interference factor	[-]
S	Area	[m^2]
S_a	Airborne distance	[m]
S_g	Ground roll	[m]
S_{wet}	Wetted area	[m$^{2]}$
T	Thrust	[N]
T	Moment	[N.m]
t	Thickness	[mm]
V	Velocity	[m/s]
v_i	Induced velocity	[m/s]
V_{stall}	Stalling speed	[m/s]
V_{tip}	Propeller tip speed	[m/s]
W	Weight	[N]
X	Distance between propeller and glider c.g	[m]
y	Hinge point	[-]
Z	Number of pulley teeth	[-]

Greek symbols

α	Angle of attack	[°]
β	Pitch angle	[°]
β	Angle of wrapping	[°]
ζ	Velocity ratio	[-]
η_{pr}	Propeller efficiency	[-]
θ	Induced angle	[°]
θ_{OB}	Angle of flight path	[°]
ρ	Air density	[kg/m^3]
σ	Propeller solidity	[-]
σ_{cr}	Critical stress	[MPa]
σ_{max}	Maximum bending stress	[MPa]
σ_y	Yield stress	[MPa]
τ_{avg}	Average shear stress	[MPa]
ω	Angular velocity	[rad/s]

Subscripts

AGL	Above Ground Level
avg	Average
c.g	Center of gravity
Cr	Critical
CS-22	Certification specification for sailplane and powered sailplane
ISA	International Standard Atmosphere
JS-1	Jonker Sailplane
MSL	Mean sea level
NACA	National Advisory Committee for Aeronautics
OB	Obstacle height
Prop	Propeller
S.F	Safety factor
St.	Station
T/O	Take off
tip	Propeller tip

1. INTRODUCTION

1.1 Background

Humanity's desire to fly possibly first found expression in China from the sixth century AD. In the west, the Wright Brothers were the pioneers who built gliders to develop aviation. After the First World War gliders were built in Germany for sporting purposes. The sporting use of gliders rapidly evolved in the 1930's and this is by now their main application. As their performance improved, gliders began to be used to fly cross-country, and they are now regularly flown thousands of kilometers.

A pure glider is an unpowered aircraft. A modern glider is a very efficient machine that uses rising air to climb after which it is able to cruise at a very flat glide angle.

Although many gliders don't have engines, there are some that use engines occasionally. The manufacturers of high-performance gliders now often list an optional engine and retractable propeller to allow the glider to take-off on its own.

The self-launching retractable propeller motor gliders have sufficient thrust and initial climb rate to take-off safely without assistance, or may be launched as with a conventional glider.
The purpose of the retractable system is to avoid the performance penalty of a non-retractable engine installation. After the engine is retracted the outside aerodynamic surface is undisturbed, thus restoring the original performance of the glider.

The JS-1 sailplane is a high performance 18m class glider that has been developed at the Jonker sailplanes in conjunction with the North-West University in 1999. This glider has a full composite structure (glass-fiber, carbon fiber and Kevlar). The JS-1 glider is a pure glider, but provision was made in the initial design for an engine system.

1.2 Problem statement

The problem for this study is to design a self-launching system for the JS-1 glider.

1.3 Objective of study

The objectives of this project are:

- Develop specifications for a self-launching engine system.
- Select a suitable engine.
- Calculate performance of system.
- Design propeller.
- Design retraction mechanism.

The design of the self-launching system for JS1 glider will be according to CS-22 Airworthiness requirements (certification specification for sailplanes and powered sailplanes).

1.4 Layout of the thesis

The layout of the thesis is as follows:

In Chapter 2, the literature study, the related topic of the self-launching system design methods will be discussed. Chapter 3 discusses the preliminary design, the comparative study, the results necessary for the preliminary design and the engine selection result. Chapter 4 provides the propeller design, the aerodynamic geometry design process with the use of numerical methods as well as the results obtained. Chapter 5 deals with the retraction system design, and will discus the frame design and the design of folding mechanism of the system. Chapter 6 discussed the design calculation of some critical parts of the system are discussed. A short performance comparison between the JS1 with the self-launching system and the other self-launching glider will be given in Chapter 7. Chapter 8 concludes the study with a short overview of the thesis with suggestions for further research.

2. LITERATURE STUDY

2.1 Introduction

In this section, the methods and tools to design the self-launching system for a glider will be discussed and previous work reviewed. This will identify the relevant tools and methods to be used in this study.

2.2 Design specification

The first step in the design of a self-launching system for a glider is to set the design specifications. An initial client requirement for the self-launching system is as follows:

"The self-launching retractable system is design to allow the glider to take-off without any external assistant, and to prevent any performance losses."

This overall specification must be kept in mind when designing the literature survey. The design of a self-launching glider depend on a number of variables, divided into the following groups: performance calculations, engine selection, propeller design, and the retraction system design. The literature study will be conducted for these groups.

2.3 Performance calculations

The performance of a self-launching glider depends on lift-to-drag ratio, the thrust-to-weight ratio and the wing loading.

2.3.1 Lift to drag ratio

The lift-to-drag ratio, or the "glide ratio" L/D, is equal to the lift generated, divided by the drag produced by the glider. At subsonic speeds the L/D is most directly affected by two aspects of the design: wing span and wetted area. The drag at subsonic speeds is composed of two parts. Induced drag is the drag caused by the generation of lift. This is primarily a function of the wing span. Zero-lift-drag is the drag which is not related to lift. This is primarily skin-friction drag, and directly proportional to the wetted area (Raymer, 1989:19).

The L/D change with speed and the performance of a glider is defined by the maximum glide ratio. When the L/D is a maximum value, the zero-lift-drag equals the induced drag (Anderson, 2001: 207). The L/D can thus be expressed in the following equation, where the drag due to lift factor (k) decrease when the aspect ratio increase and hence increases the lift to drag ratio.

$$\left(L/D\right)_{\max} = \sqrt{\frac{1}{4k \times C_{Do}}} \tag{2.1}$$

In the conceptual design stage we can make a crude approximation for the value of $\left(L/D\right)_{\max}$ based on data from existing gliders (Anderson, 2001:214).

2.3.2 Power loading

The power loading ratio, P/W is perhaps the parameter with the strongest influence on the dynamic performance characteristics of the powered glider. Rate of climb and take-off performance are the two main flight characteristics determined by the Power loading ratio.
When designer speak of an aircraft's power loading ratio they generally refer to the P/W during sea-level zero-velocity, standard-day conditions at design take-off weight and maximum throttle setting (Raymer, 1989:78).

The term "thrust-to-weight" is associated with jet-engine aircraft, and the term of "power loading" is related to the propeller-driven aircraft, this power loading is numerically equal to the weight of the glider, divided by its horsepower.

In the conceptual design stage, the statistical estimation can be used to find the value of power loading (Raymer, 1989: 80) to develop a curve-fit equation based upon maximum velocity for different classes of aircraft.

$$\left(hp/W\right) = AV_{\max}^{C} \tag{2.2}$$

Where: A=0.043 and C=0 for the power glider.
(Anderson, 2001: 412) prefers to obtain the value of T/W by examining the rate of climb, take-off distance, and maximum velocity.

The method of obtaining the value of P/W and T/W by examining the rate of climb, and take-off distance will be used in this study and will be compared to the curve-fit equation.

2.4 Engine selection

The general type used in self-launching gliders is piston (reciprocating) engines. The reason for this is mostly: operational cost, fuel availability, installed weight and drag of the integrated propulsion system**.**

2.4.1 Piston Engines

In piston engines, the combustion process is intermittent as opposed to continuous. Piston engines are normally configured as four-stroke, two-stroke and rotary engines using either spark ignition or compression ignition.

The compression ratio of a piston engine is a ratio of the cylinder volume with the piston at the bottom to that with the piston at the top. Compression ratios range from around 6:1 in spark ignition engines to around 16:1 in compression ignition engines (Roskam & Lan, 2003: 208).

The power delivered to the output shaft is referred to as shaft-horse-power (SHP), P_{shp}. When the output shaft drives a propeller which provides a thrust, T at a speed, V then the product TV is defined as the power available, P_A. The ratio of power available to shaft-horse-power is called the propeller efficiency, η_p. This ratio will be discussed in the propeller design section.

Factor affecting the power output of piston engines:

1. Heat release per pound of air
2. Charge per stroke
3. Maximum permissible RPM
4. Effect of altitude
5. Effect of air temperature
6. Supercharging
7. Compounding

The power output of a piston engine is classified in terms of power ratings. Typically these ratings are as follows:

1. Take-off power: the maximum power allowed during take-off.
2. Maximum continues power (normal rated power). Used for maximum climb performance and for maximum level speed.

3. Cruise power. There are two cruise power ratings:
    a. Performance cruise: 75% of take-off power at 90% of maximum RPM.
    b. Economy cruise: 65% of take-off power.

The engine selection matrix will be used in this study to obtain the suitable engine for the JS1 glider. Detailed explanations about this method are described in Chapter 3.

2.5 Propeller design

A propeller is a rotating Aerofoil that generates thrust in the same way as a wing generates lift. Like a wing, the propeller is designed to a particular flight condition. The propeller Aerofoil has a selected design lift coefficient, and the twist of the Aerofoil is selected to give the optimal Aerofoil angle of attack at the design condition.

Since the tangential velocities of the propeller Aerofoil sections increases with distance from the hub, the Aerofoils must be set at progressively reduced pitch-angles going from root to tip. The overall pitch of a propeller refers to the blade angle at 75% of the radius.

In this chapter the theory related to propellers and their performance is discussed.

2.5.1 Momentum theory

This section briefly discusses the fundamentals of incompressible momentum theory for propeller with reference to Figure 2.1.

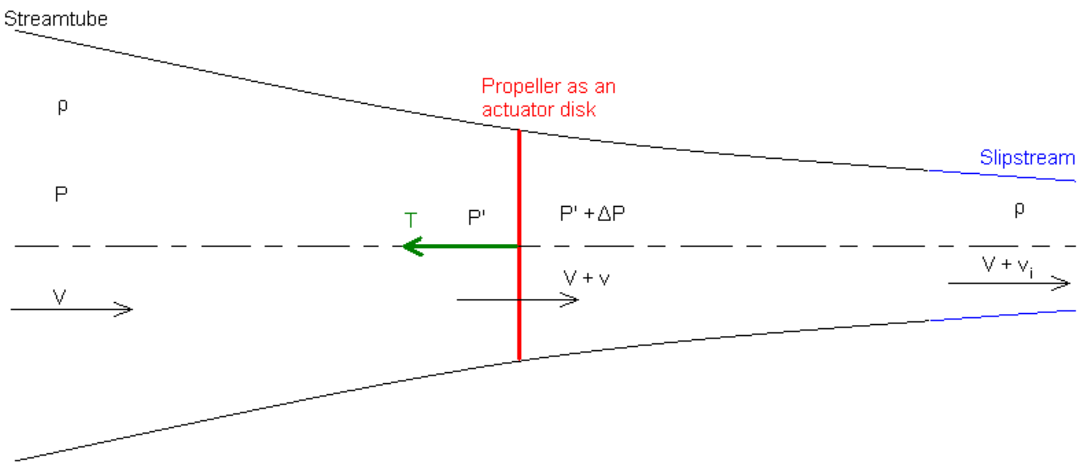

Figure 2.1: Stream tube through a propeller disk

With simple incompressible momentum, where the rotating blades are assumed to be an actuator disk, the thrust generated by a propeller is derived with the use of Bernoulli's equation.

$$T = 2.\rho \cdot A(V + V_i)V_i \quad (2.3)$$

Where: V_i is the induced velocity downstream, V the forward velocity of the disk, ρ is the air density and A is the disk area created by the rotating blades. The ideal propeller efficiency is stated as

$$\eta_{ideal} = \frac{V}{V + V_i} \quad (2.4)$$

It can be seen from this that if the air is left undisturbed by the propeller i.e. V_i =0, that the efficiency would be 100% (Roskam & Lan, 2003: 266).

From Equation 2.4 and confirmed by (Weick, 1930), according to the momentum theory, the following can be said about the ideal efficiency:

- An increase in forward velocity V, leads to an increase in efficiency.
- The ideal efficiency decreases with an increase in thrust.
- An increase in propeller diameter and fluid density increases the efficiency.

These statements are important to consider during the design phase of a propeller, and as is usual in engineering, compromises have to be made when considering the combination of the above parameters.

2.5.2 Blade element theory

In Figure 2.2 the elemental forces dL and dD are the differential lift and drag forces respectively. dT is the thrust component, while dQ/r is the force producing the propeller torque. α is the blade element angle of attack and β is the geometric blade pitch angle.
From force balance in the horizontal and vertical direction it is found that:

$$dT = dL.\cos\phi - dD.\sin\phi \quad (2.5)$$

$$dQ = (dL.\sin\phi + dD.\cos\phi).r \qquad (2.6)$$

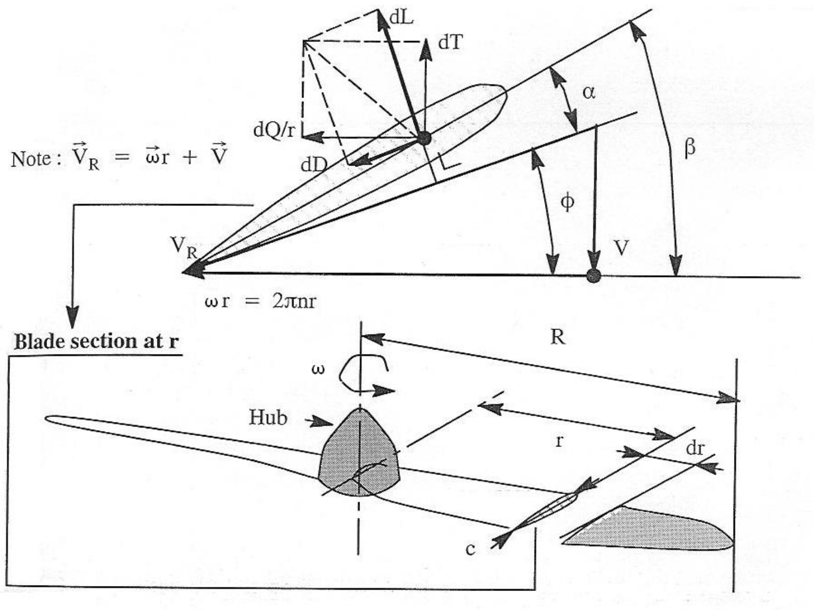

Figure 2.2: A propeller showing an infinitesimal blade element (Roskam & Lan, 2003: 275).

Knowing the blade geometry, the equations can be written as:

$$dT = \frac{1}{2} \cdot \rho \cdot V_R^2 \cdot c \cdot (C_l \cdot \cos\phi - C_d \sin\phi) \cdot dr \qquad (2.7)$$

$$dQ = \frac{1}{2} \cdot \rho \cdot V_R^2 \cdot c \cdot r(C_l \cdot \sin\phi + C_d \cos\phi) \cdot dr \qquad (2.8)$$

2.5.3 Combined blade element momentum theory

The momentum theory is valid if the downstream induced velocity is measured and used to calculate the thrust by a propeller of given diameter and forward velocity. The theory is limited in its use as one can not calculate the blade geometry. The blade element theory allows for this deficiency, and consequently the geometry can be analyzed. In contrast to the momentum theory, the blade element theory does not account for the induced velocity created by the downwash over the blades. The solution is then to combine the theories set out above (Roskam & Lan, 2003: 277).

2.5.4 Useful relationships for propellers

As for the wing, the properties of a propeller are expressed in coefficient form. Experimental data for design purposes are expressed using a variety of parameters and coefficients, as described below.

- Advance ratio: is related to the distance the aircraft moves with one turn of the propeller.

$$J = V/nD \tag{2.9}$$

- The power and thrust coefficients are non-dimensional measures of those quantities, much like the wing lift-coefficient.

$$c_P = \frac{2P}{\rho V^3 \pi R^2} \tag{2.10}$$

$$c_T = \frac{2T}{\rho V^2 \pi R^2} \tag{2.11}$$

- The activity factor is a measure of the amount of power being absorbed by the propeller. Activity factors range 90-200.

$$AF = \frac{10^5}{D^5} \int_{.15R}^{R} cr^3 dr \tag{2.12}$$

- The propeller efficiency is the ratio of power converted from the engine to thrust power (power driving the aircraft forward). The propeller efficiency can also be expressed in terms of the advance ratio and the thrust and power coefficients.

$$\eta = \frac{TV}{P} = J\,\frac{c_T}{c_P} \tag{2.13}$$

2.5.5 Propeller design methods

Several methods are in existence to design a propeller. Some are more advanced than others. Some authors, such as McCormick (1979), prefer to calculate the induced velocity instead of the induced angle, which may be due to personal preference.

2.5.5.1 Method described by McCormick

A procedure for the design of a new propeller is as found in (McCormick, 1979) is described in brevity. With reference to Figure 2.3, the following must hold:

$$\omega r \cdot \tan(\phi + \theta) = \text{constant} \tag{2.14}$$

Defining $V_0 \equiv V_i$ as,

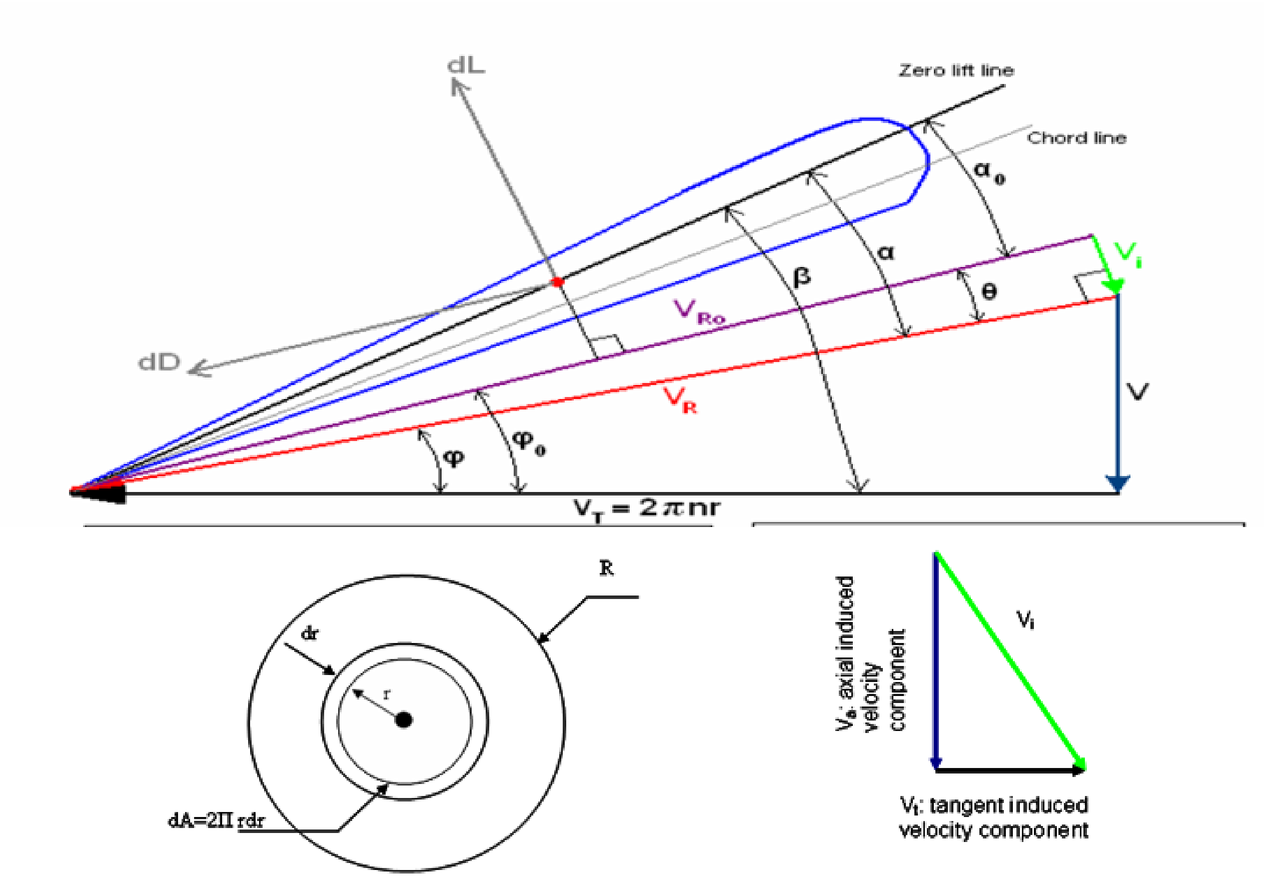

Figure 2.3: Blade element for use in combining the blade element and momentum theories

$$V_0 = \omega r \tan(\phi + \theta) - V \tag{2.15}$$

The induced angle is solved with

$$\theta = \tan^{-1}\left(\frac{\left(\frac{V_0}{V_T}\right)x}{x^2 + \xi\left(\xi + \left(\frac{V_0}{V_T}\right)\right)} \right) \tag{2.16}$$

with ξ a non-dimensional ratio of velocities, $V/\omega r$.

The bound circulation and the tangential velocity component is calculated next.

$$\Gamma = \frac{1}{2} c \cdot C_l \cdot V_{Ro} \tag{2.17}$$

$$V_t = V_R \cdot \theta \cdot \sin\phi \tag{2.18}$$

For use in calculating the thrust and torque with

$$T = B \cdot \rho \int_0^R (\omega r - V_t)\Gamma \cdot dr \tag{2.19}$$

$$Q = B \cdot \rho \int_0^R r \cdot (V - V_a)\Gamma \cdot dr \tag{2.20}$$

The calculations above can be iterated to provide the blade geometry that will satisfy certain parameters such as required thrust or torque.

2.5.5.2 Minimum induced loss propeller design technique

This is a method developed by the late Prof.E.E. Larrabee. The equations for use his method in propeller design was obtained from Royal Aeronautical Society website♣. An Excel ® spreadsheet applying these equations was also found at Royal Aeronautical Society website, but Visser (2006) decided to program them in a Matlab® script.

To use the equations for this method, the following must be known:

- The number of blades
- The power input or thrust
- The rotation rate
- The propeller diameter
- The blade section C_l and C_d

Start by calculating P_c, if power is prescribed

$$P_C = \frac{2P}{\rho V^3 \pi R^2} \tag{2.21}$$

♣ http://www.raes.org.uk/cmspage.asp?cmsitemid=SG_hum_pow_download

$$\lambda = \frac{V}{\omega R} \tag{2.22}$$

Then for each radial station along the blade the following is calculated

$$\xi = \frac{r}{R} \tag{2.23}$$

$$x = \frac{\xi}{\lambda} \tag{2.24}$$

$$f = \frac{B}{2}\frac{\sqrt{\lambda^2+1}}{\lambda}(1-\xi) \tag{2.25}$$

$$F = \frac{2}{\pi}.\cos^{-1} e^{-f} \tag{2.26}$$

$$G = \frac{Fx^2}{x^2+1} \tag{2.27}$$

I_1, I_2, J_1 and J_2 are numerically integrated and used to calculate ζ, the displacement velocity ratio ($\zeta = \frac{V_{\text{induced downstream}}}{V_{\text{induced after disk}}} = 2$, from the slip velocity of the momentum theory of propellers). Simpson's rule is used to carry out the numerical integrations.

$$I_1 = 4\int_0^1 G\left(1-\frac{C_d/C_l}{x}\right)\xi d\xi \tag{2.28}$$

$$I_2 = 2\int_0^1 G\left(1+\frac{C_d/C_l}{x}\right)\left(\frac{1}{x^2+1}\right)\xi d\xi \tag{2.29}$$

$$J_1 = 4\int_0^1 G(1+(C_d/C_l)x)\xi d\xi \tag{2.30}$$

$$J_2 = 2\int_0^1 G.(1+(C_d/C_l)x)\left(\frac{x^2}{x^2+1}\right)\xi d\xi \tag{2.31}$$

$$\zeta = \frac{J_1}{2.J_2}\left[\sqrt{1+\frac{4P_C.J_2}{J^2}}-1\right] \tag{2.32}$$

and hence T_c, P_c and the efficiency can be calculated

$$T_C = I_1.\zeta - I_2.\zeta^2 \tag{2.33}$$

$$P_C = J_1.\zeta - J_2.\zeta^2 \tag{2.34}$$

$$\eta = \frac{T_C}{P_C} \tag{2.35}$$

$$\phi = \tan^{-1}\left[\left(\frac{\lambda}{\xi}\right)\left(1+\frac{\zeta}{2}\right)\right] \tag{2.36}$$

The blade angle is given by

$$\beta = \phi + \alpha_{design} \tag{2.37}$$

Finally the blade chord, torque and thrust are calculated from

$$\frac{W}{V} = \sqrt{x^2 + 1 - (\zeta \cos\phi / 2)^2} \tag{2.38}$$

$$\frac{C}{R} = \left(\frac{4\pi\lambda}{B}\right)\left(\frac{G}{W/V}\right)\left(\frac{\zeta}{C_l}\right) \tag{2.39}$$

$$Q = \frac{1}{2} T_C \rho V^2 \pi R^2 \tag{2.40}$$

$$T = \frac{P_C \rho V^3 \pi R^2}{2\omega} \tag{2.41}$$

The minimum induced loss propeller design method will be used in this study.

2.6 Retraction system

The basic function for the retractable system is a complete extraction of engine and propeller into the slipstream. A bad choice for the retracted system position can increase the glider weight, and create additional aerodynamic drag. An example of the types of the self-launching system in the glider is shown in Figure 2.4.

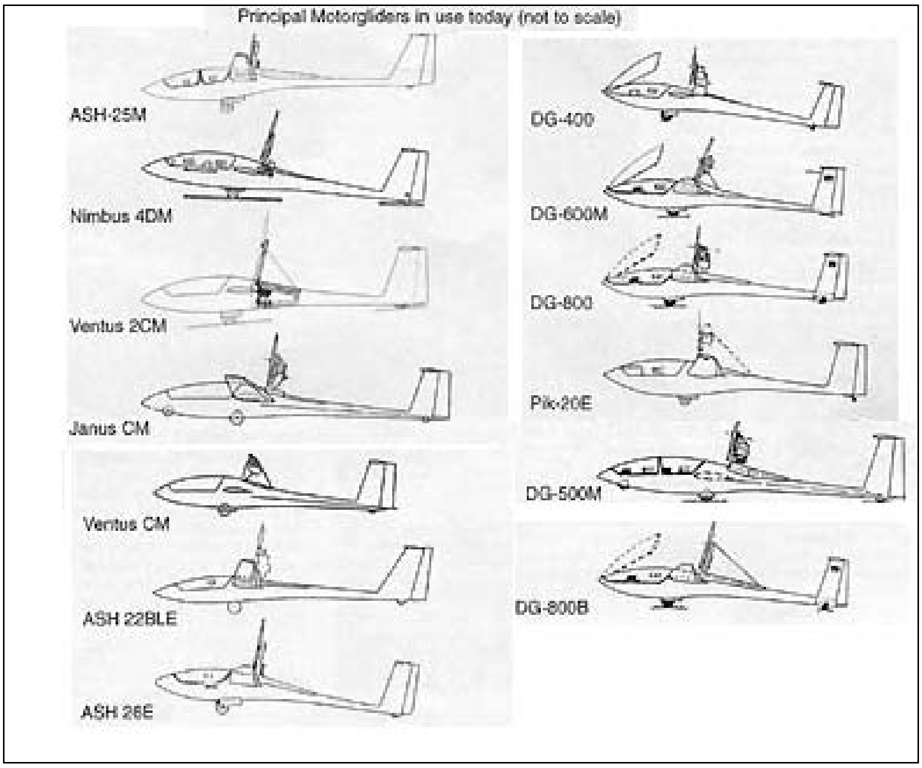

Figure 2.4: Examples of self-launching gliders (DG, 2008)

The retractable propeller is usually mounted on a mast that rotates up and forward out of the fuselage, aft of the cockpit and wing carry-through structure. The fuselage has engine bay doors that open and close automatically, similar to landing gear doors.

A thorough research regarding existing retracting propulsion of self-launching gliders had to be performed to execute the project. Valuable observations of the functioning of the systems could be obtained to determine what concepts were used in existing systems. and its appearance could be studied to make the necessary deductions.

With the examination it was found that there is not a great variety of concepts used. Three basic concepts of retracting propulsion for gliders were identified. They are discussed shortly:

Figure 2.5: Concept 1 (DG, 2008).

2.6.1 Concept 1

In concept 1 (see Figure 2.5) the engine is mounted behind the propeller at the top of the retracting arm. Usually in this instance no belt propulsion system is used. The propeller is directly connected to the prop shaft of the engine. If the shaft speed of the engine does not meet the required propeller speed, a belt propulsion system is used. In this instance it is true that the engine is not static but is pushed out and retracted with the retracting arm. The engines used in this instance are usually air-cooled engines.

The mass of the engine is critical in this concept, because it can have a negative effect on the extracting forces. The retracting arm must also be designed so that it is strong enough to provide for the extra weight of the engine. The projected area in the direction of the motion of the engine is also important because a larger area will cause larger shearing forces, which will cause an increase in the extracting forces size.

Figure 2.6: Concept 2 (DG, 2008).

2.6.2 Concept 2

In some models such as the DG-800C Fig 2.6, the engine is positioned lower on the retracting arm (closer to the body) although it is still showing above the body of the glider in the final extracted position. As with concept 1 the engine is not in a static position. In this instance belt propulsion is used between the prop shaft of the engine and the propeller. The size of the projected area in the direction of motion of the engine has a smaller influence on the push-out forces during extraction, because the resulting force caused by the shearing force is closer to the hinge point of the retracting arm. The force thus has a shorter lever arm (distance between the resulting force and the hinge point) and can have a smaller moment of rotation when compared to concept 1. Air-cooled engines are used most often in this concept.

Figure 2.7: Concept 3 (Alexander, 2003).

2.6.3 Concept 3

The most important aspect of this concept is the fact that the engine remains in a static position during the in- and out-folding (Figure 2.7). Only the retracting arm with the propeller and the cooling stack that is mounted to it moves during the extracting process. There is only a point just above the front of the engine’s propulsion - the axis around which the retracting arm hinges. The fact that it is not necessary to move the engine has a large influence on the design of the whole mechanism, because the forces are much smaller than the forces in the instances of concepts 1 and 2. Since the engine and propeller is quite a distance from each other a belt propulsion system can be used. Therefore the aim with the design of the retracting arm is to design it in such a way that the belt is protected against the wind. The belt is protected so that it does not vibrate in the wind and is damaged in that way.

In this concept water cooled engines are used. In the design of the retracting arm it is necessary to leave space for the mounting of the cooling stack. The influence of the cooling stack on the system is that it increases the shearing force of the structure causing an increase in the extracting forces. The increase in the extracting forces is less in comparison to the increase in forces when the entire engine has to be moved.

After the consideration of the three concepts, it was decided to use concept 3. With concepts 1 and 2, anytime the engine and propeller pylon is moved many parts must move, including the engine and propeller, the fuel lines to the carburetors, the wiring bundles to the ignition, the muffler and cooling system if installed.

This complexity is part and parcel of the self-launching glider and is subject to vibration, slipstream forces and ground taxi forces. In comparison, concept 3 is quite simple, since the engine and its system do not move and vibrations are absorbed by the engine mounts.

2.6.4 Power transmission

Power transmission between the engine shaft and propeller can be accomplished in a variety of ways. Gears and flexible elements such as belts and chains are commonly used.

Belt drive propellers are typically used in applications requiring a reduction drive system. Two stroke engines require a belt reduction drive to keep the propeller tip speed within their specified limits. The four principal types of belts are flat belts, round belts, V-belts and timing belts. In all cases, the pulley axes must be separated by a certain minimum distance, depending upon the belt type and size, to operate properly.

Modern flat-belt drives consist of a strong elastic core surrounded by an elastomer; these drives have advantages over V-belt drives. A flat-belt drive has an efficiency of about 98 percent. On the other hand, the efficiency of a V-belt drive ranges from about 70 to 96 percent (Wallin, 1978:265). Flat-belt drives produce very little noise and absorb more tensional vibration from the system than V-belt drives.

A timing belt, also known as toothed belts, is made of rubberized fabric with steel wire to take the tension load. It has teeth that fit into grooves cut on the periphery of the pulleys; these are coated with a nylon fabric. A toothed belt does not stretch or slip and consequently transmits power at a constant angular-velocity ratio. No initial tension is needed. The efficiency of toothed belt ranges from 97 to 99 percent (Juvinall & Marshek, 2000).

In the all types of belts except for toothed belts, there is some slip and creep, and so the angular-velocity ratio between the driving and driven shafts is neither constant nor exactly equal to the ratio of the pulley diameters (Shigley & Mischke, 2003: 1071).

Based on the above comparison, the toothed belt will be used in this study

In this study the location of the self-launching system for the JS1 will be in the aft fuselage. The design of the platform and the mast of the propeller will be based on the size of the engine and propeller. The selection of suitable spindle drive for the system will be discussed in the Chapter 5.

2.7 Summary

This chapter discussed the tools and methods of designing a self-launching system for the glider. It briefly investigated the performance of a self-launching glider, and provided a brief overview of the piston engine, as well as a few design methodologies for the propeller. It was decided to use the method of minimum induced loss propeller design technique to propeller design. The retraction concepts were evaluated, it was decided to use concept three. For the transmission system the tooth belt seems to be the best choice. More detailed information about certain aspects is discussed in the report body itself where the need exists.

3. PRELIMINARY DESIGN

3.1 Introduction

The design process is a creative process; there is no absolute or exact method to describe how it should be done. However, it makes sense to follow a structured plan to verify progress along the way and to plan the later phases in advance.

3.2 Development of engine system specifications

The first step in any design process is to lay down the specifications of the proposed design. Without a clear statement of the desired design outcomes of the self-launching system, the design cannot start. The initial client requirement was given in Chapter 2. With consultation a more specific set of design specifications was developed. They are given below:

- A minimum rate of climb for the JS1 glider at maximum weight must not be less than 3 m/s at MSL (mean sea level).
- The maximum allowable weight of the system is 75kg.
- The system must fit inside the JS1 fuselage without modification to the current shape.
- The system must not detract from the performance of the glider.
- The maximum allowable all up weight of the JS1 glider is 600kg.

It is clear that the given requirements are by no means a complete list of specifications, only a basic framework. In fact, some very important parameters such as take-off distance is not mentioned. Accurate initial estimates are required to assist in the design to ensure that a realistic design is created, therefore a study of similar existing self-launching gliders will be done to determine if the above requirements are realistic and to determine additional information.

The specifications of the JS1 pure glider are given in Table 3.1.

Table 3.1: JS1 pure glider specifications

Wing span	18m
Aspect Ratio	28.8
Wing area	11.2 m2
Wing Loading (max)	53.3 kg/m2
Wing Loading (min)	31.2 kg/m2
Max all up weight	600 kg
Max Speed (V_{ne})	290 km/h
Maneuver speed (V_b)	201 km/h
Max Glide Ratio (L/D)	53

3.3 Comparative study

There are some the self-launching gliders currently in use. The following table (Table 3.2) is a summary of the available performance specifications of five self-launching gliders. All data in the table was obtained from datasheets of the respective self-launching gliders. The same information is not available on all the systems, the system of units of some parameters also differ from one manufacturer to another. For completeness, all available data is included, and all units converted to the same system of units.

Table 3.2: Technical data for self-launching gliders

Parameter	Self-launching Gliders				
	Ventus-2cxM	**ASH26**	**DG800A**	**DG808C**	**LS8-st**
Wing span [m]	18	18	18	18	18
Wing area[m^2]	11.03	11.68	11.81	11.81	11.43
Aspect ratio	29.5	27.74	27.43	29.43	28.35
Range of wing loading min-max [kg/m^2]	35.8-51.24	37-45	-	-	-
Maximum permitted speed with propeller retracted[km/h]	285	270	270	270	270
Stall speed[km/h]	-	71	-	68at420kg	-
Minimum sink rate [m/s].	.55 at 470 kg	0.48	-	.51 at (420kg)	.58 at 480 kg
Best glide ratio		50@ 96 km/h	50	50 @ 110km/h	>47
Engine	SOLO 2625-01	Diamond AE50R	Rotax 505	SOLO 2625-01	SOLO 2625
Power [hp]	52at 6000RPM	50	42.5at 6100RPM	52.3 at 6300 RPM	55
Gear reduction	1:3	-	-	1:3	-
Take-off distance 15m [m]	-	-	-	306 at 600kg	350
Rate of climb @ S.L [m/s]	-	3.4 @ 525Kg	-	3.6 @ 600kg	-

The data in the tables is useful to verify whether the initial requirements of the self-launching system design are realistic for performing the task at hand:

- The best glide ratio for 18m glider is about 50. The specific value for the JS1 is not calculated yet, but all indication seems to be greater than 50. The value of 50 can be used to predict system power requirements.

- CS-22 under section 22.51 describes the specifications to which a sailplane or glider has to comply with. It states in sub-paragraph (a):

  "For a powered sailplane the take-off distance at maximum weight and in zero wind, from rest to attaining a height of 15 m must be determined and must not exceed 500 m when taking off from a dry, level, hard surface. In demonstration of the take-off distance, the powered sailplane must be allowed to reach the selected speed promptly after lifting off and this speed must be maintained throughout the climb." (CS, 2003:1-B-2).

The take-off distance is strongly dependent on the power of a self-launching glider; it decreases with increase in power (Anderson, 2001: 376). The take-off distance for self-launching gliders in Table 3.2 varies between 306m and 350m. These values are less than the CS-22 requirement. The value of 310m will be used for the JS1 glider at this stage to avoid any penalty of exceeding the CS-22 requirement.

- The data in the Table 3.2 can also give us some idea about the engines used in the self-launching gliders. Three of the gliders in the Table 3.2 using SOLO 2625, one using Rotax 505 and one using Diamond AE50R Wankel rotary.

Taking all of this into account, a revised specification list of requirement can be complied:

- Maximum Rate of climb $(R/C)_{\max} \geq 3m/s$
- Maximum weight of the system 75kg.
- The system must fit inside the JS1 fuselage without modification to the current shape.
- The maximum all up weight (W) = 600kg.
- The best glide ratio $\left(L/D\right)_{\max} = 50$.
- The take-off distance (to clear a 15m obstacle at sea level, standard ASI, level smooth tar surface, with no wind, max T/O weight) (S_g+S_a) =310m.

Enough realistic requirements are now set to continue the design process. As the design continues, more details can be added and the performance updated.

3.4 Prediction the power for the system

The power available is the power provided by the self-launching system of the glider.

The shaft power of the engine (P) was calculated using Equation 3.1

$$P = \frac{P_A}{\eta_{\Pr}} = \frac{T_A \times V_\infty}{\eta_{\Pr}} \qquad (3.1)$$

The propeller efficiency η_{Pr} is always less than 1. Hence, the power available is always less than the shaft power (Anderson, 2001).

The value of thrust-to-weight ratio (T/W) determines in part the take-off, and the value of power loading (P/W) determines in part the rate of climb. in order to obtain the design value of (T/W) and (P/W), we have to examine the take-off distance and rate of climb constrains.

3.4.1 The take-off distance constrain

First, the ground roll (S_g) must be calculated using Equation 3.2. Where $(C_L)_{\max}$ is that value with the flaps only partially extended, consist with their take-off setting.

$$s_g = \frac{1.21\left(W/S\right)}{g\rho_\infty (C_L)_{\max}\left(T/W\right)} \tag{3.2}$$

The ground roll is in proportion to the square weight of the glider, and it is dependent on the ambient density.

Second, the airborne distance S_a was calculated using Equation 3.3.

$$S_a = R\sin\theta_{OB} \tag{3.3}$$

The Figure 3.1 shows the flight path after lift-off. Where R is the turn radius and θ_{OB} is the included angle of the flight path between the point of take-off and that for clearing the obstacle of height h_{OB}.

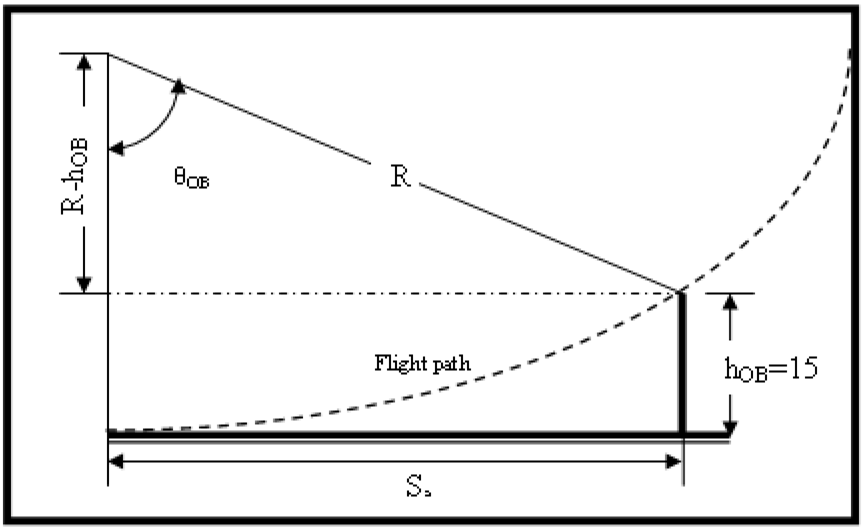

Figure 3.1: Sketch for the calculation of distance while airborne.

During the airborne phase, CS-22 required that "The selected speed must not be less than $1{\cdot}15 V_{stall}$, that is shown to be safe under all reasonably expected operating conditions, including turbulence and complete engine failure." (CS-22, 2003: 1-B-3).

$$R = \frac{6.96 (V_{stall})^2}{g} \qquad (3.4)$$

For the take-off constrain, the total power must be great than 51hp.

3.4.2 The rate of climb constrain

The zero lift drag coefficient was calculated using Equation 3.5 with a beast glide ratio of 50.

$$C_{Do} = \frac{1}{4 \times K \times \left(L/D\right)^2_{\max}} \qquad (3.5)$$

The power prediction for the JS1 was calculated using the rate of climb Equation 3.6, after we solved for power term.

$$\left(R/C\right)_{\max} = \frac{\eta_{pr} P}{W} - \left(\frac{2}{\rho_\infty} \sqrt{\frac{K}{3C_{Do}}} \frac{W}{S}\right)^{1/2} \frac{1.155}{\left(L/D\right)_{\max}} \qquad (3.6)$$

For the rate of climb constrain, the total power must be great than 47hp.

The results from this section is summarized by in Table 3.3, which shows the two constraints on power required for JS1. The specification of the take-off of 310m is the determining factor of the required power from the engine. For the JS1, the engine should be capable of producing a power of 51hp or greater.

Table 3.3: Power required for JS1

Constrains	**Power [hp]**
Take-off	$P \geq 51$
Rate of climb	$P \geq 47$

For a reciprocating engine/propeller-driven glider, the shaft power is essentially constant with the velocity, whereas the thrust decreases with velocity. To excerpt the power to weight ratio makes more sense. The power loading is the weight of the glider divided by the power. The power loading for the JS1 is 25.64 lb/hp. For powered sailplanes the value of power loading is 25 lb/hp (Raymer, 1989: 80). So our estimation appears to be very reasonable.

The detailed calculation steps for the power required for the JS1 self-launching system are given in Appendix A, section A.1.

3.5 Engine selection

The selection of the engine is extremely important in the first stage of the development the self-launching system. The choice of the engine and the rest of the system is directly dependant on each other. The factors of the engine that will influence the design of the system are:

- Dimensional size
- Weight
- Power
- Interface dimensions
- Cooling of the engine

All the available engines that fulfill the design specifications were examined. In the end 3 types of engines fulfilled the specifications: Rotex, Midwest and SOLO.

The Table 3.4 provides a summary of the comparative engine data.

Table 3.4: Engines specifications

Engine	Rotax 582ul	Midwest AE50	SOLO 2625-01
Dimensions (mm) LxWxD	510x240x366	420x256x340	408x238x288.5
Weight (kg)	44	33	23
Power (hp)	64.4	50	53
Cost ($)	6397	10356	7103
TBO (hours)	300	300	400

The importance of making the right decision in selecting an engine requires that a detailed selection process is followed. A detailed selection matrix will be used. Weighted values are assigned to all the identified engine related requirements using the rating system indicated below:

Relative Performance	Rating
Very good	5
Good	4
Average	3
Poor	2
Very poor	1

Table 3.5: Engine selection matrix

	Engine	Rotax 582ul		Midwest AE50		SOLO 2625-01	
Selection criteria	weight	rating	weighted Score	rating	weighted score	rating	weighted score
Dimensions	**30%**	2	0.6	3	0.9	5	1.5
Weight	**25%**	3	0.75	4	1	5	1.25
Power	**20%**	5	1	4	0.8	4	0.8
Cost	**15%**	3	0.45	1	0.15	2	0.3
TBO	**10%**	3	0.3	3	0.3	4	0.4
Total score		3.1		3.15		4.25	
Rank		3		2		1	

The engine selection matrix shows that the SOLO 2625-01 is the most appropriate engine for the requirements of the JS1. Although it did not perform the best in each required category, overall it is the best. The SOLO 2625-01 was developed by the German company SOLO especially for the self-launching sailplane with retractable power plant. The technical data and operating limitations that are available in Appendix B, section B.1 and drawing the most important dimensions of the engine in Appendix B, section B.2.

3.6 Propeller sizing

At this stage, we are not concerned with the details of the propeller design, the blade shape, twist, chord length, thickness of blade, Aerofoil section, etc., but we need to found the propeller diameter, because that will dictate the length of the propeller mast.

The propeller diameter should be as large as possible for good propulsive efficiency. Limitations such as structural clearance, noise, compressibility and blade stress levels my dictate an upper bound. Noise, compressibility and blade stress levels are all related to the tip speed.

For the purpose of initial sizing, Raymer (1989) gives an empirical relation for propeller diameter (D) as a function of engine horsepower.

$$D = 22(HP)^{1/4} \qquad (3.7)$$

With Equation 3.7 the diameter of propeller can be determined in inches.

$$D = 22(53)^{1/4} = 59.35in \approx 1.5m$$

To avoid the compressibility effects at the tip we have to check the tip speed according to Equation 3.8. V_∞ is the forward speed and πDn the propeller rotational velocity.

$$V_{tip} = \sqrt{(\pi Dn)^2 + V_\infty^2} \qquad (3.8)$$

From Equation 3.8 the value of V_{tip} is179m/s, and doesn't exceed the speed of sound at standard sea level (340m/s).

3.7 Summary

This chapter explained the conceptual design process, with emphasis on the importance of design requirements to constrain a conceptual design. The initial project requirements were investigated and updated by comparing the self-launching system design for the JS1 to similar self-launching gliders. The power required was there calculated and was found to be P≥51hp. This estimate was based on the take-off distance and rate of climb constraints. The engine was selected using the engine selection matrix. Lastly the propeller sizing was done. The results on the self-launching system can be summarized as follows:

- Power 53hp (39KW)
- Engine: SOLO2625-01
- Propeller diameter 1.5m
- Take-off distance 310m
- Lift to drag ratio 50
- Gear reduction 1:3

These specifications and selections will be used in the further design of the system.

4. PROPELLER DESIGN

4.1 Design envelope

In this section the design of a propeller suitable to the JS1 self-launching system will be developed. This will be powered on the engine selected and specification developed in Chapter 3. The first step is to determine the design envelope of the propeller. Sources determining this envelope are the engine and its characteristics, the JS1 and its dimensions and deductions made from the propeller design theory described in Chapter 2.

First of all a new propeller design has to match the engine it will operate on. The engine in this case is the SOLO2625-01. From the data sheet of the SOLO2625-01 the take-off power was obtained as 39KW at 2083rpm (with reduction gear 1:3) [Appendix B1]. The corresponding torque is found from Equation 4.1 as 179Nm. If a propeller absorbs less power at a rated rotation rate, the engine will be under-utilized. The other case is that the propeller requires more power than the engine can deliver and the engine might overheat. This case would have severe consequences as the engine is at the current margin in terms of overheating. The propeller would thus be required to absorb 39kW at 2083rpm.

$$\max.Torque = \frac{power}{2\pi n/60} \qquad (4.1)$$

In Figure 4.1 the drag characteristics of the JS-1 glider is plotted. From basic aerodynamic theory it is known that for unaccelerated, level flight that the thrust should be approximately equal to the drag. To accelerate further the available thrust would have to be higher than the drag at a certain engine rotation rate and flight speed. From the Figure 4.1 we can fix the JS-1 speed at 35 m/s (~ 126 km/hr) at which the propeller should be optimized. From the drag curve at 35m/s, the aircraft drag is roughly 122 N. The absolute minimum thrust should then be about 130 N to contend with any uncertainty in the data.
The take-off thrust for the JS1 was estimated using Equation 4.2 (Anderson, 2001: 457).

$$T_A = \frac{\eta P}{0.77V_{stall}} \qquad (4.2)$$

This was calculated to be T_A=975 N. this will be used as the required thrust from the propeller.

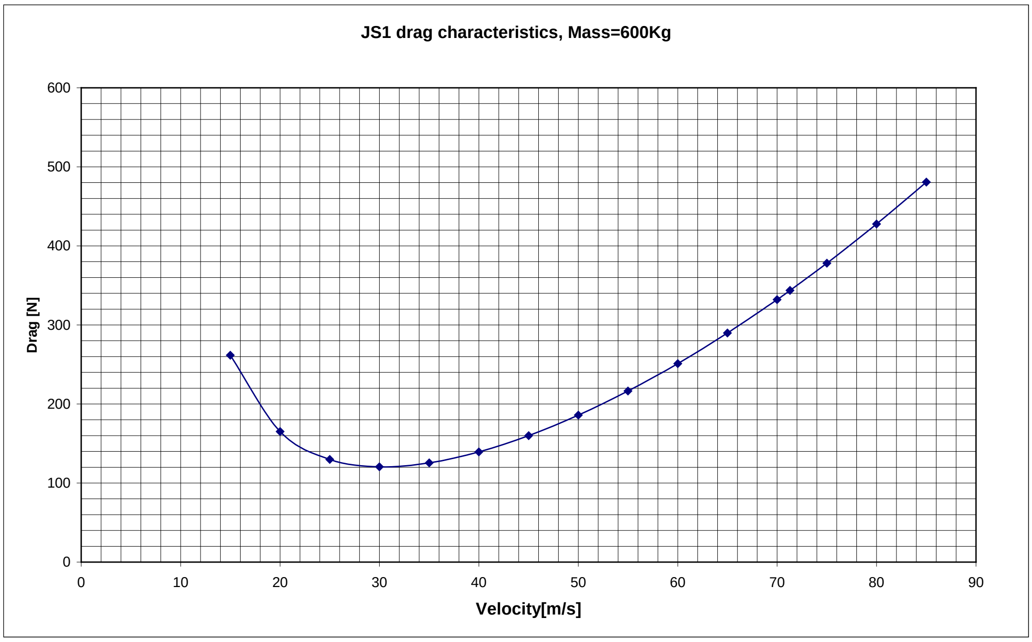

Figure 4.1: JS1 drag characteristics.

4.2 Aerofoil Selection

The most commonly used blade Aerofoil sections are the RAF-6, Clark Y and NACA-16 series of Aerofoils. As a general rule, the RAF-6 section has high camber and offers good take-off thrust. The Clark Y section has moderate camber and low minimum drag. The NACA-16 sections are designed for high speed applications and are not normally used with engines below 700hp. (Roskam & Lan, 2003: 324).

On this design the Clark Y Aerofoil section will be used. Another reason the Clark Y section is used is that it eases the manufacturing process, because of the flat lower surface.

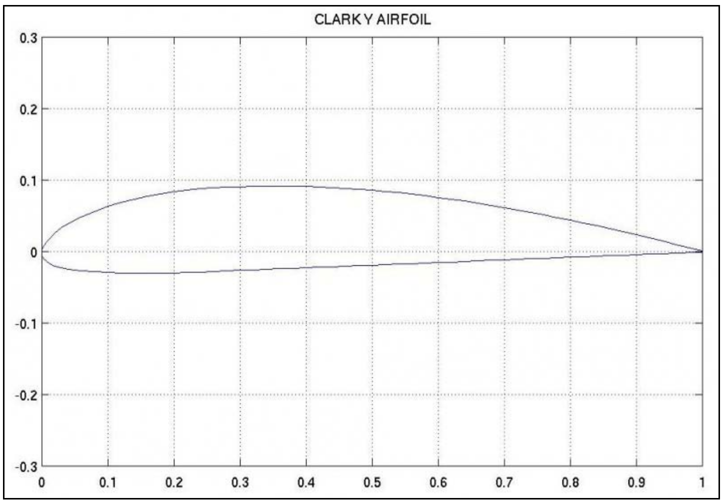

Figure 4.2: A Clark-Y Aerofoil (Silverstien, 1935).

4.3 Aerodynamic Design

For the chosen Aerofoil to be used for the blade profiles of the propeller, the aerodynamic characteristics had to be studied. The analysis of the Clark-Y Aerofoil was done with a software package, freely available on the internet, called XFLR5. The Aerofoil had to be analyzed over the range of operating conditions that the blades are expected to experience. From a few short calculations, assuming some blade dimensions and sailplane speeds, the Reynolds number can be plotted as a function of the radius along the blade. This distribution is shown in Figure 4.3 and the range of Reynolds numbers likely to be expected is from about $2x10^5$ to $2.5x10^6$.

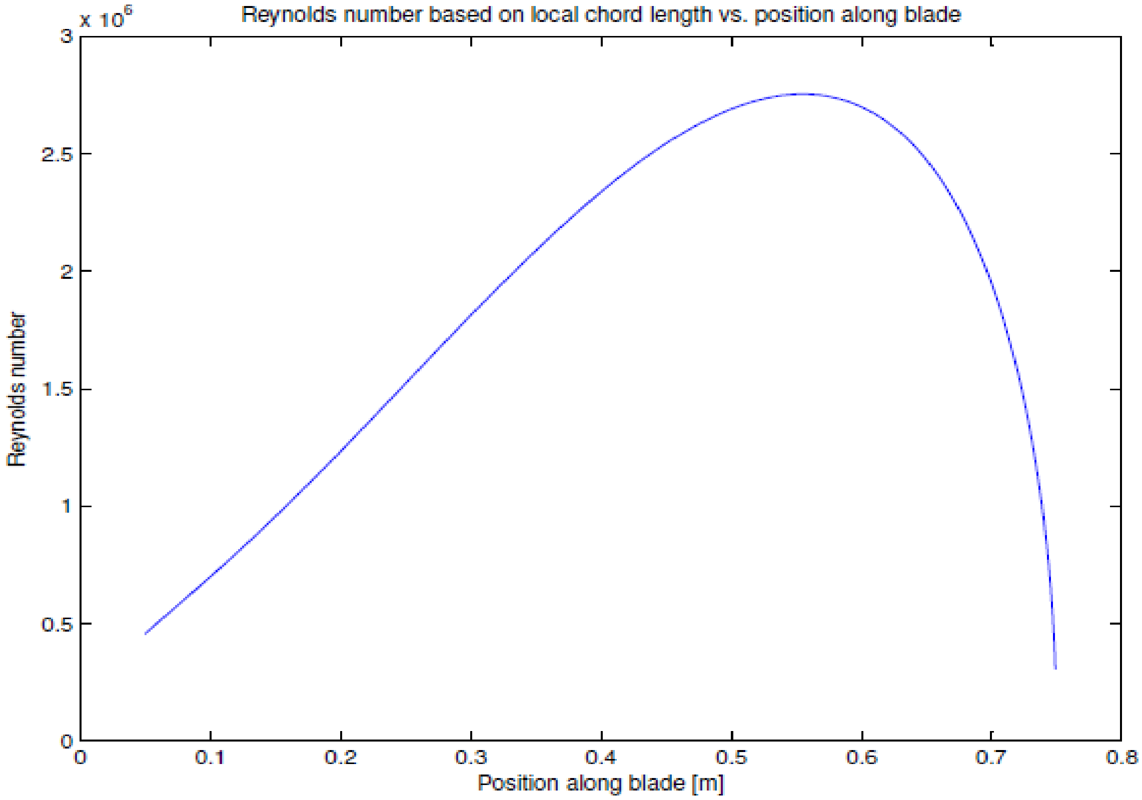

Figure 4.3: Expected Reynolds number along blade.

With this information, the analysis for the Clark-Y was run by the software package and the main result of the lift coefficient versus angle of attack is shown in Figure 4.4. In conjunction with this plot, the drag polar is needed to determine the necessary Aerofoil characteristics to be used in the design process.

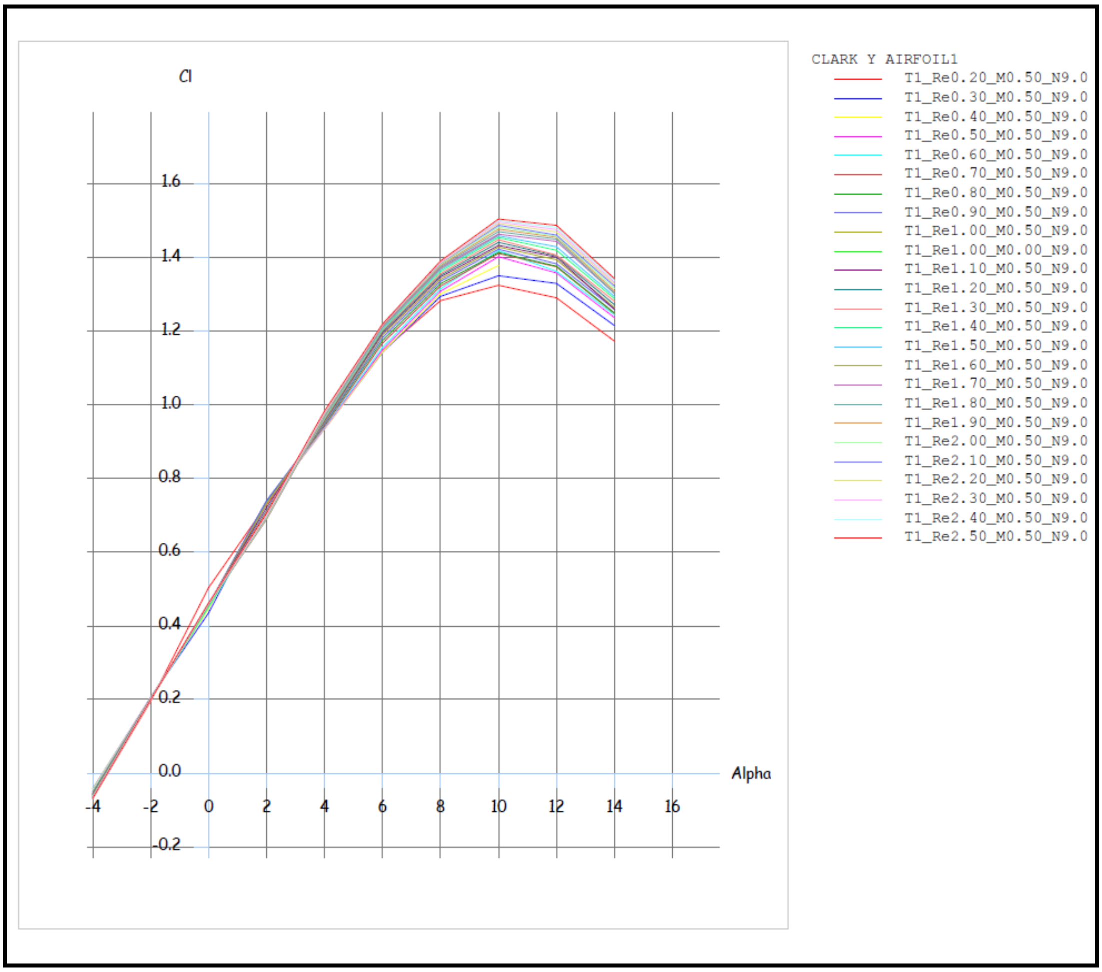

Figure 4.4: Lift coefficient versus angle of attack for Clark-Y Aerofoil.

The results were verified by wind-tunnel test results. Valuable information is available on National Advisory Committee for Aeronautics (NACA) reports center (Silverstien, 1935), and a report documenting these results was obtained and is shown in Figure 4.5.

The software generated plot confirms well with the wind-tunnel results. The results from the wind-tunnel were obtained with a wing of aspect ratio 6. To convert this information to two-dimensional the Equation 4.2 is used (McCormick & Wiley, 1979).

$$C_L = \frac{C_l AR}{2 + \sqrt{4 + AR^2}} \qquad (4.3)$$

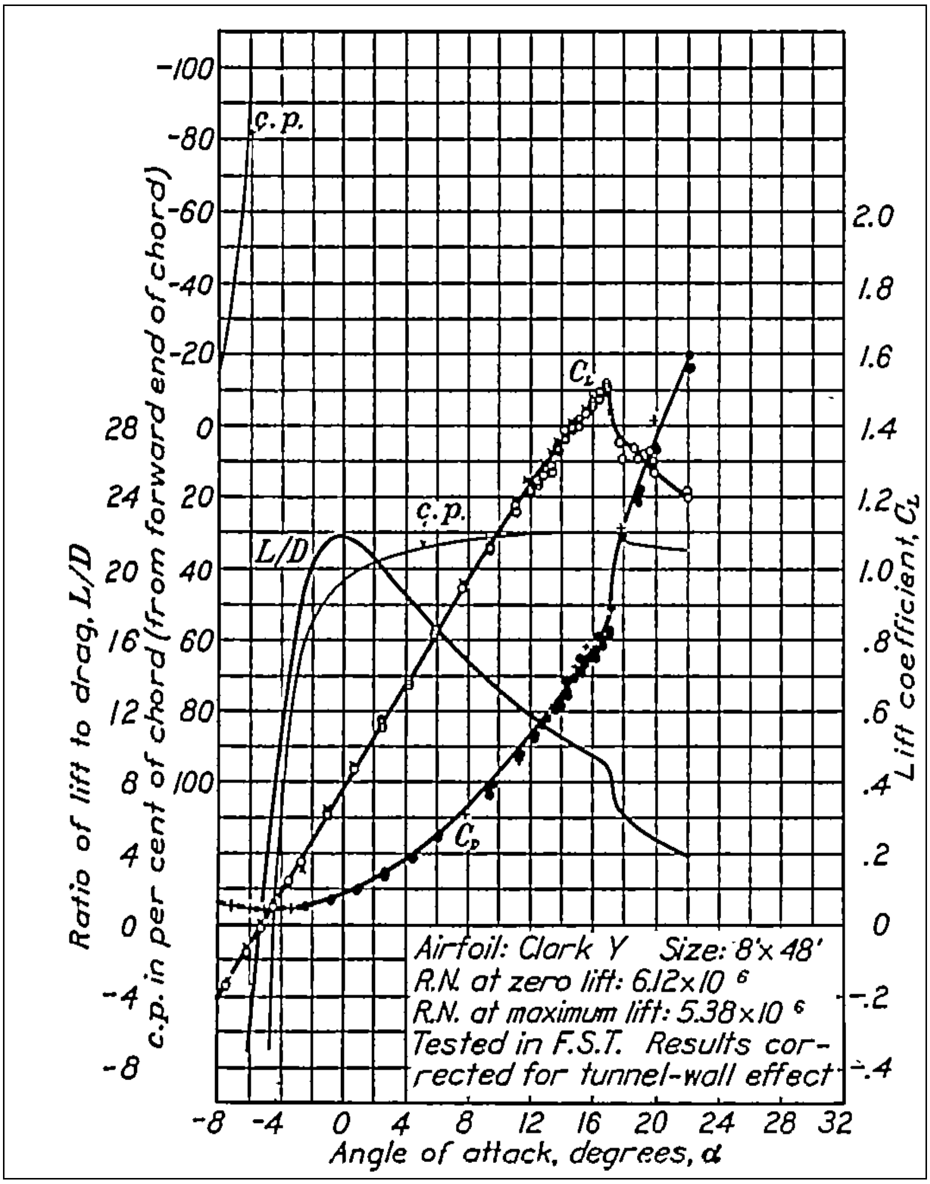

Figure 4.5: Wind tunnel testes results on a wing with Clark-Y Aerofoils (Silverstien, 1935)

This relation gives the 2D lift coefficient as about 1.11 (software analysis ≈1.16) at an angle of attack of 6°. At a 4° angle of attack, the 2d lift coefficient is roughly .97 (software analysis ≈.93). This seems to correlate very well with the software generated values, with a band of error of about 4%.

To have as little drag loss as possible, the Aerofoil should operate at some optimum point. This point is a tangent point of a line from the origin to the drag polar curve (Roskam & Lan, 2003: 138). The curve in Figure 4.6 shows this point. The curve was evaluated at a Reynolds number of $0.2X10^6$ (C_L~0.9).

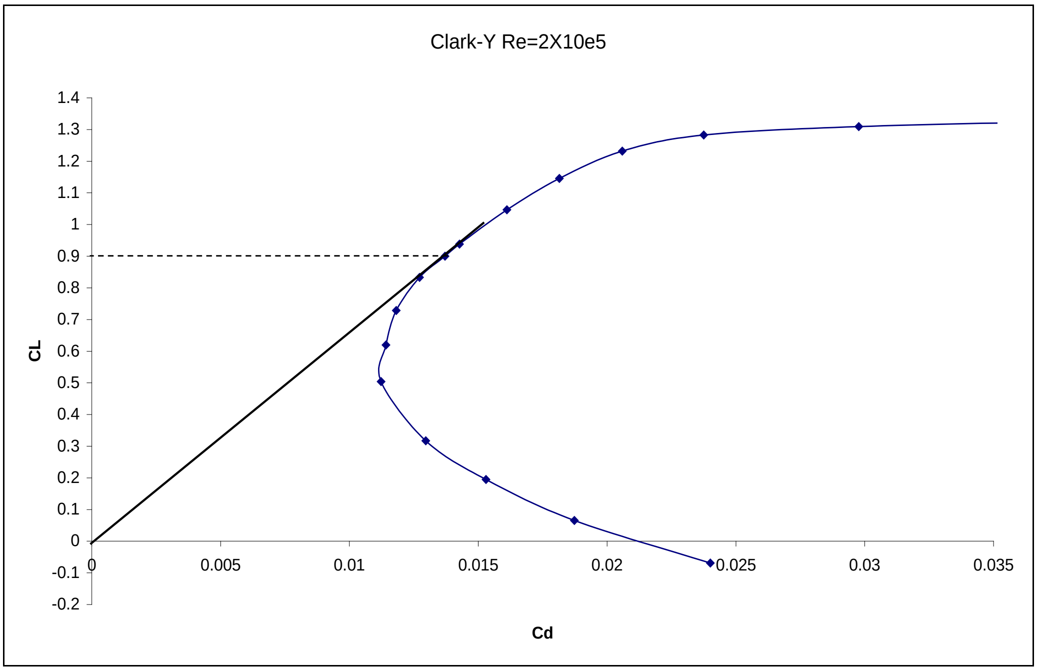

Figure 4.6: Lift coefficient versus drag coefficient for Clark-Y.

In correspondence with propeller manufacturers and Dr. Hepperle (2009), the angle of attack of a Clark-Y on existing propeller is 3^o. The slightly lower angle than the optimum is used in the aviation industry because of the part of induced drag that it does not account in the 2D analysis. The angle of attack of 3^o will be used during the design process. According to this angle of attack, the section lift coefficient is 0.8 and the drag coefficient is 0.0085. The zero lift angle of attack is found as -3.6. Figure 4.7 shows a comprehensive drag polar for the Clark-Y.

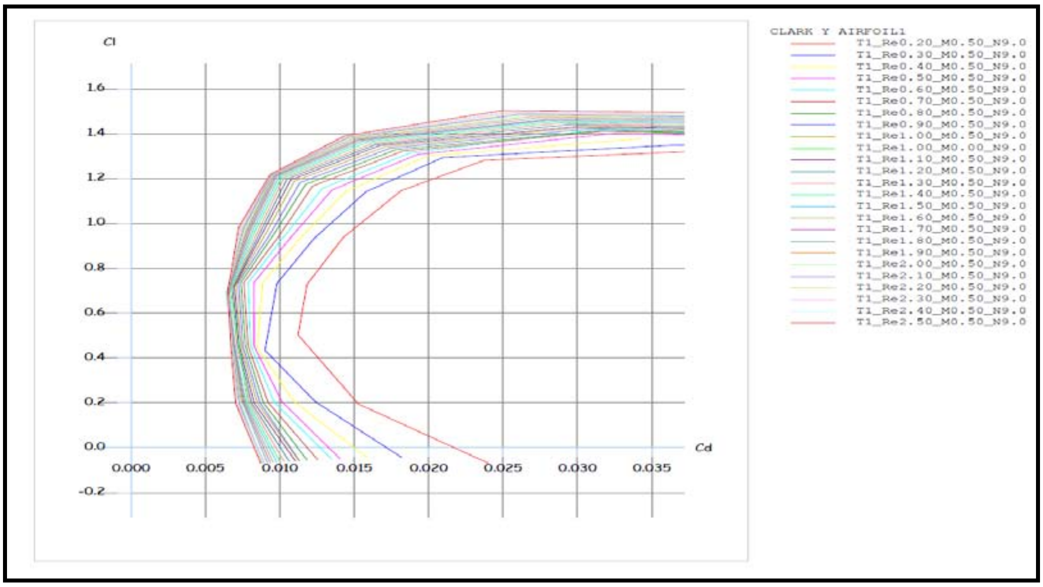

Figure 4.7: Lift coefficient versus drag coefficient for Clark-Y.

4.4 Software Description, usage and output

As was stated earlier in Chapter 2, the method of minimum induced loss propeller technique that was developed by Larrabee (1984) was programmed in Matlab® script by Visser (2006). In this section the Visser (2006) Matlab® script was used for the propeller design.

The following inputs are needed to run the program, and the blade geometry can be obtained by numerical analysis and a prediction towards the thrust and torque can be obtained by numerical integration.

All the inputs necessary to commence with the design has been determined and they are listed in Table 4.1 below.

Table 4.1: Propeller design parameters

Variable	**Value**
Aircraft speed, V	35m/s
Propeller diameter, D	1.5 m
Torque $_{max}$, Q	179Nm @ 2083RPM
Take-off Thrust, T	975N
Aerofoil	Clark-Y
Angle of attack, α	3º
C_l	0.8
Cd	0.0085
Number of blades	2
Hub diameter	125mm
Design operating altitude	At sea level

4.4.1 Propeller design Results

The above design inputs were used and provide the following outputs at each blade station:

- Blade angles
- Chord length
- Induced angles
- Helix angle
- Thrust and Torque coefficient

The entire graphics output is shown in Appendix C.

Propeller outputs are:

- Static Thrust, [N]
- Predicted thrust, T_{calc} [N]
- Predicted torque by the propeller, Q_{calc} [N.m]
- Propeller activity factor, AF
- Advance ratio, J
- Propeller efficiency, η
- Integrated design lift coefficient
- Text files (x, y and z coordinates) to import directly into Solidworks® to construct the propeller

Table 4.2: Propeller design results

Specification	Value
Diameter, D	1.5m
Number of blades, B	2
Maximum chord, C_{max}	182 mm
Static thrust, T_{stat}	908 N @ 2083RPM
Aerofoil	Clark Y
Aircraft speed, V	126 km/h
Take-off thrust, T	975 N
Activity factor, AF	130
Advance ratio, J	0.67
Thrust coefficient, C_T	0.121
Power coefficient, C_P	0.1
Efficiency, η	81%

4.5 Summary

This chapter reported on the aerodynamic design for the propeller with the use of minimum induced loss propeller design technique. The design envelope for the propeller was developed. The Clark Y Aerofoil was selected to be used for the blade profiles of the propeller. The analysis of the Clark Y Aerofoil was done with the XFLR5 software.

5. RETRACTION SYSTEM DESIGN

5.1 Geometrical restrictions on the system

In the initial phase of the project the geometrical restrictions connected to the system were determined first. Provision has thus been made for the installation of the retractable propulsion system and therefore the parameters regarding the installation space are fixed. The geometry of the available space was determined by measuring the body of the JS1 glider. With the measurements of the installation space known fixed boundaries could be determined by which the system should be designed and installed. For simplicity purposes and the irregular form of the space has been simplified.

The form of the space is simplified to the following basic form (Figure 5.1) with the indicated dimensions.

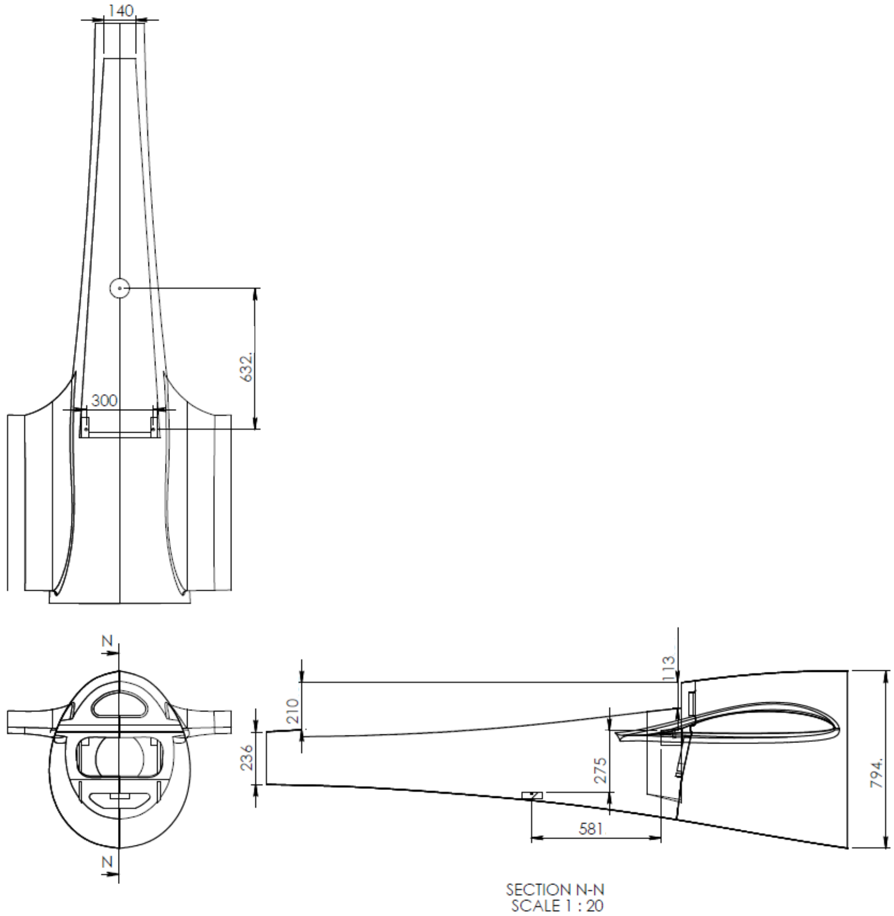

Figure 5.1: The top and side view of the installation space.

The relative positions of the hinge points that can be used are connected to the geometry of the space. Three strong points were identified through visual examination. These three strong points will be used in the interest of the design and the installation of the retracting propulsion. The relative position of the points to each other can be seen in Figure 5.2. These points can however be moved slightly if required.

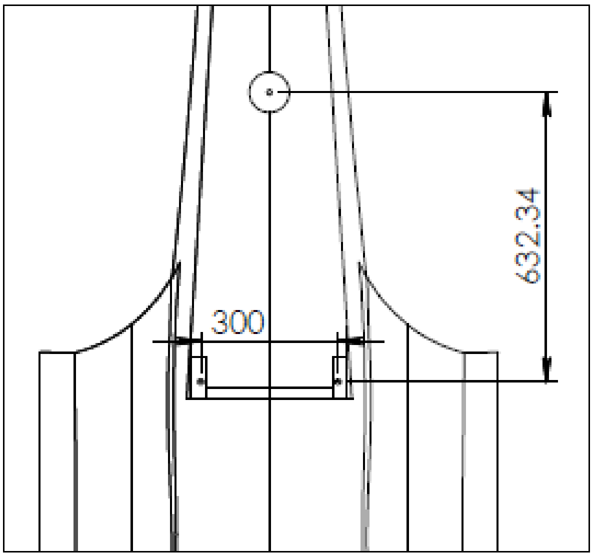

Figure 5.2: Relative position of hinge points (top view)

To simplify the design of the retractable frame, the author decided to model the SOLO2625-01 engine in a SolidWorks® according to the engine dimensions (provided by the manufacturer) [see Appendix B2]. Figure 5.3 shows an isometric sketch of the SOLO 2625-01engine.

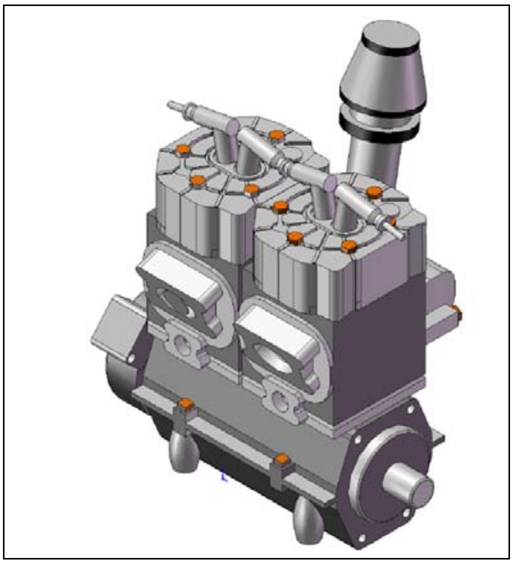

Figure 5.3: SOLO 2625-01 Engine.

Because the engine will also take up space and volume and its form is fixed, it is seen as a geometrical restriction. The purpose with the CAD model is to simplify the design of the retractable frame. The model is thus seen as a good designing aid. The model was put into the installation space and an idea was developed of the available amount of space available for the frame and the retracting mechanism. The model also showed what likely interface should be used between the engine and the frame.

5.2 External Forces on the system

Three external forces were identified that exerts force on the mechanism:

1. The forces working on the system because of the mass of the retracting arm.
2. The shearing forces caused by air resistance on the retracting arm.
3. The gyroscopic force caused by the rotation of a propeller.

The gyroscopic force will be discussed later in Chapter 6.

5.2.1 Forces caused by air resistance

Part of the primary purpose of the retracting propulsion is that the system can be deployed during the flight to increase the aid the glider needs to gain height. It is therefore necessary to calculate the air resistance load on the extended system.

Firstly one has to realize that the air resistance or drag will have an influence on the design of the steel frame and the (folding) retracting mechanism. The forces that will be needed to create the push out of the system will be larger if the effect of drag is considered.

The retracting mechanism will be designed so that it can be deployed if the maximum possible forces are applied to it. That will happen when the glider is flying at the maximum recommended deployment glider speed (CS-22) of 140 km/h. In the fully deployed position the retracting arm is perpendicular to the direction of the motion.

The total effects of the drag forces on the unfolding mechanism were determined by determining the effect on each sub-part of the retracting arm and then add it to each other.

The retracting arm has the following main components as indicated in Figure 5.4. The areas of each of these components will be used in calculating the drag forces. The components are:

1. Propeller
2. Top pulley
3. Radiator for water cooling
4. Pylon

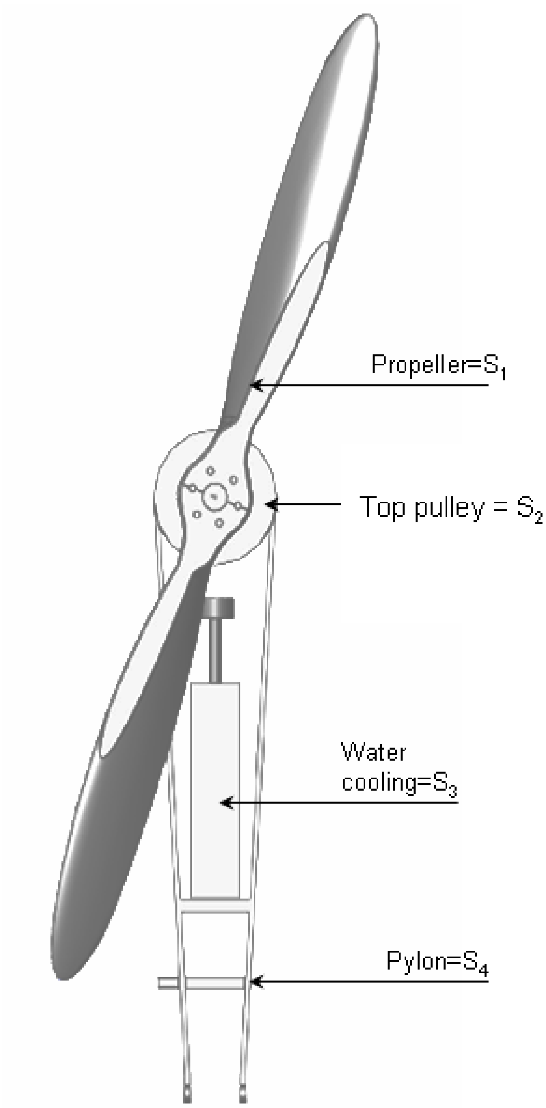

Figure 5.4: Main parts of the retracting arm with indicated areas that were used for calculations.

The drag forces are shown on a simple free body diagram in Figure 5.5.
The drag force of a stopped propeller is calculated by using Equation 5.1.where σ is propeller solidity, S is propeller disk area and q is a dynamic pressure (Raymer, 1989: 287).

$$D/q = 0.8\sigma S_{propellerdisk} \qquad (5.1)$$

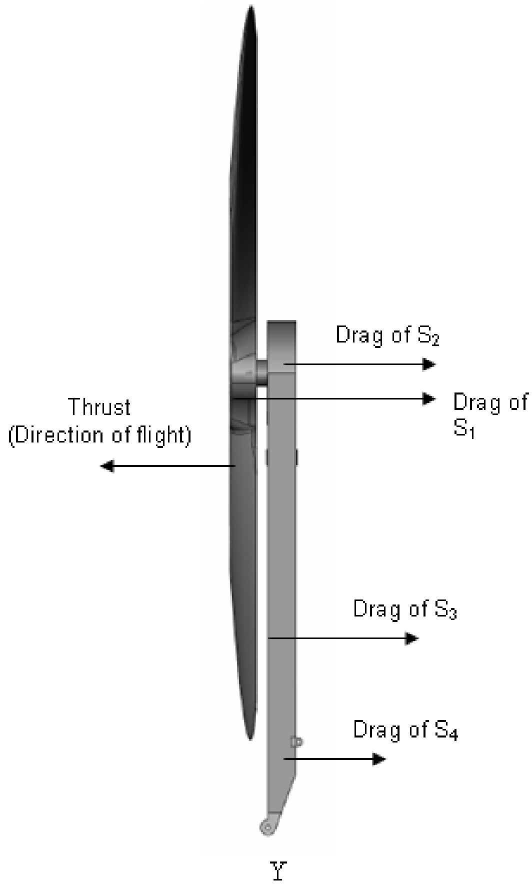

Figure 5.5: Forces diagram of unfolding arm (side view) caused by wind resistance.

The drag force for the propeller top pulley and for the water cooling stack can be adequately estimated using the same methodology used for the determining the fuselages drag Equation 5.2 (Raymer, 1989: 279).

$$C_{D_o} = \frac{C_f . Q . FF . S_{wet}}{S_{ref}} \tag{5.2}$$

Equation 5.3 was used to calculate the drag force for the propeller pylon, (Roskam & Lan, 2003: 162).

$$C_{D_o} = R_{wf} R_{Ls} C_f \left\{1 + L'\left(t/c\right) + 100\left(t/c\right)^4\right\} \frac{S_{wet}}{S} \tag{5.3}$$

The results of the calculations of the drag force are provided in Table 5.1. It must be emphasized once more that these are the results when the system is fully extracted. The values of the areas were determined by examining the existing retracting arms and make assumptions according to this.

Table 5.1: Results of drag force calculations.

Items	Area S[m^2]	Drag coefficient C_d	Drag force D[N]	Distance from Y[m]	Moment around Y M[N.m]
Propeller	0.163	0.0116	120.68	1.03	124.30
Top pulley	0.096	0.0039	40.38	1.01	40.73
Radiator for Water cooling	0.0755	0.0039	40.27	0.615	24.77
Propeller pylon	0.037	0.0037	38.38	0.435	16.69
Total			239.66		206.50

By summating the moments around Y it is found that the drag force on the extended system will cause a moment of 206.5 Nm around the hinge point. The folding mechanism was thus designed for this maximum value. It must also be kept in mind that 206.5 Nm is the maximum value for the effect of the drag forces. The value starts as a minimum (zero) when the system starts to ascend, and increases as the retracting arm is unfolding. It then reaches the maximum calculated value when the arm is fully extended.

Figure 5.6 shows the increase in drag forces with the corresponding increase in the moment around Y as the unfolding angle increases. The unfolding angle is an angle of 90˚ through which the arm has to rotate. The angle is taken as zero if the system is in the fully retracting position and 90˚ if the arm is fully extended.

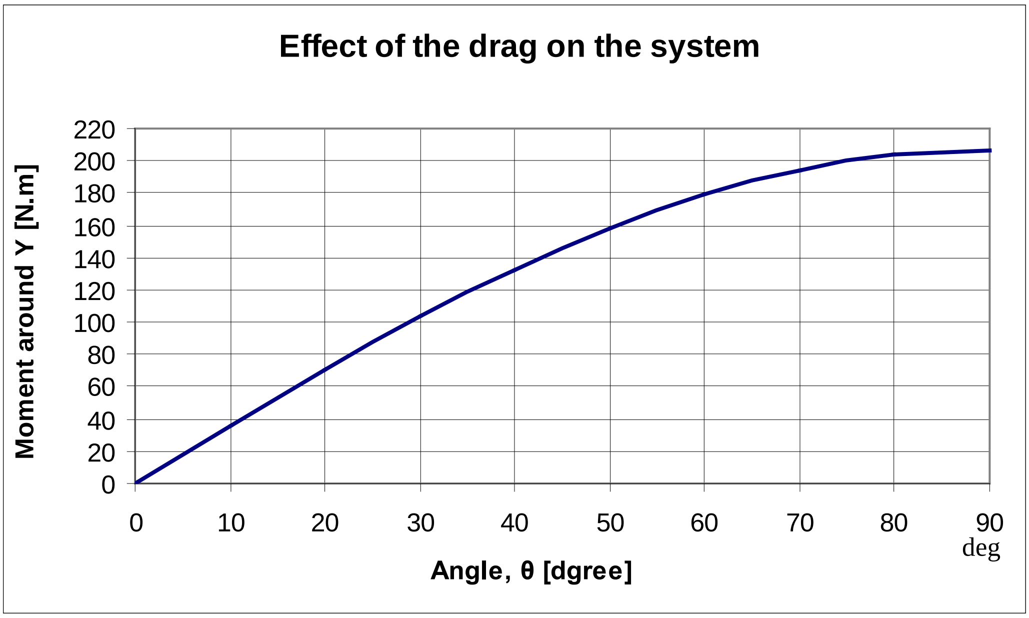

Figure 5.6: Effect of the drag forces on the system.

5.2.2 Forces caused by mass of the system

The force caused by the mass of the system has an opposite effect on the system than the effect of the drag forces. The mass of the system has a maximum value (moment around Y) if the system is retracted and declines to zero when the arm is fully extended. Because the design of the retracting arm and the propeller has not been done, existing systems was examined to determine good values for the masses of the different components.

Table 5.2: Results of weight calculations

			n=1g	n=2g
Items	mass[kg]	W[N]	M [Nm]	M [Nm]
Propeller	5	49.05	50.52	101.04
Top pulley	1.5	14.715	14.86	29.72
Radiator water cooling	1.4	13.734	8.45	16.89
Unfolding legs(pylon)	2	19.62	8.53	17.07
Total	9.9	97.119	82.36	164.73

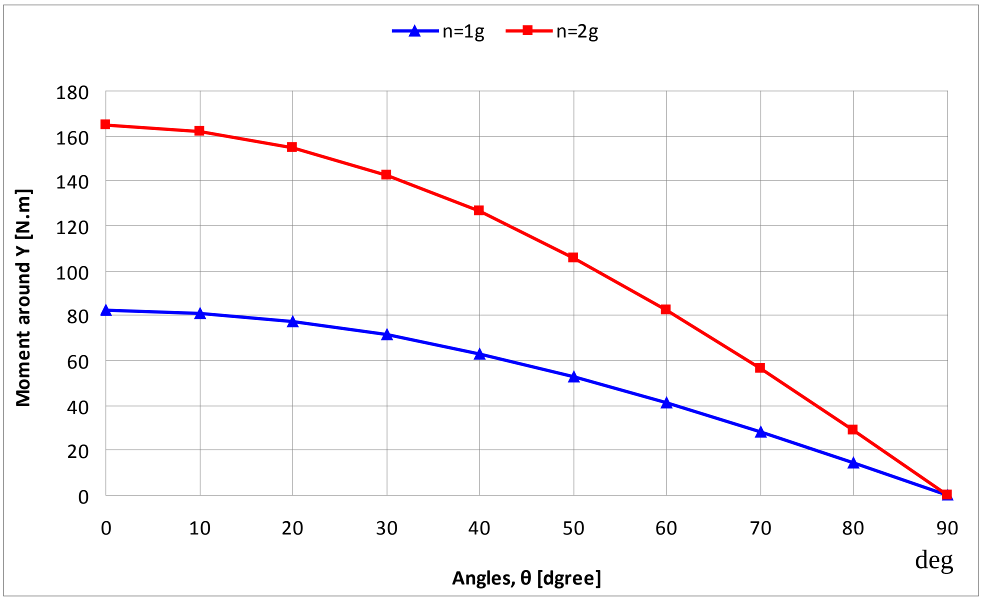

Figure 5.7: Effect of the mass forces on the system.

By combining the effect of the drag forces and the effect of the mass forces on the system, the total external forces of the system can be calculated as indicated in Figure 5.8. Figure 5.8 represents the values of the forces that will be used in the design.

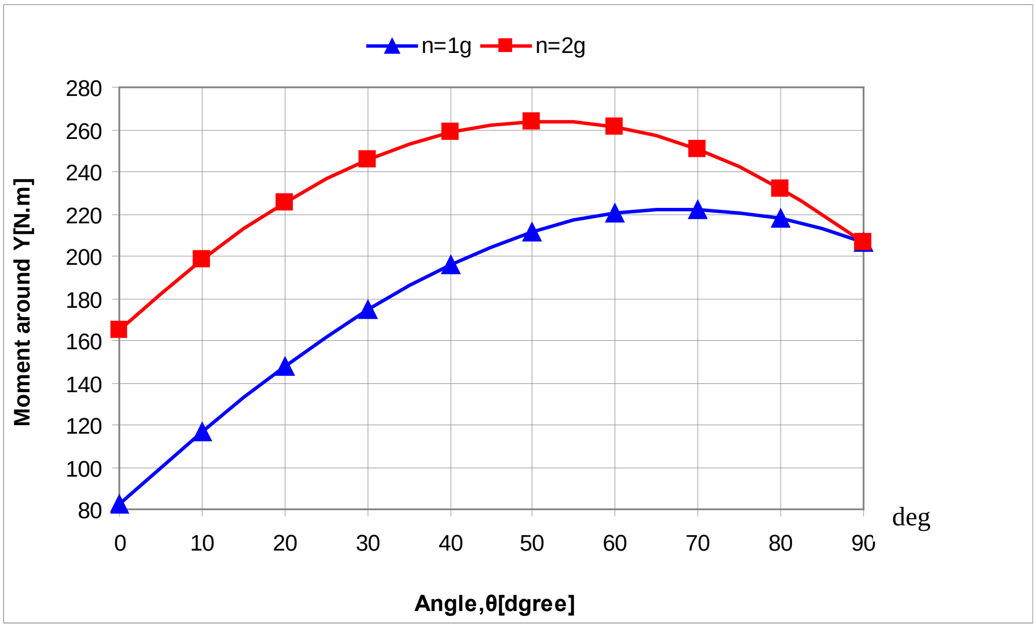

Figure 5.8: Effect of the total external forces on the system.

5.3 Frame design

The following design requirements and restrictions must be kept in mind during the design of the frame:

- Components like the engine and the retracting arm must be connected to the frame to ensure strength of the system.
- The frame must be strong enough to provide resistance (without failure) to all the forces that exercise an effect upon the system.
- The frame must be sturdy with minimum deflections at all critical points.
- The frame must isolate the body of the glider from all engine vibrations.
- The size of the frame must be determined by the allotted area for the frame.
- The frame must be designed to use the three existing strong points Figure 5.2 for the mounting of the system in the glider.
- The mass of the frame must be kept to a minimum. Therefore not only the strength but also the mass of the frame must be optimized.
- The frame must be 100% reliable.

During the project a large number of failed frame designs were made, the cause being the available space for the installation (Figure 5.1) of the frame and the engine are restricted and has a complicated shape. Ideas for the frame that looked good on paper did not work in practice, because there was always a part of the frame that did not fit or the entire design was impractical when compared to the available space. The decision was then made to build a model out of wire that will fit into the installation space. By using an alternating build and fit method it was easy to see whether the frame will fit or not. The alternating build and fit method implies that a part of the frame was built and then fitted into the specific part of the installation space. The needed modifications (if necessary) can then be made to the frame before continuing with the detailed design. Figure 5.9 shows an isometric sketch of the framework. All rods in the figure are steel tubing. All this was done in the CAD software SolidWorks®.

It should be noted that because concept three was chosen and the engine is fixed, the drive belt needs to bend during retraction, but needs to be tight during engine operation. This was done by putting the folding mechanism hinge point in front of the belt. This will allow the belt to go slack during retraction, but to tighten up during extension.

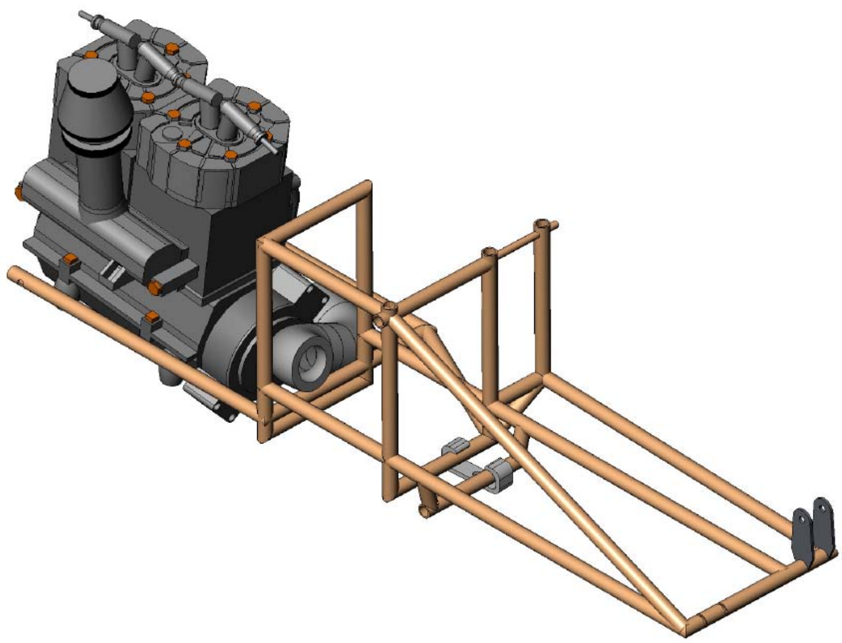

Figure 5.9: Frame for the JS1 self-launching system.

5.4 Concepts for the functioning of the folding mechanism

Three concepts were examined for the functioning of the folding mechanism. Figures 5.10, 5.11 and 5.12 indicate the action of the three concepts. The dotted lines in each figure indicate the position of the system when folded back.

In Figure 5.10 the force necessary for the folding mechanism is provided by a linear actuator. The actuating force and its connecting position is indicated by the arrow. In Figures 5.11 and 5.12 the force and relative connection positions are also indicated by arrows.

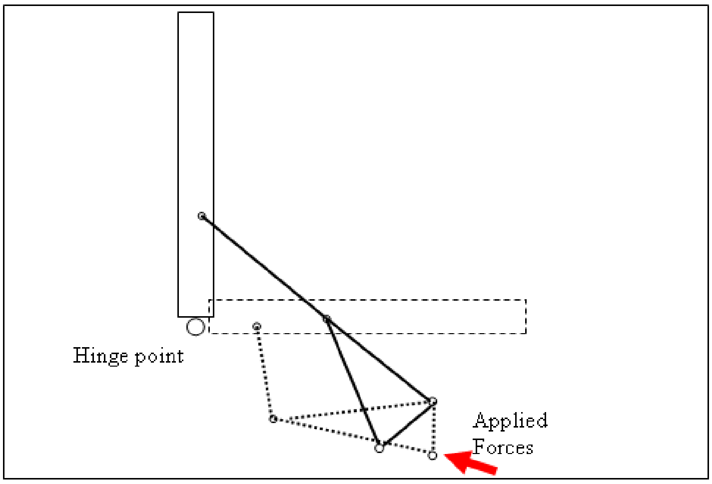

Figure 5.10: Concept 1 of folding mechanism

Concept 2 has a simple set-up. The force is also provided by a linear actuator.

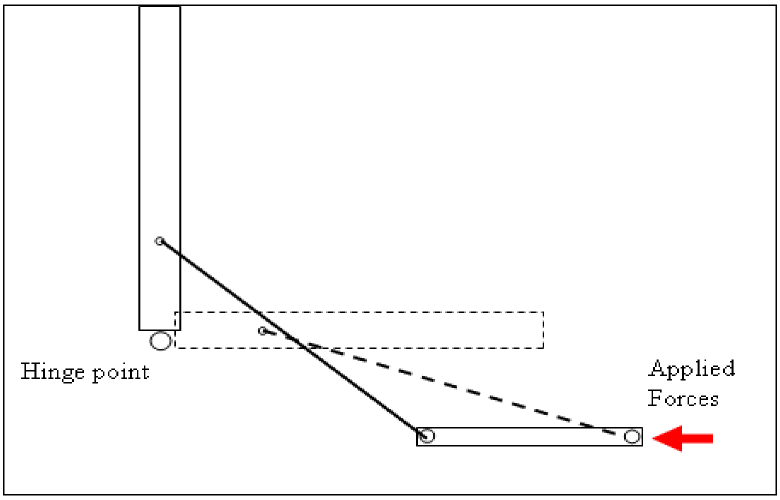

Figure 5.11: Concept 2 of folding mechanism

In the final concept a moment of rotation is used as a force and not a linear force. The moment of rotation is provided by an electrical motor.

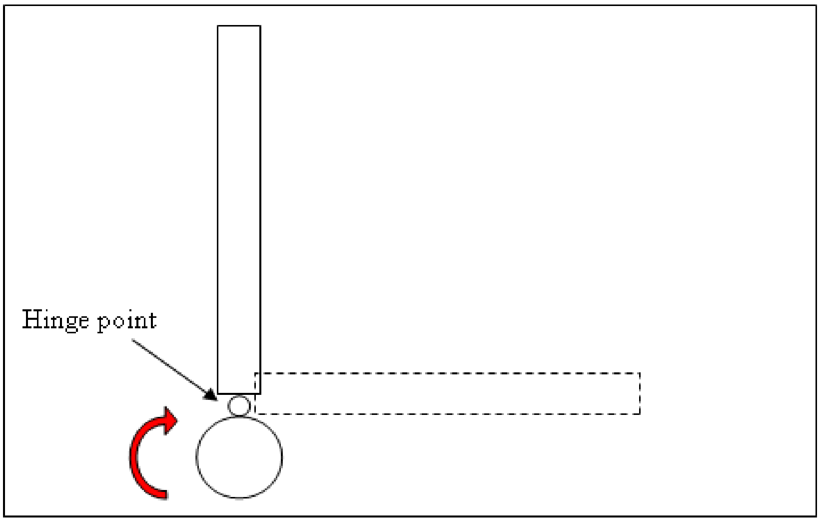

Figure 5.12: Concept 3 of folding mechanism

After the initial considerations it was decided that only the first two concepts would be considered. Concept three was eliminated early on. Certain aspects led to the early elimination of concept three:

- Complexity of the system.
- Space restriction for the set-up type in the installation space.
- Lubricating system necessary for ratchet.
- Regular maintenance needed for the system.

Thereafter the advantages and the disadvantages of the two remaining concepts were considered. These advantages and disadvantages were weighed against each other to decide which concept will be used for the functioning of the folding mechanism. A discussion of the advantages and disadvantages of each concept will now be discussed.

The actions of both concepts are very simple. For both instances the linear actuator has relatively the same position regarding the installation space. There is thus not a difference in the design of the frame when it comes to provision for the connection of the actuator. In the second place the space that is taken up by the frame and the folding mechanism would both fit in the allotted installation space. The set-up of concept two is of such a nature that it is smaller than that of concept 1. The volume taken up by concept two is not only smaller than that of concept one but also more favourable. This conclusion has been made by looking at the interfaces of the folding mechanism with the engine and the available space. According to space concept two is thus more favourable. In the third place the forces necessary to deploy the system is in the same order for the different set-ups. This aspect thus did not really have an influence on choice. Another important fact that had to be considered at this point is the ease with which the system can be optimized for the minimum actuator forces needed for the functioning of the folding mechanism. The design of concept two allows for the force to be optimized easily by altering the design only slightly to determine the minimum force needed. This is not the same for concept one though, since the process to optimize the system is more complex because a few aspects influence the system in a way. The relationship also determines the position of the arm when after being retracted away which is important to ensure that the system will fit into the space when retracted. The mass of the two set-ups is also important, and the mass of concept one was slightly lower than that of concept two.

The last consideration, and possibly one of the most important ones, is the ease with which the systems can be manufactured. In this instance everything indicates that concept one is preferable, because the manufacturing of the pushing arm’s movement and the design of the frame to keep it steadily on the track is seen as problematic areas.

After all the considerations have been completed and a few aspects that have not been mentioned, it was decided to chose concept one for further development.

5.5 Optimizing of the concept

Concept one (Figure 5.10) was developed further to develop optimal functioning of the folding mechanism. Optimal functioning implies that the placing and dimensions of the folding mechanism and the actuator is determined in such a way that minimum force is needed for the extracting and retracting of the system.

The first step in optimizing the system is to determine the position of the folding mechanism. The position is determined by looking at the available space that is right after the engine and frame has been put in the installation space. The position that has been decided upon was of such a nature that the functioning of the folding mechanism is not influenced by the engine, frame or fuselage of the glider.

It is possible to model retraction system mechanism using spreadsheet programs. This is a method developed by A.S. Jonker. The spreadsheet model is a parametric model and it gives a simple visual presentation of the control system with interactive movement. It is also possible to use this model to calculate the loads in each member as a function of the inset load (Jonker, 2006).

5.5.1 Simulating retraction system

The spreadsheet model was used in the design of the JS1 sailplane retractable system mechanism. This mechanism is automatically operated by the electrical actuator. Figure 5.13 shows a typical retraction system, consisting of an actuator at the end of the frame, a rod A, rod B to the propeller pylon and then the propeller pylon.

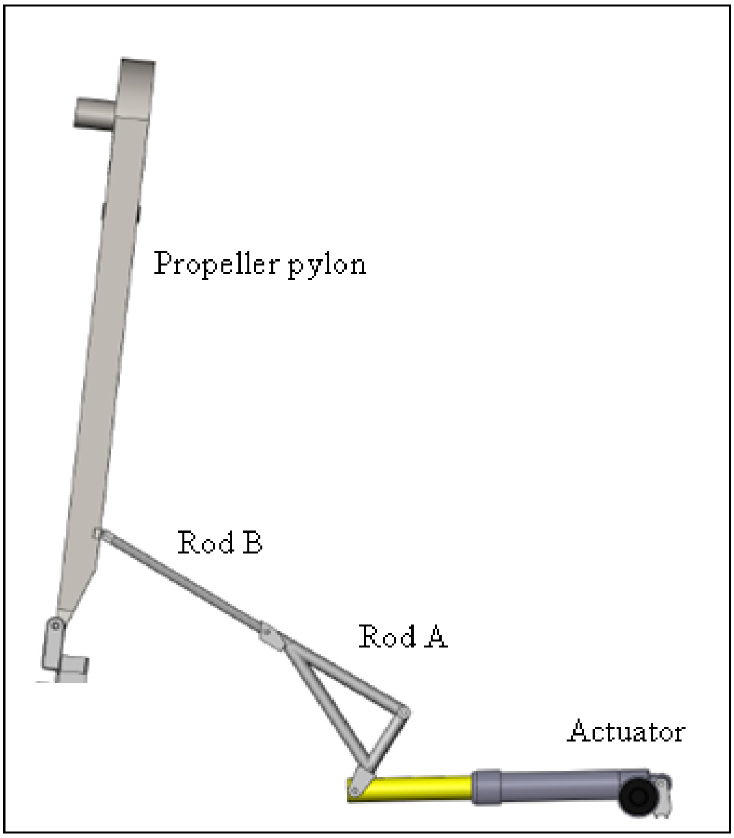

Figure 5.13: Retractable system mechanism for the JS1

All the geometrical data is filled in for every element after which the coupling is performed. The output result is the graphical representation in the Figure 5.14. The input to the simulation is linked to the actuator length.

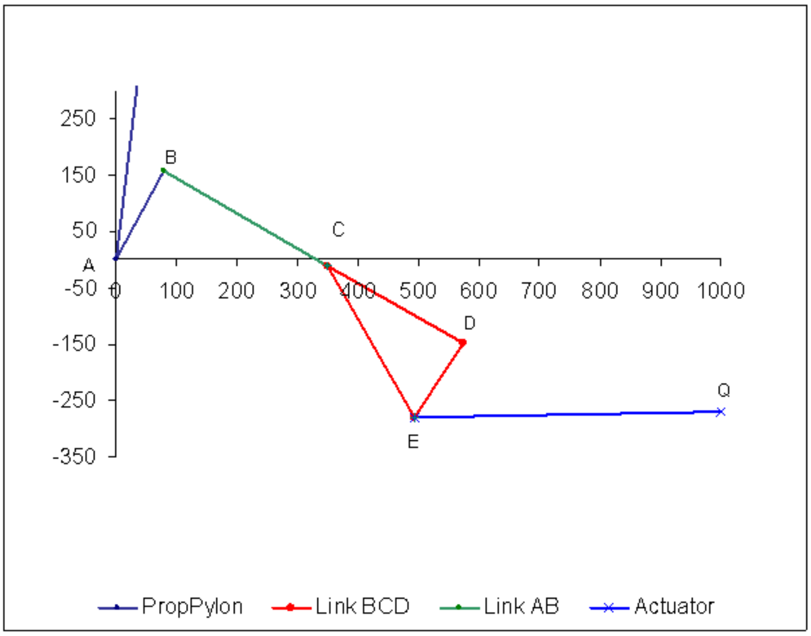

Figure 5.14: Linkage layout for a Retractable system.

5.5.2 Load calculations

The spreadsheet model was used in the design of the JS1 sailplane retractable propeller pylon mechanism. This mechanism is automatically operated by the actuator. The design requirements is thus the operational load not be higher than 4450N which is the maximum load possible by the actuator (Motion Systems, 2009).

The actuation loads were calculated using a spreadsheet model and is shown in Figure 5.15. The maximum load is 1895N at n=1g and 2493 N at n=2g was considered acceptable.

The axial forces for the retraction mechanism system were calculated in each member as a function of the actuator stroke position in Appendix A section A.2.

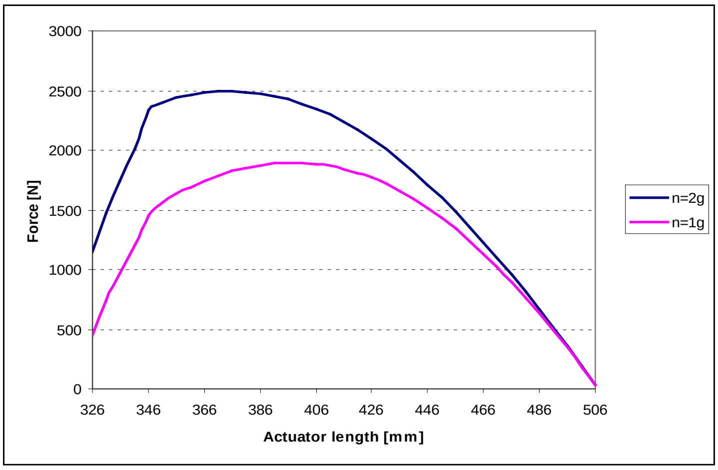

Figure 5.15: Actuation load against Actuator stroke length.

Actuator specifications in Table 5.3 as determined from the retraction system simulation and the loads needed to operate the system.

Table 5.3: Actuator specifications

Actuator length [mm]	326
Stroke length [mm]	180
Dynamic Load [N]	4450
Static load [N]	13345
Gear ratio	20 : 1
Motor	12 VDC, 3000RPM

Figure 5.16 shows the time of extension the self-launching system vs. the load that exerted on the system, the system need 11.36 second to extend at the maximum load of 2493N.

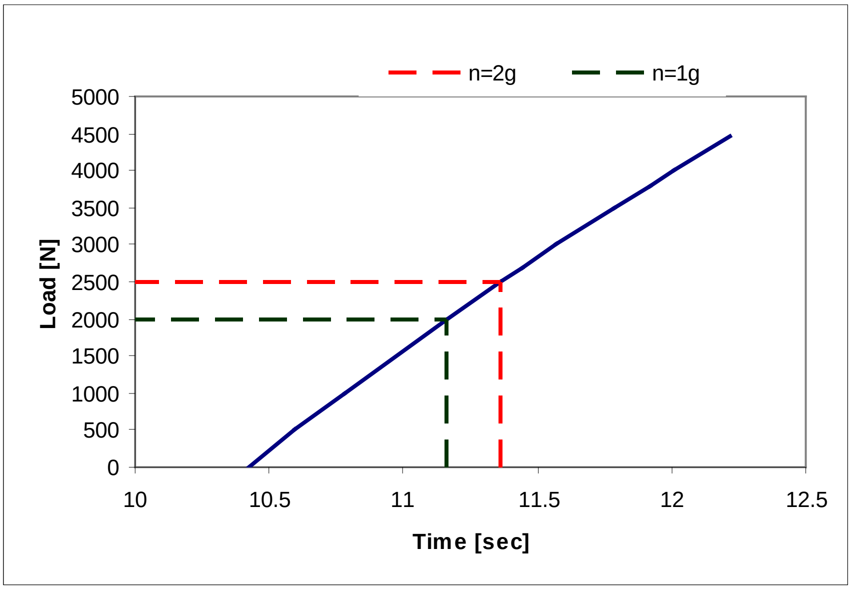

Figure 5.16: Actuation load against extension time.

The actuator of ‘Motion System Corporation’ meets all the system requirements. The specifications of the actuator are given in Appendix E.

Figure 5.17 shows the installation of the self-launching system in the glider. The detailed sketches of the self-launching system can be seen in Appendix F.

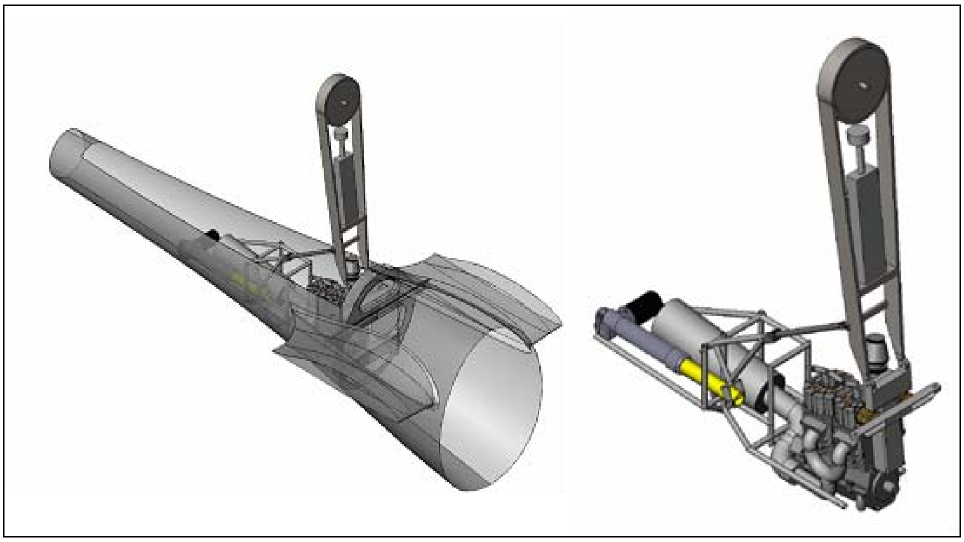

Figure 5.17: The self-launching system model.

5.6 Summary of retraction system design

In this chapter, the geometrical restrictions connected to the system were selected. The external force on the system was calculated. The design requirements for the frame design were briefly discussed. The retraction system mechanism and calculating axial load was modeled using spreadsheet programs.

A summary of the calculated results from this chapter:

- Drag force caused by the system: 240N.
- Mass force caused by the system at:
    1. n=1g: mass force= 97N.
    2. n=2g: mass force= 194.24N.
- Moment around hinge point: 206.5N.m
- Time for extension the system at n=2g: 11.4 second.
- Axial load at each rod of retraction mechanism:

Table 5.4: Maximum loads on rods of retraction mechanism

Rod	Max load [N] n=1g	Max load [N] n=2g	Length [mm]
AB			175.43
BC	1777.13	1830.25	318
CD	-1576.62	-2174.84	265
DE	1196.47	1391.34	155.8
CE	2189.14	2821.12	307.41
EQ	1894.53	2492.93	326-506

6. DESIGN CALCULATIONS

In this chapter the design calculations for the system will be discussed, the following items will be calculated:

- Gyroscopic load on the propeller pylon
- Belt design calculations
- Bending moment and shear force diagrams for the pylon
- Euler knuckle joints of rods with axial forces exerted on them
- Lugs calculations

In this chapter the solution method, relevant theory with applicable equations and the result of the calculations will be provided and all the calculations are provided in Appendix D and Appendix E.

6.1 Gyroscopic load on extension arms

When the glider flies in a circle with the engine running a gyroscopic force is generated by the propeller. This force is reacted by the extension arms. Any time a force is applied to deflect the propeller out of its plane of rotation. The resulting force is 90° ahead of and in the direction of rotation and in the direction of application, causing a pitching moment, a yawing moment, or a combination of the two depending upon the point at which the force was applied (Pilot School, 2006). This is shown in Figure 6.1

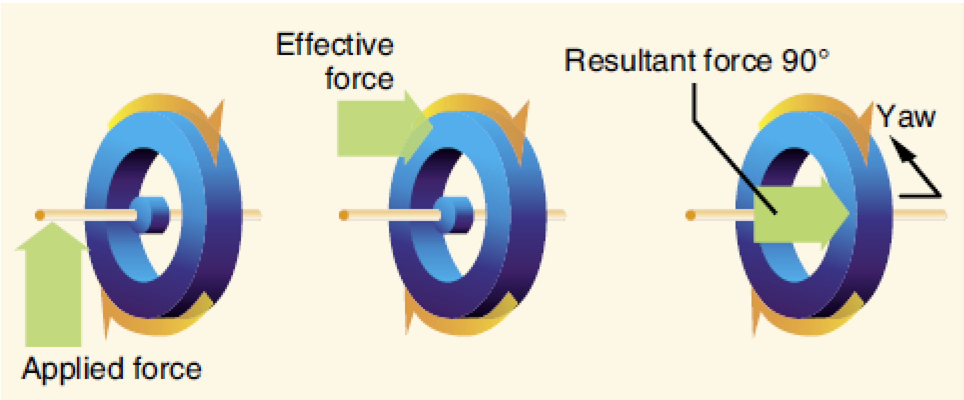

Figure 6.1: Gyroscopic precession (Pilot School, 2006).

The propeller pylon structure will be designed for gyroscopic loads resulting from maximum continuous r.p.m. (CS-22, 2003: 1-C-6).

The gyroscopic force (F_{gyro}) is determined with Equation 6.1 (Zaic, 1952: 50). This equation is in the Imperial units.

$$F_{gyro} = 0.00043 \times \frac{W \times N \times V_{\infty} \times r^2}{X \times R} \qquad (6.1)$$

With	W	=	Mass of the propeller in pounds (lbs).
	N	=	Propeller rpm.
	V_{∞}	=	Speed of flight (MPH).
	r	=	Propeller diameter (ft).
	X	=	Distance of propeller from the C/G of the glider (ft).
	R	=	Turn radius (ft).

The turn radius in Equations 6.2 and 6.3 (Anderson, 2001) depends only on flight speed V_{∞} and the load factor n.

Level turn
$$R = \frac{V^2_{\infty}}{g\sqrt{n^2 - 1}} \qquad (6.2)$$

For the pull up the turn radius, R was calculated at the load factor, n=1.15, and the velocity, V_{∞}=164 km/h.

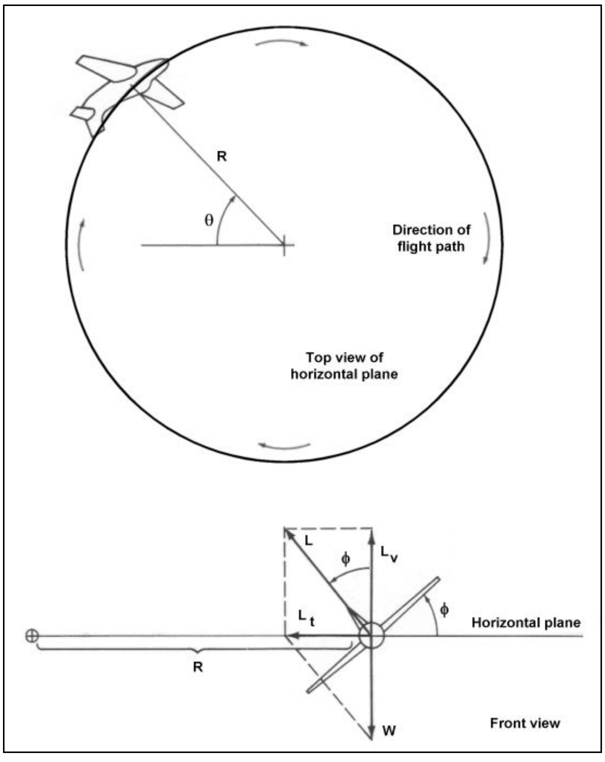

Figure 6.2: The level turns (Anderson, 2001).

Pull-up $$R = \frac{V^2_\infty}{g(n-1)} \quad (6.3)$$

For the pull up the turn radius, R was calculated at the load factor, n=5, and the velocity, V_∞=164 km/h.

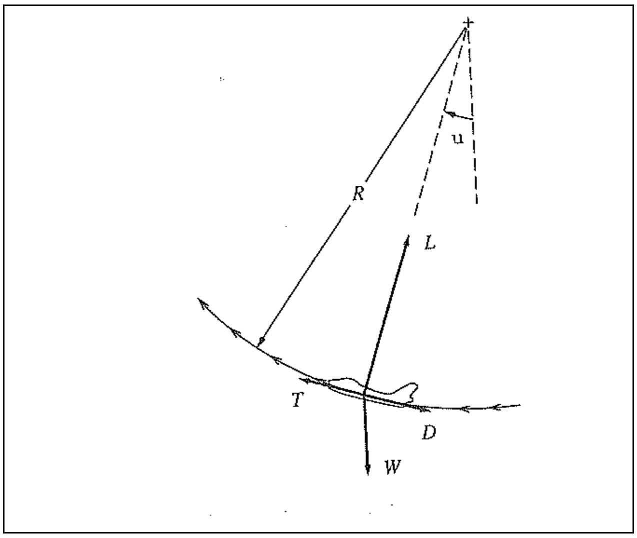

Figure 6.3: The pull up maneuver (Anderson, 2001).

During the flight the weight of JS1 sailplane will change (decrease) due to the consumption of fuel and dumping of the water in the wing. This change will lead to change the location of the JS1 sailplane center of gravity (C.G).

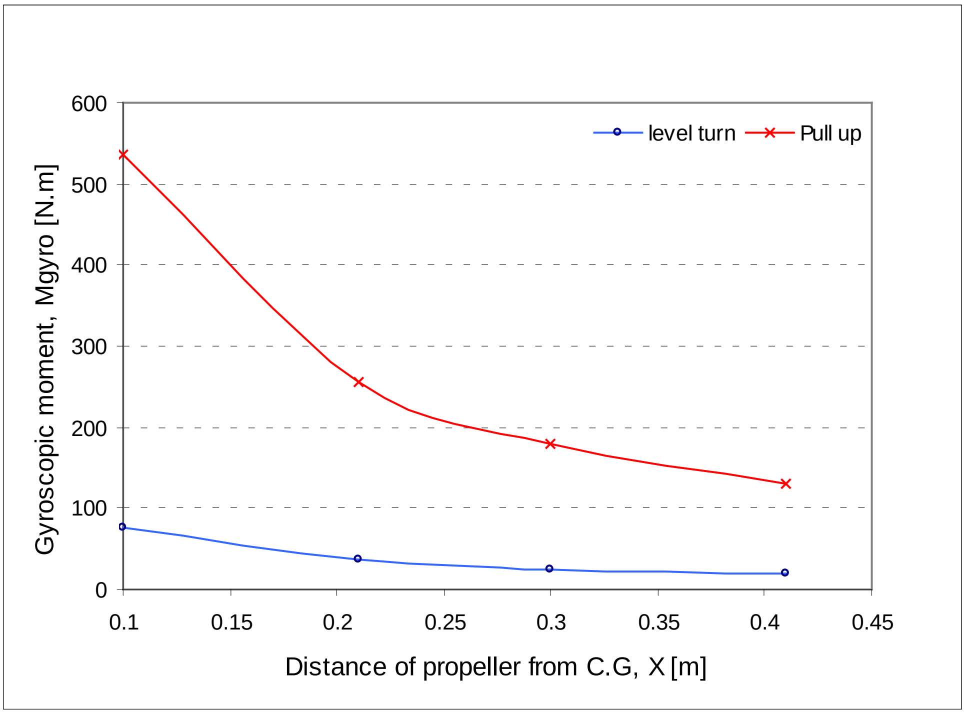

Figure 6.4: Gyroscopic moment vs. propeller distance from the JS1 center of gravity.

From Figure 6.4 it can see that M_{gyro} is increasing when X decreasing. The maximum value of M_{gyro}=535.69 N.m (at pull-up maneuver) will act on the two legs of the propeller pylon. To determine the average shear stress on the propeller pylon, Equation 6.4 will be used, with T=0.5 M_{gyro}.

$$\tau_{avg} = \frac{T}{2tA_m} \tag{6.4}$$

The shear flow (q) is the product of the tube's thickness and the average shear stress.

$$q = \tau_{avr} t \tag{6.5}$$

Because the pylon cross sectional area is change along the propeller pylon, the values of shear flow and average shear stress will also change. Figure 6.5 shows the distance of each station from the pylon hinge point. For simplicity and as a first order approximation, the cross-sectional area was taken to be rectangular.

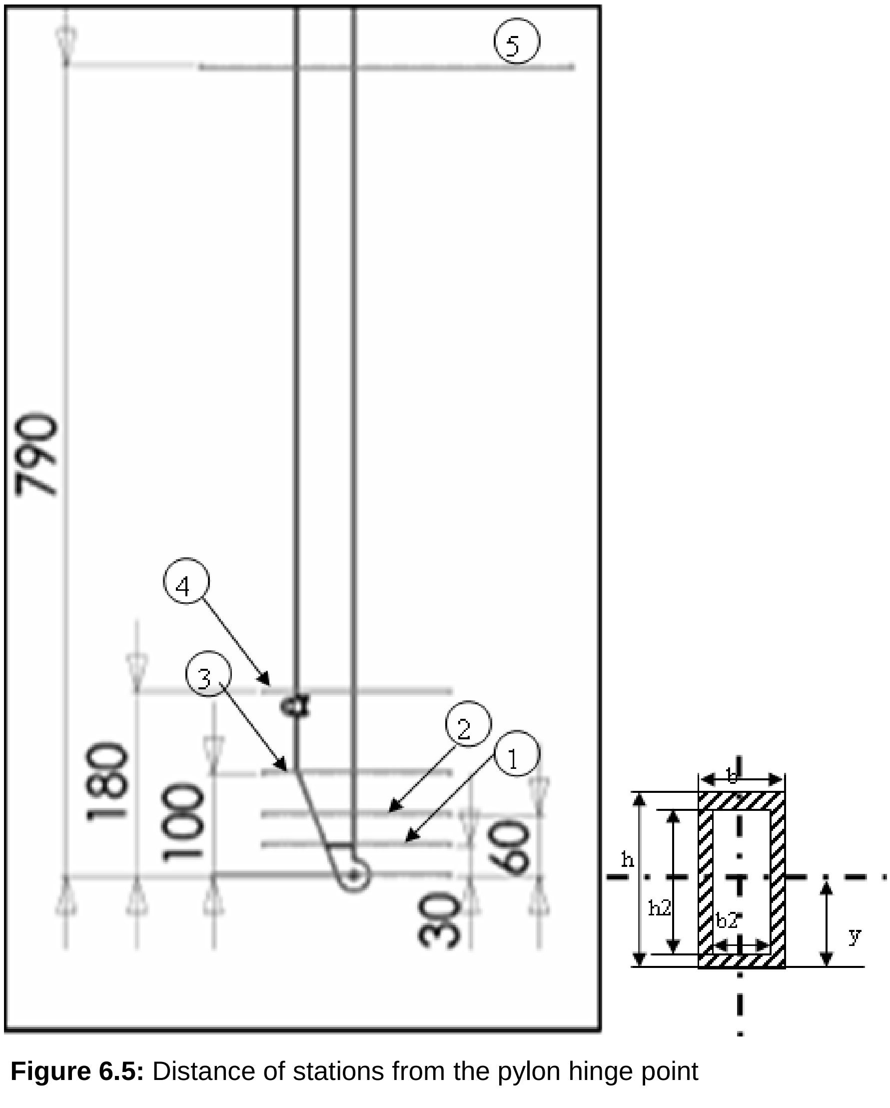

Figure 6.5: Distance of stations from the pylon hinge point

Table 6.1: Shear flow and average shear stress results

Flight conditions		Level turn		Pull up	
Section	dist.[mm]	q[N/mm]	τ_{avg} [MPa]	q[N/mm]	τ_{avg} [MPa]
1	30	29.34	9.78	206.67	68.89
2	60	20.12	6.71	141.72	47.24
3	100	22.37	7.46	157.56	52.52
4	180	21.51	7.17	151.50	50.50
5	790	21.51	7.17	151.50	50.50

From Table 6.1 the maximum value of the shear flow q= 206.67 N/mm is at station 1 of the propeller pylon. The detailed calculation steps for the shear flow are given in Appendix A, section A.3.

6.2 Belt design calculations

In this section the selection of a belt system for the JS1 self-launching system will be developed. The belt system will transfer the power from the engine selected in Chapter 3 to the propeller designed in Chapter 4.

The spreadsheet program of MITCalc® will be used for this design. This spreadsheet solves the following tasks:

- Selection of the type of belt with a suitable output power
- Selection of an optimum transmission alternative in view of power, geometry and weight
- Calculation of all necessary strength and geometrical parameters
- Calculation of power parameters and axis loads

All the inputs necessary to start the design calculations has been determined in Chapters 3 and 4, and they are listed in Table 6.2.

Table 6.2: Belt system design parameters

Variable	value
Transferred power	39 KW
Pulley speed for driving wheel	6250 RPM
Pulley speed for driven wheel	2083 RPM
Type of driving machine	Heavy shocks
Type of driven machine	Higher duty
Daily loading of the transmission	Less than 8 hours

The design parameter in Table 6.2 was used and the belt system design results are given in Tables 6.3 and 6.4.

Table 6.3: Belt system design results

Variables	value
Selection of a synchronous belt	8M HTD (synchroforce CXP III)
Width of the synchronous belt, B	40mm
Number of belt teeth	360
Belt length	2896mm
Effective pull force, F_U	1800 N
Initial belt tension, F_O	1746 N
Force in forced belt strand, F_1	2700 N
Force in unloaded belt strand, F_2	900N
Total radial force on the shaft, F_r	3488 N

The guide pulleys will be used to avoid any interference between the belt and the pylon. The axis distance between the driving pulley and driven pulley is 1230.45mm.

“The radial clearance between the blade tips and the sailplane structure must be at least 25mm” (CS, 2003: 1-E-1). The distance between the propeller tips and the fuselage is 60mm. this value does not exceed the CS-22 requirements.

Table 6.4: Pulleys design results.

	Driving Pulley[1]	Guide pulley[2]	Driven Pulley[3]	Guide Pulley[4]
Number of pulley teeth, z	26	20	80	20
Pulley pitch diameter, Dp	66.208 mm	50.93 mm	203.718 mm	50.93 mm
The angle of wrapping, β^o	149.37^o	23.26^o	164.11^o	23.26^o

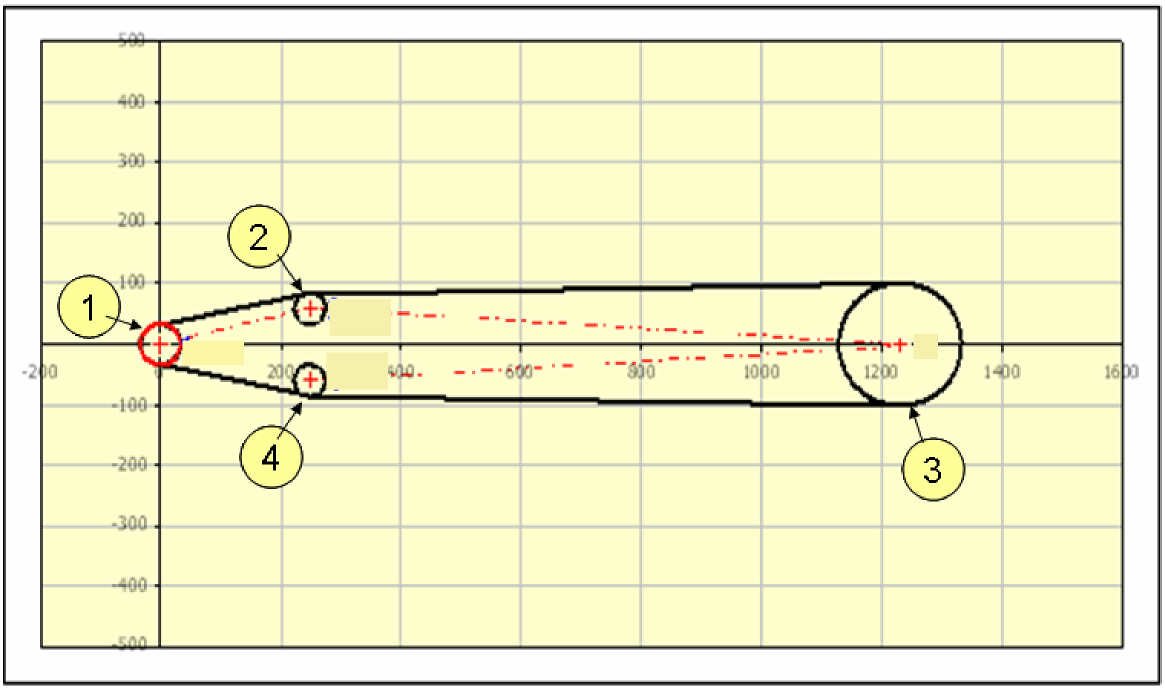

Figure 6.6: Dimensions of the pulleys (Top view).

6.3 Bending moment and shear force diagrams for the pylon

A propeller pylon can be approached with a forces diagram as indicated in Figure 6.7. Force (D sin θ_0+Wcos θ_0) represent the combination force of the drag and weight of the system. Forces R_1 and R_2 are the retraction forces at the supporting points of the pylon. F_1 and F_2 are the equivalent loadings on the axis of the pylon. The support reactions have been calculated in Chapter 5, and the shear and moment diagrams are shown in Figure 6.8 and Figure 6.9 respectively. From Figure 6.8 the maximum shear force= 1342N and maximum bending moment= 192N.m.

Figure 6.7: The side view of propeller pylon.

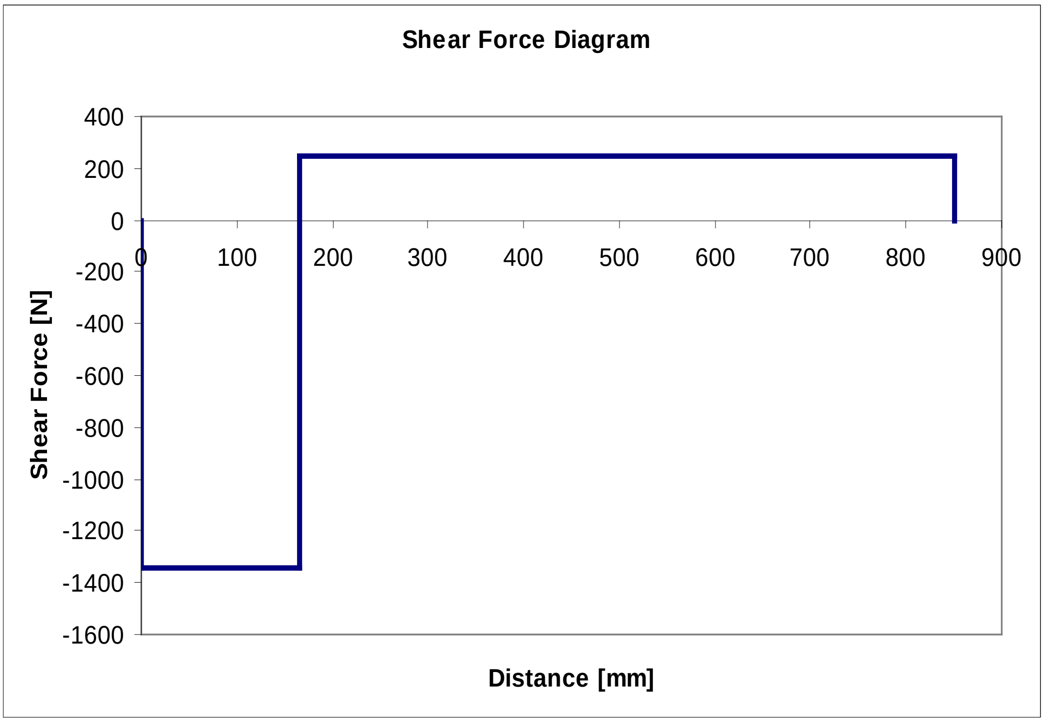

Figure 6.8: The shear force diagrams.

The maximum stress at each station on the propeller pylon was calculated using Equation 6.6.

$$\sigma_{\max} = \frac{M_{\max} y}{I} \tag{6.6}$$

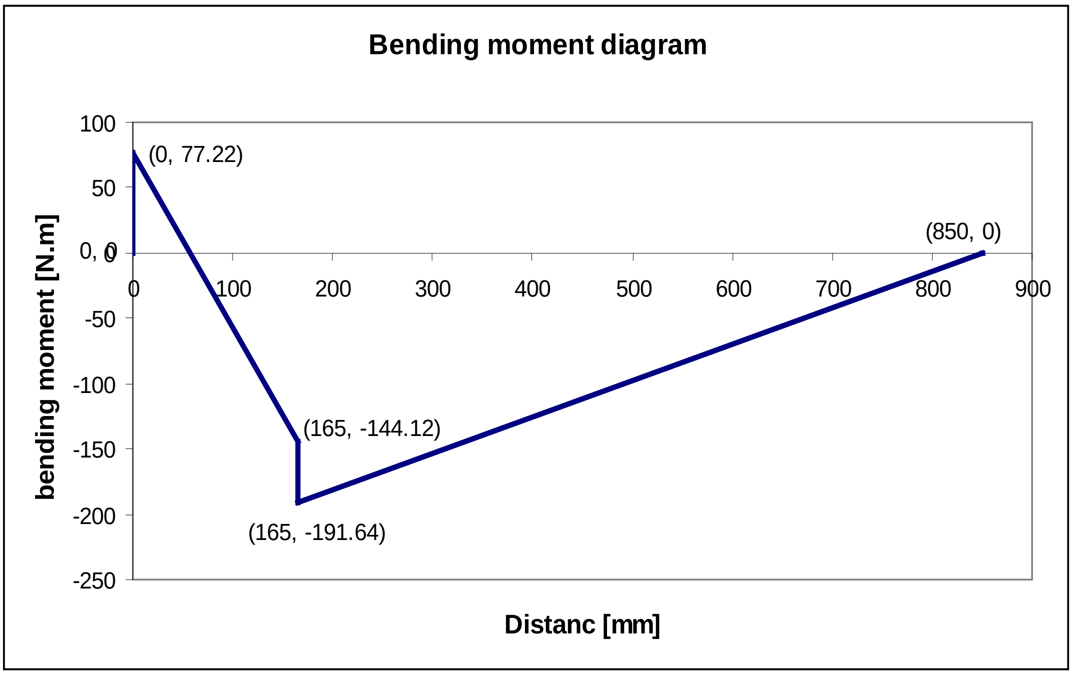

Figure 6.9: The bending moment diagrams.

The results of the calculations of bending stress for a pylon are given in Figure 6.10.

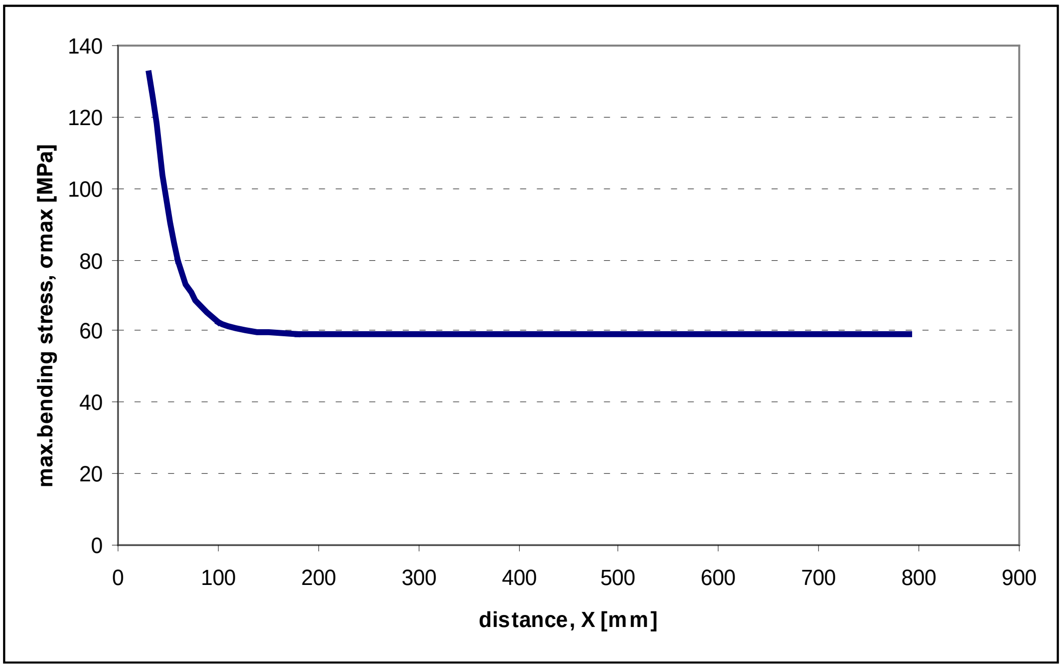

Figure 6.10: The bending stress.

The maximum stress of $\sigma_{\max}$ = 131.98 MPa is at station 1 at 30mm from the pylon hinge point. The propeller pylon is manufactured from carbon fiber, with a yield stress of 400MPa. This gives a minimum safety factor of S.F=3. The detailed calculation steps for the bending stress for the propeller pylon are given in Appendix A, section A.4.

6.4 Euler knuckle

For all the rods that are subjected to axial forces the maximum allowed stress is determined in the rod. This includes the stress in rods BC, CD, DE and CE. The critical stress σ_{cr} in each rod is determined by Equations 6.7 and 6.8 (Hibbeler, 2008: 699).

$$\sigma_{cr} = \frac{\pi^2 E}{\left(L/r\right)^2} \tag{6.7}$$

$$r = \sqrt{\frac{I}{A}} \tag{6.8}$$

With

σ_{cr}	=	critical stress in rod [MPa].
E	=	elastic modulus of material [MPa].

L	=	length of rod [mm].
r	=	radius of gyration [mm].
I	=	moment of inertia of the rod [mm^4].
A	=	cross-sectional area [mm^2].

The Euler formula is valid only for critical stress σ_{cr} below the materials yield point σ_y (Hibbeler, 2008: 700). For the ASI 4130 steel the yield stress is σ_y = 435MPa [E = 205GPa], and the smallest acceptable slenderness ratio L/r = 68. In Figure 6.11 the slenderness ratio of rods BC, CD, DE and CE are less than 68. In this case the critical stress for the rods will be 435 MPa.

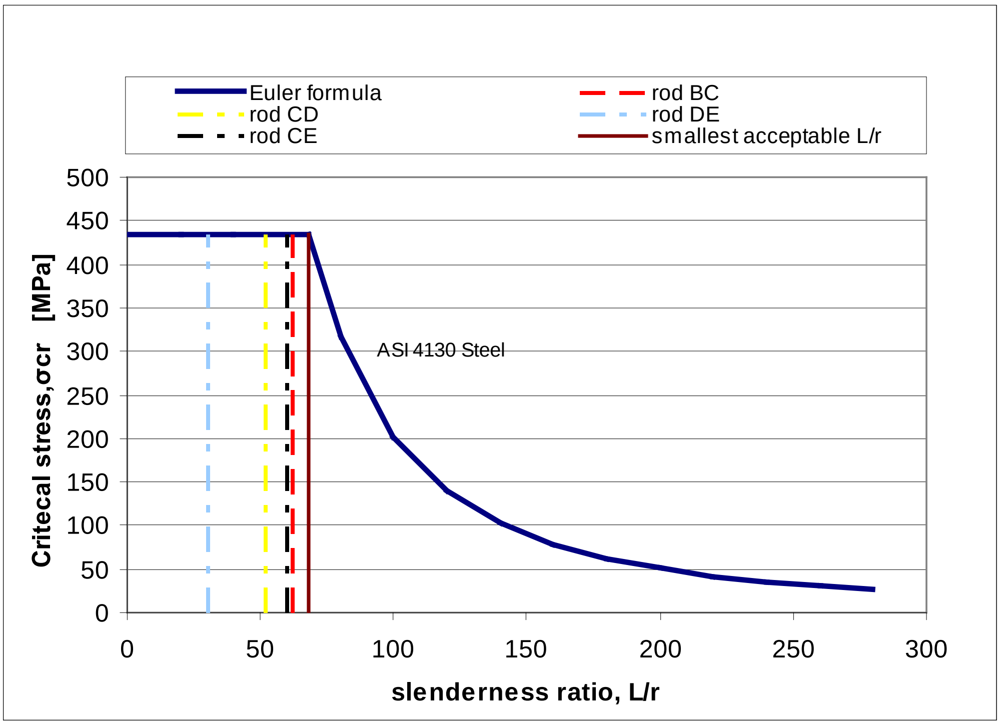

Figure 6.11: Critical stress vs. the slenderness ratio for ASI 4130 steel.

The calculations of the values in Figure 6.11 can be seen in Appendix A, section A.5.

6.5 Lugs calculations

In this section the lugs at Q, E, B and A (Figure 6.12) are designed. Empirical data from Appendices D1 to D3 is used, along with the method of application as described in (Young, 1990).

The results of calculations are provided in Table 6.6. These results led to the decisions to choose wall thicknesses of 3mm and to use bolts with a diameter of 8mm. The reasons for these decisions are:

- Deflections of connecting pieces are restricted with thicker walls
- It was decided to use standard bolts that can be bought from the shelves as far as possible
- The choice of the bolt saved the manufacturing of a special bolt for the system

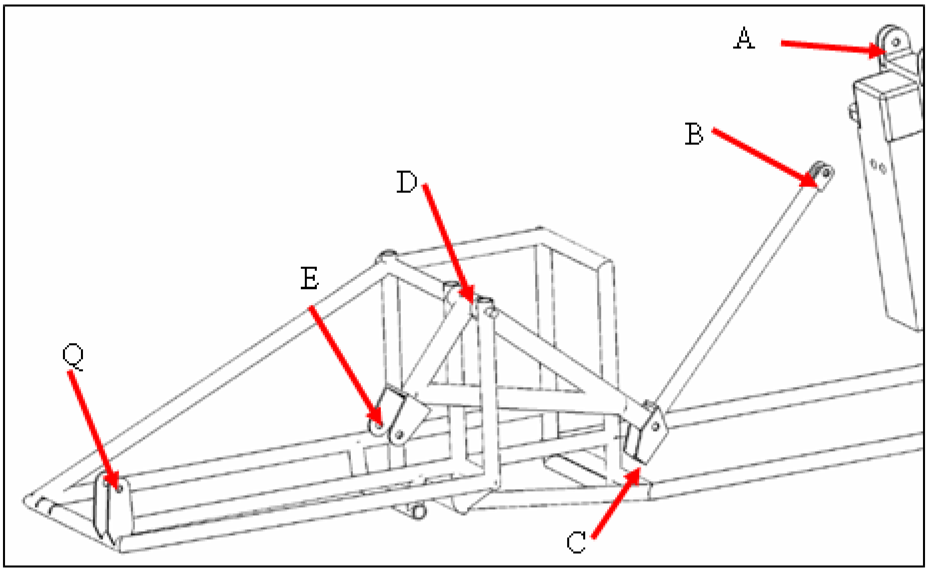

Figure 6.12: Frame with folding mechanism.

Table 6.5: Lugs calculations results.

	P_{tu} (N)		P_{br} (N)		P_{tru} (N)		P_{ob} (N)		P_{um} (N)	
	Ultimate	Max	Ultimate	Max	Ultimate	Max	Ultimate	Max	Ultimate	Max
E	45989	335	22512	335	22512	2847	21598	2493	9682	2847
B	15758	1847	17688	1847	13346	874	14163	1830	4636	874
Q	59697	170	33768	170	33768	2172	17847	2493	7596	2172
A	39798	3229	28944	3229	27014	1543	19500	2941	12563	1543

The calculation of the values in Table 6.5 can be seen in Appendix A section A.6.

6.6 Frame

The final design analysis of the frame was not performed as part of this study. This will be performed in a follow up project which will perform the detail design of the complete system.

6.7 Summary

This Chapter comprised the design calculation for the system. The gyroscopic force and then the gyroscopic moment were calculated at the level turn and pull-up maneuver. The shear flow and average shear stress on the propeller pylon were calculated. The design of the belt system for the self-launching glider was performed. The bending stress for the pylon was calculated. The maximum allowable stress for the rods of the retraction system was determined. Finally the lugs calculations for the system were done.

7. PERFORMANCE ANALYSIS

7.1 Introduction

In this chapter the overall performance of the JS1 glider with the engine system will be discussed. The performance calculations are the rate of climb, the flight range and the take-off distance. The performance calculated was compared with the performance of other self-launching systems.

7.2 Rate of climb Performance

The rate of climb performance for a JS1 glider with the self-launching system was calculated at different altitudes and take-off masses. The same method previously described in Chapter 3 was used to calculate the rate of climb. Figure 7.1 shows the rate of climb for the JS1 compared to the DG-808C for two masses. The JS1 clearly has better rate of climb performance through the altitude range. The maximum rate of climb obtained is 4.26m/s, with a maximum weight of 600Kg.

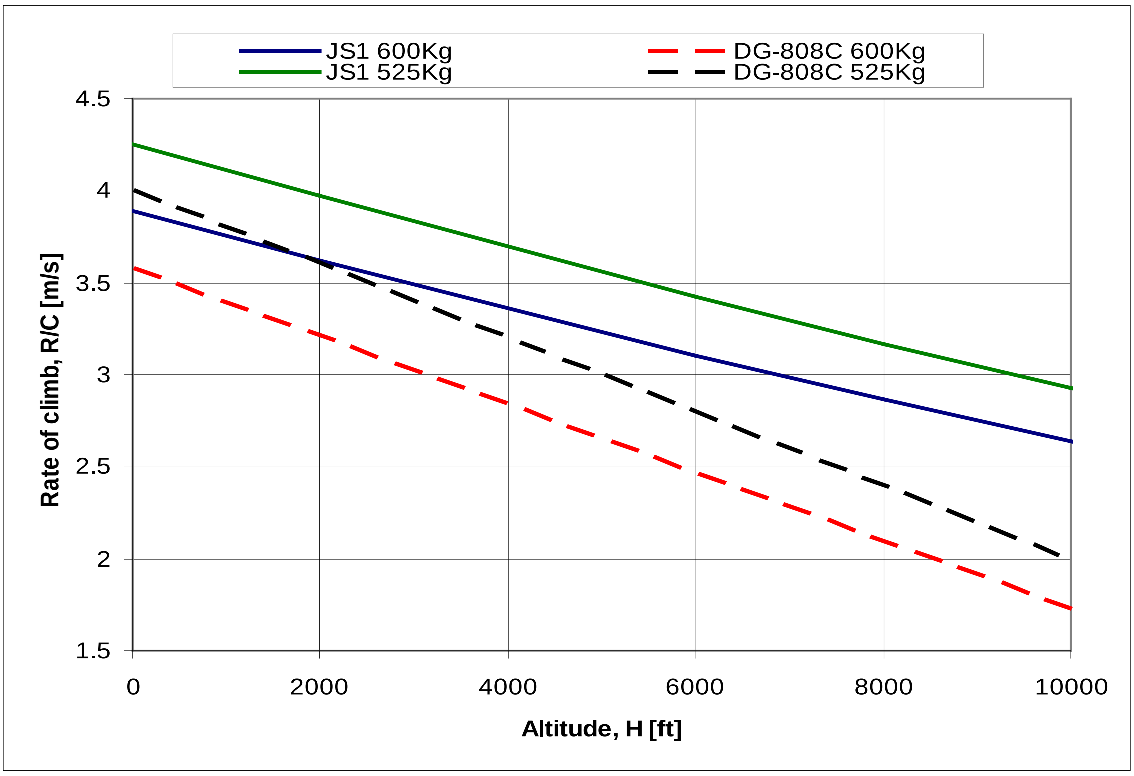

Figure 7.1: Rate of climb performance comparison between the JS1 and DG-808C

7.3 Range

The calculation of the range performance is a very important to estimate the capacity of fuel that we need it of the JS1 self-launching glider. The total fuel consumed during the mission is that consumed from the moment the engines are turned on at the airport to the moment they are shut down at the end of the flight. Between these moments there are different missions. Figure 7.2 shows the simple profile mission. It starts at the point 0, when the engine is turned on. The take-off segment is denoted by the line segment 0-1. The climb to cruise altitude was donated by the line 1-2. Segment 2-3 represent the cruise. Segment 3-4 refers to the descent. And finally segment 4-5 represents landing.

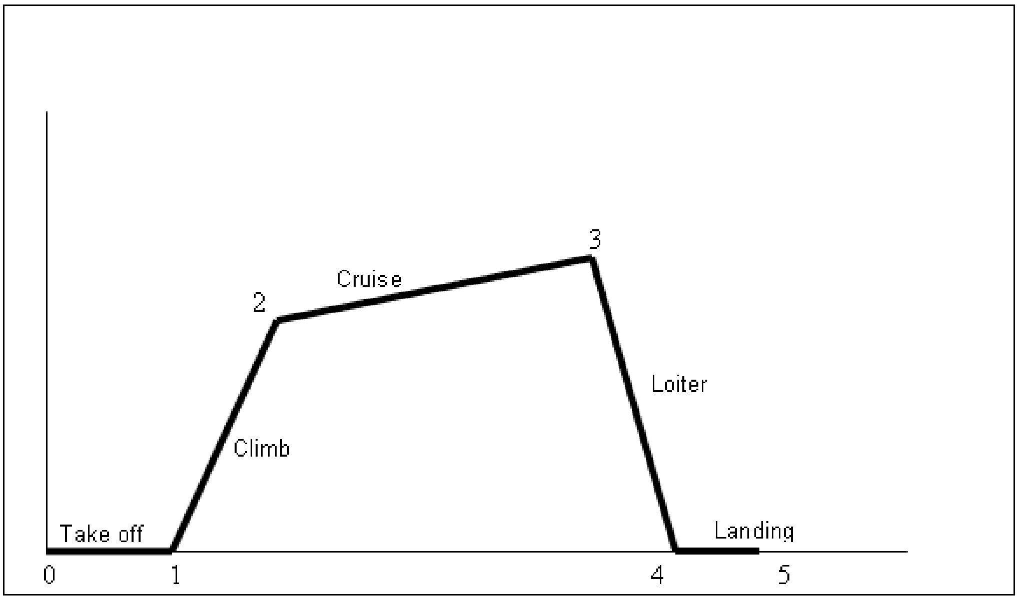

Figure 7.2: Mission profile for a simple cruise.

The use of the self-launching engine in mainly to allow unassisted take-off. There is however sometimes a need for the glider to be used in a cruise fashion to ferry the glider to another destination.

In this section the fuel requirements of the system will be determined. The following was calculated.

1. Range take-off only to 500m AGL.
2. Ranges take-off to 300m AGL +200km cruise.

The fuel consumption was calculated as follows:

Equation 7.1 shows the value of the ratio of the fuel weight, W_f to the ratio of the JS1 gross weight, W_0. The 6% allowance was made for the reserve and trapped fuel.

$$\frac{W_f}{W_0} = 1.06\left(1 - \frac{W_5}{W_0}\right) \tag{7.1}$$

Where the value of $\frac{W_5}{W_0}$, is the ratio of the sailplane weight at end of the mission to the initial gross weight.

$$\frac{W_5}{W_0} = \frac{W_1}{W_0}\frac{W_2}{W_1}\frac{W_3}{W_2}\frac{W_4}{W_3}\frac{W_5}{W_4} \tag{7.2}$$

The consumption of fuel for the take-off segment is 0.97. These values were obtained from the historical data (Raymer, 1989:16). For the cruise mission, the Breguet range equation (Anderson, 2001: 401) was used.

$$R = \frac{\eta_{\mathrm{Pr}}}{c}.\frac{L}{D}.\ln\frac{W_2}{W_3} \tag{7.3}$$

The propeller efficiency, η_{pr} was obtained in Chapter 4 as 81%, form Chapter 3 the value of the maximum lift to drag ratio was used, and the specific fuel consumption, c is $0.505\, lb/hp.h$.

The required fuel was calculated as follows:

1. Size fuel for take-off to 500m: 0.099 gallons (0.38 litres).
2. Size fuel of take-off 300m+ 200km cruise: 5.7 gallons (21.7 litres).

The maximum fuel tank size is thus: 5.7 gallons (21.7 litres) in mission 2.

7.4 Take-off distance

The take-off distance for the JS1 self-launching glider was calculated. The same method previously described in Chapter 3 was used to calculate the take-off distance. The take-off distance to 15m obstacle for the JS1 with the full up weight is 321m. This value is clearly far less than the specified take-off distance of 500m as stated in CS-22 requirements.

7.5 Summary

In this chapter the performance analysis for the JS1 self-launching glider was calculated. The rate of climb performance for the JS1 glider was obtained and compared to the DG-808C self-launching glider. The take-off distance was calculated and the fuel tank capacity was calculated using the Breguet range equation.

8. CONCLUSIONS AND RECOMMENDATIONS

8.1 Conclusions

The conclusions of the study are as follows:

- The final preliminary design of a self-launching system for the JS1 glider meets all the requirements and restrictions that were set out initially.

- The JS1 self-launching system in comparison to the DG-808C self-launching glider shows better performance. Calculations show a maximum rate of climb of 4.26m/s under ISA conditions with maximum weight (600 kg).

- The aerodynamic geometry for the propeller blade was designed with the use of numerical methods.

- The retraction mechanism for the system was designed with the parametric spreadsheet modeling method.

- The parametric spreadsheet modeling method allows real time simulation of control kinematics with the ability to make quick and easy parametric changes to the retraction system at any stage of the design.

- The optimizing of the retraction mechanism made provision for the minimum forces required during extracting and retracting.

- The retraction system was designed in such a way that the hinge point of the propeller pylon was in front of the belt to ensure the belt contract and relax during the folding in and out of the system.

- The dimensions of the frame deliver a good interface between the frame, installation and engine. Adequate space was also left for the connection of the engine mounting piece to the frame.

8.2 Recommendations for further studies

For future improvements and studies the following recommendations can be considered:

- For the mounting of the engine to the frame standard engine mounting pieces should be bought from the manufacturer to minimize engine vibrations to the body.

- Because the system will be installed in a glider and mass of the glider always plays a vital role in the optimal performance of the glider, the mass of the rods, frame and propeller must be minimized as much as possible.

- The deflection of point Q (Figure 6.12) must be calculated using a finite element method to determine an accurate deflection value.

- The detailed structural analysis for the propeller pylon must be performed.

- The shape of the propeller pylon must be a low drag shape to optimize the performance of the glider by minimizing the drag of the JS1 self-launching glider.

- The ground test of the total system before the installation of the system in the glider must be performed.

- A suitable fuel tank must be designed according to the CS-22 specifications.

- The restraining cable that connect between the rear of the engine box and the rear of the propeller pylon must use. Because this cable restrains the pylon in case of a sudden stopping of the glider.

REFERENCES

Alexander Schleicher, 2003, ASH 26 specifications, Poppenhausen, Germany, viewed 11 November 2007, <http://www.alexander-schleicher.de/index_e.htm>

Anderson, J.D., 2001. Aircraft performance and design, McGraw-Hill, Singapore

Certification Specifications, 2003, CS-22 for sailplanes and powered sailplanes, European Aviation Safety Agency, German

DG Flugzeugbau GmbH, 2008, DG Company, German, viewed 6 September 2007, <http://www.dg-flugzeugbau.de/buying-motorglider-e.html>

Hepperle, M. (Martin.Hepperle@dlr.de), 2009, Questions on design point for Clark-Y Aerofoil: [Email to:] Nogoud, Y.A. (yasserh77@gmail.com).

Hibbeler, R, C, 2008, Mechanics of Materials, 7th edition, Prentice Hall, Singapore

Jonker, A, S. 2006, PARAMETRIC LINK DESIGN USING SPREADSHEETS, SACAM, Cape Town, 16-18 January 2006, South Africa.

Jonkersailplane, 2007, JS1 specifications, Potchefstroom, South Africa, viewed 1 September 2007, <http://www.jonkersailplanes.co.za/specifications.htm>

Juvinall, Robert C, Marshek, Kurt M, 2000, Fundamentals of Machine Component Design, 3rd edition, John Wiley & Sons, Inc, New York

Larrabe E E, 1984, Minimum induced loss propeller design spreadsheet and theory, Royal aeronauticalsociety,UK,viewed,15May2008,<http://www.raes.org.uk/cmspage.asp?cmsitemid=SG_hum_pow_download>.

McCormick, B.W, 1979, Aerodynamics, Aeronautics and Flight Mechanics, 1st edition, Jr, Wiley & Sons, Inc, New York

Motion Systems Corporation, 2009, Ball Drive Actuators, Eatontown, New Jersey, USA, viewed 2 March 2009, <http://motionsystem.thomasnet.com/Asset/85199_2.pdf>

Pilot School, 2006, gyroscopic effect, USA, viewed, 17 February 2009,<http://www.free-online-private-pilot-ground-school.com/propeller aerodynamics.html>

Raymer, D, P, 1989, Aircraft Design: A Conceptual Approach, 2^{ed} edition, American Institute of Aeronautics and Astronautics, Washington.

Roskam, J. and Lan, C.E., 2003. Airplane Aerodynamics and Performance, 3rd printing, DAR corporation, Kansas

Shigley, Joseph E. Charles R. Mischke, 2003, Mechanical Engineering Design, sixth edition, McGraw-Hill Book Company, New York.

Silverstien, A, 1935, Scale effect on Clark Y Aerofoil characteristics from N.A.C.A full scale wind-tunnel testes, NACA central, Cranfield, UK, viewed 13 August 2009, < http://naca.central.cranfield.ac.uk/reports/1935/naca-report-502.bdf>

Visser, HP 2006, New Propeller for an unmanned Aerial Vehicle, B.sc final report, University of Pretoria, Pretoria, South Africa.

Wallin, A. W, 1978, “Efficiency of synchronous Belts and V-Belts,” proc. Nat. conf. Power Transmission, vol. 5, Illinois Institute of Technology, Chicago, 7-9 November 1978, USA

Weick, F.E., 1930. , Aircraft Propeller Design, 1st edition, McGraw-Hill, New York.

Young Niu M.C, 1990, Airframe structural design, 5th edition, Commilit press ltd, Hong Kong.

Zaic, F, 1952. Model Aeronautic Year Book 1951-52, Model Aeronautic Publications, New York.

APPENDIX A: CALCULATION EXAMPLES.

A.1 Power required and propeller sizing calculations

1-Take-off constrain	
S_a+S_g [m]	310
V $_{stall}$ @ Cl=1.4	24.76
R [m]	434.82
ρ@ S.L [kg/m^3]	1.225
W/S [N/m^2]	525.54
S_g * (T/W)	37.80
θ_{OB} [rad]	0.26
θ_{OB} [deg]	15.09
S_a[m]	113.22
S_g[m]	196.78
T/W	0.19
V[m/s]	19.93
P_R [KW]	22.53
P [KW]	37.55
P[hP]	51.03

2-Rate of climb constrain	
AR	28.93
e	1
L/D	50
Propeller efficiency, η	0.6
max.mass [kg]	600
ρ @S.L [kg/m^3]	1.225
W/S [N/m^2]	525.54
K	0.011
C_{do}	0.009
R/C [m/s]	3
(η.P)/W	3.54
PR [KW]	34.72
P [hP]	47.18

W/P	25.92

Propeller sizing	
D [in]	59.36
D [m]	1.51
$V_{tip\ static}$ [m/s]	164.47
V max [m/s]	73
$V_{tip\ helical}$ [m/s]	179.94
a @ S.L [m/s]	340
below the sonic speed	

A.2 Retraction mechanism calculation

Prop Pylon		super arm
θ_{ref}	0.000	0.000
θ_1	20.000	0.349
θ_0	63.535	1.109
r1	175.43	
r2	850.000	
	X	Y
OFFSET	0.000	0.000
in	78.181	157.046
mid	0.000	0.000
out	95.708	844.595
Coordinates		
x	y	R
78.181	157.046	175.430
0.000	0.000	850.000
0.000	0.000	
95.708	844.595	

Link B		Link	Calculated values		
r1	175.430		l	348.658	
r2	318.000		θ_3	1.478	84.684
x1	348.502		θ_1	0.525	30.066
y1	-10.437		θ_2	1.139	65.250
x2	0.000		l1	275.213	
y2	0.000		l2	73.445	
xn	78.181		θ_4	0.030	1.715
yn	157.046		y3	-2.198	
Invert	1.000		x3	73.412	
Coordinates			θ_{10}	1.541	88.285
x	y	r	h	159.316	
348.502	-10.437	318.000	θ_5	1.109	116.465
78.181	157.046	0.000		-271.444	0.000

$\theta_2-\theta_4$	63.535	1.1088933
$\theta_4+\theta_1$	31.781	0.55468454
$\theta_2+\theta_4+\theta_5$	180.000	3.14159265
$\theta_{10}+\theta_4$	90.000	1.57079633

Link A		super arm
θ_{ref}	0.000	0.000
θ_1	270.000	4.712
θ_0	-121.272	-2.117
r1	155.800	
r2	265.000	
	X	Y
OFFSET	575.000	-148.000
in	494.123	-281.164
mid	575.000	-148.000
out	348.502	-10.437
Coordinates		
x	y	R
494.123	-281.164	155.800
575.000	-148.000	265.000
575.000	-148.000	
348.502	-10.437	

Actuator					
r1	155.800		l*	442.164	
r2*	506.000		θ_3*	1.003	57.463
x1	1000.000		θ_1*	0.302	17.281
y1	-270.000		θ_2*	1.837	105.256
x2*	575.000		l1*	483.159	-425.000
y2*	-148.000		l2*	-40.995	
xn	494.123		θ_4*	3.421	196.017
yn	-281.164		y3*	-136.689	
Invert	1.000		x3*	535.596	
Coordinates			$\theta_{10}*$	-1.850	-106.017
x	y	r	h*	150.310	150.310
1000.000	-270.000	506.000	θ_5*	-2.117	-121.272
494.123	-281.164	0.000		-344.900	150.310
		0.000			

θ_4	16.0165929	0.27954228
$(\theta_1)*$	17.281	0.30160677
$\theta_4-\theta_1$	-1.264	-0.02206449
$\theta_2+\theta_4+\theta_5$	180.000	3.14159265

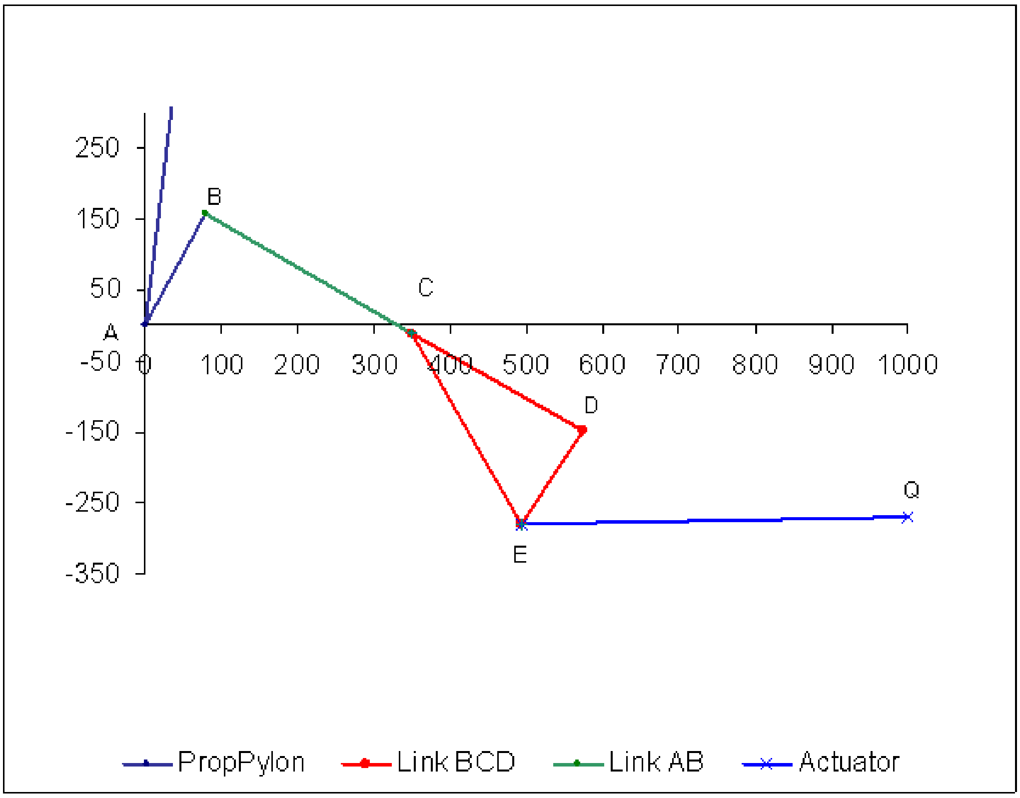

Figure A.1: Rods layout for a Retraction System.

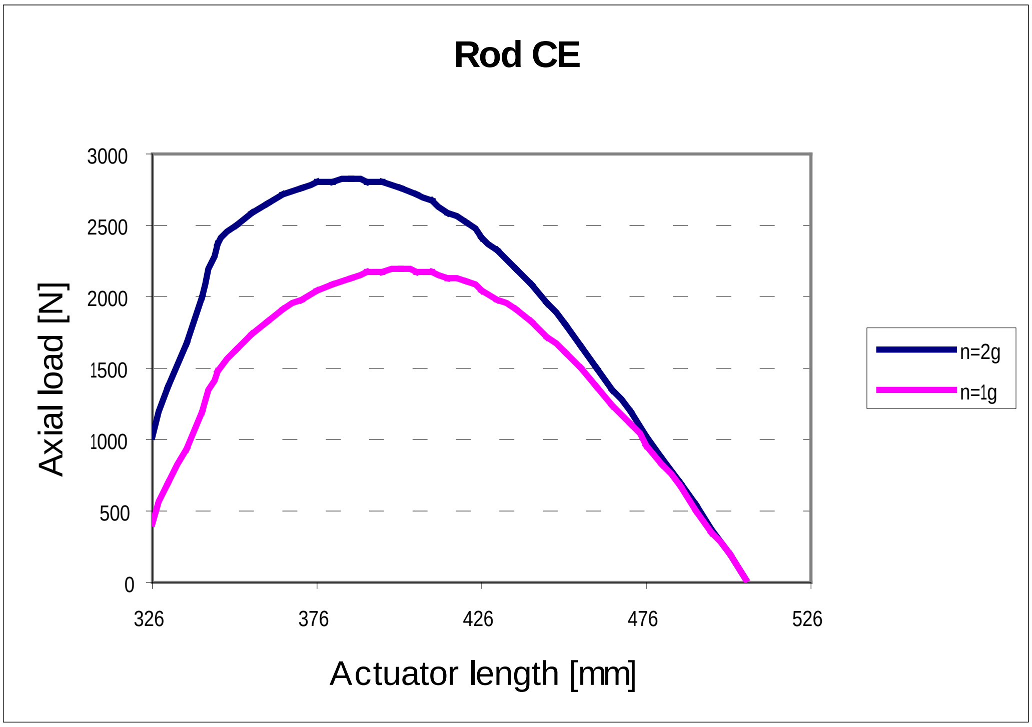

Figure A.2: Axial load vs. actuator length for rod CE.

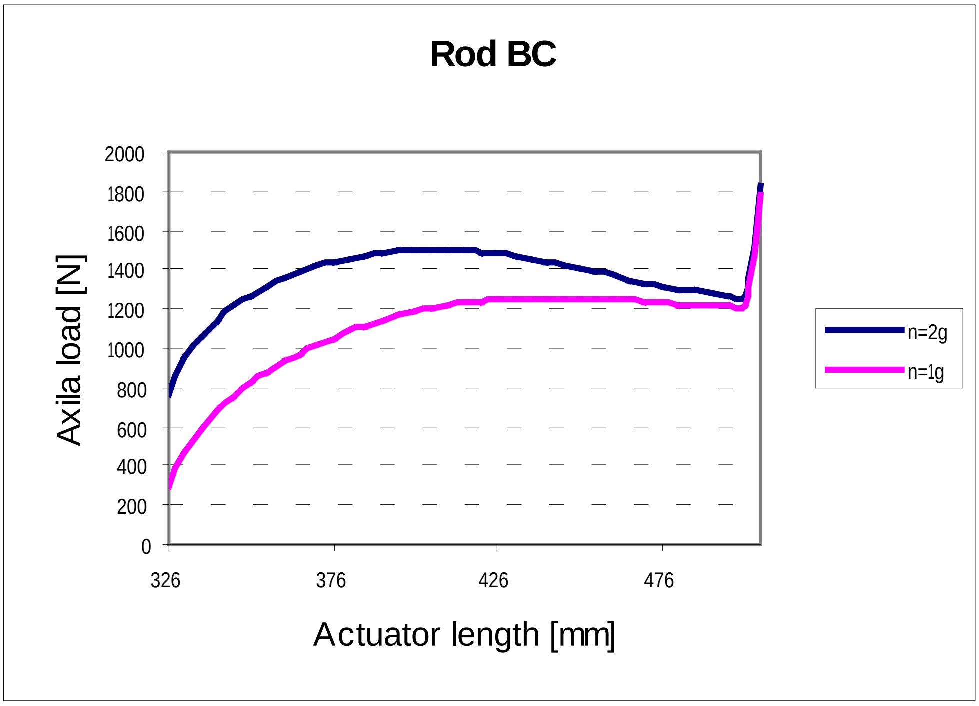

Figure A.3: Axial load vs. actuator length for rod BC.

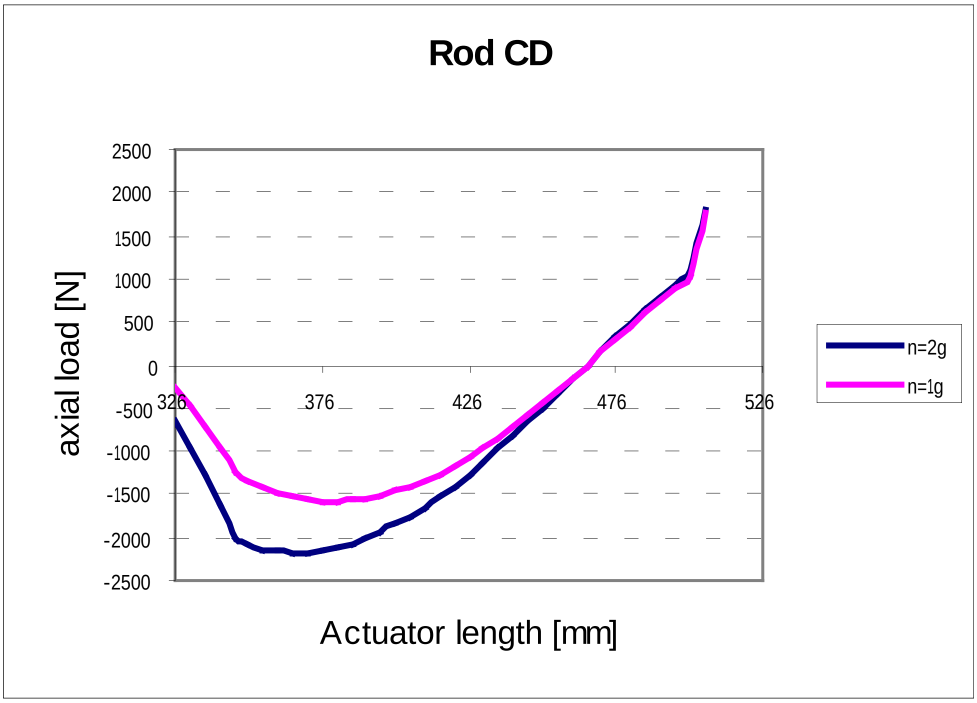

Figure A.4: Axial load vs. actuator length for rod CD.

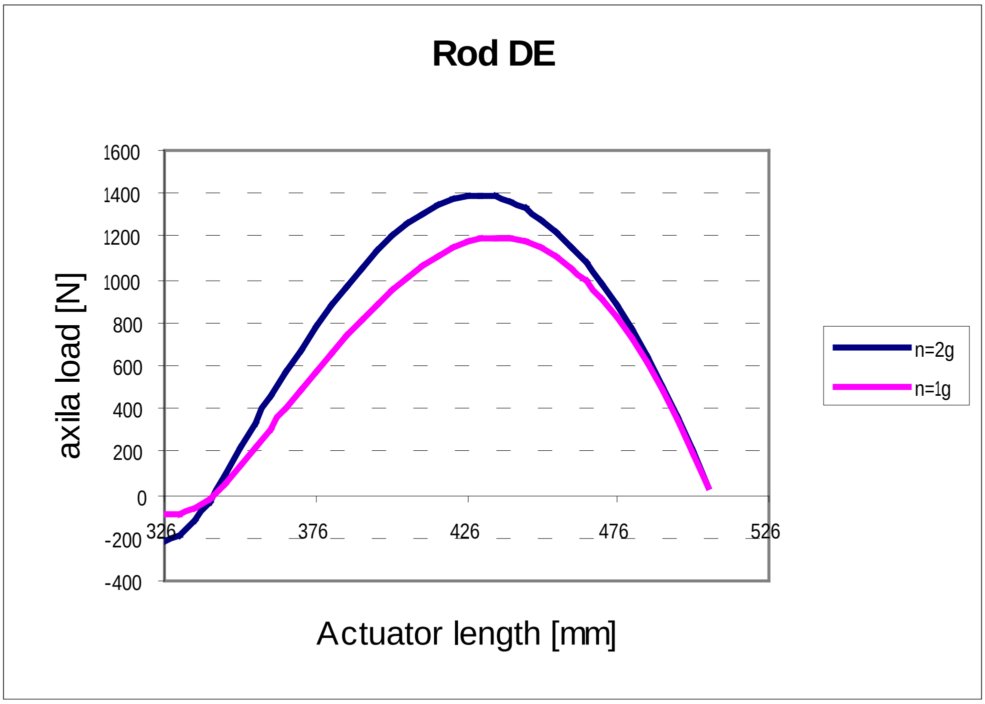

Figure A.5 Axial load vs. actuator length for rod DE.

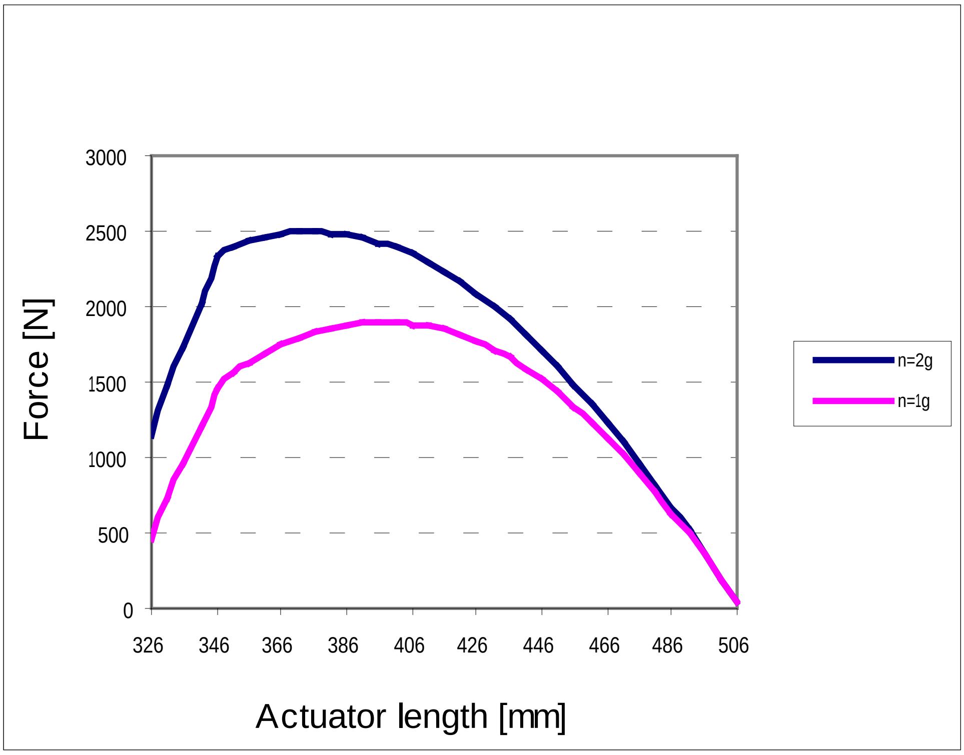

Figure A.6 Actuation load vs. actuator length for Actuator.

A.3 Gyroscopic load calculation

$$R = \frac{V^2_\infty}{g(n-1)}$$ Pull up

$$R = \frac{V^2_\infty}{g\sqrt{n^2-1}}$$ Level turn

	English units	SI units
W	22.05	10 Kg
N	2083 rpm	2083 rpm
V_∞	101.905 MPH	164 Km/h
r	2.461 ft	0.75 m
X	1.345 ft- 0.689 ft	0.41m -0.21 m
g	32.185 ft/s^2	9.81 m/s^2
n	1.15	1.15
R	1222.176 ft	372.52 m
n	5	5
R	141.675 ft	43.18 m

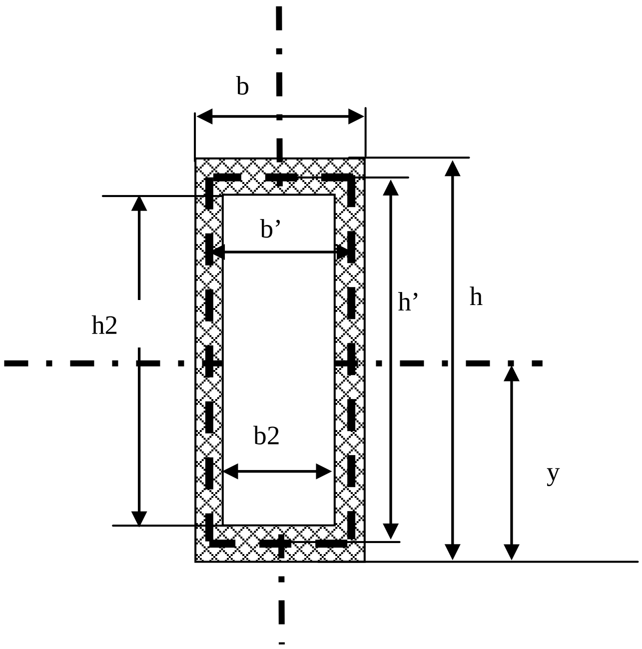

$$F_{gyro} = 0.00043 \times \frac{W \times N \times V_\infty \times r^2}{X \times R}$$

$$T = \frac{M_{gyro}}{2}$$

	Level turn			Pull up		
X[m]	F_{gyro}[N]	M_{gyro}[N.m]	T [N.m]	F_{gyro}[N]	M_{gyro}[N.m]	T [N.m]
0.41	32.98	18.55	9.27	232.28	130.66	65.33
0.3	45.07	25.35	12.68	317.45	178.56	89.28
0.21	64.38	36.22	18.11	453.49	255.09	127.55
0.1	135.21	76.05	38.03	952.34	535.69	267.84
Max	135.21	76.05	38.03	952.34	535.69	267.84

$$q = \frac{T}{2A} \qquad \tau_{avg} = \frac{q}{t}$$

Pull up

T[N.m]	b[mm]	h[mm]	t1[mm]	t2[mm]	b'[mm]	h'[mm]	Am[m^2]	q[N/m]	τ_{avg} [MPa]
267.84	30	27	3	3	27	24	0.00065	206.67	68.89
267.84	30	38	3	3	27	35	0.00095	141.72	47.24
267.84	20	53	3	3	17	50	0.00085	157.56	52.52
267.84	20	55	3	3	17	52	0.00088	151.49	50.49
267.84	20	55	3	3	17	52	0.00088	151.49	50.49

A.4 Maximum bending stress calculation

$$\sigma_{\max} = \frac{M_{\max} y}{I} \qquad I = \left[\frac{bh^3}{12} - \frac{b_2 h_2^3}{12}\right]$$

dist. [mm]	Section	b (mm)	t (mm)	h (mm)	b_2 [mm]	h_2 [mm]	I (mm^4)	y (mm)	S_y (Mpa)	σ_{max} [Mpa]	SF
30	1	30	3	27	24	21	30685.5	13.5	400	131.98	3.03
60	2	30	3	38	24	32	71644	19	400	79.56	5.02
100	3	20	3	53	14	47	127001.5	26.5	400	62.59	6.39
180	4	20	3	55	14	49	140034.5	27.5	400	58.91	6.78
790	5	20	3	55	14	49	140034.5	27.5	400	58.91	6.78

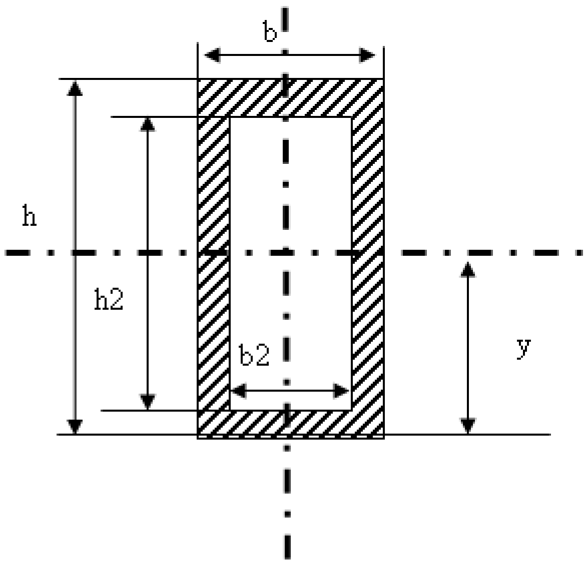

A.5 Euler knuckle

ASI 4130 Steel

Elastic modulus [GPa]	205
poisons Ratio, v	0.29
Shear modulus, G [GPa]	80
Tensile strength [MPa]	670
yield strength [MPa]	435

$$r = \sqrt{\frac{I}{A}} \qquad P_{cr} = \frac{\pi^2 EI}{L^2}$$

Max force [KN]	rod	E [Gpa]	D_o [mm]	D_i [mm]	Le [mm]	I min [mm^4]	A [mm^2]	r [mm]	L/r	σ cr [Mpa]	P cr [KN]	S.F
1.777	BC	205	21.3	16.7	318	6285.88	137.29	6.77	46.99	435	59.72	33.60
1.577	CD	205	21.3	16.7	265	6285.88	137.29	6.77	39.16	435	59.72	37.88
1.196	DE	205	21.3	16.7	155.8	6285.88	137.29	6.77	23.03	435	59.72	49.91
2.189	CE	205	21.3	16.7	307.41	6285.88	137.29	6.77	45.43	435	59.72	27.28

L/r	σ cr[Mpa]	σ Y[Mpa]
0	435	435
20	5058.17	435
40	1264.54	435
68	434.99	435
80	316.14	316.14
100	202.33	202.33
120	140.50	140.50
140	103.23	103.23
160	79.03	79.03
180	62.45	62.45
200	50.58	50.58

A.6 Lugs calculation

A.7 Fuel weight and fuel tank capacity calculations

$$\frac{W_5}{W_0} = \frac{W_1}{W_0}\frac{W_2}{W_1}\frac{W_3}{W_2}\frac{W_4}{W_3}\frac{W_5}{W_4}$$

$$R = \frac{\eta_{Pr}}{c}.\frac{L}{D}.\ln\frac{W_0}{W_1}$$

$$\frac{W_f}{W_0} = 1.06\left(1 - \frac{W_5}{W_0}\right)$$

1- Take-off 500m ALG	
W_1/W_0	1
W_2/W_1	0.9996
C [Ib/hp.h]	0.505
C [Ib*s/(ft.Ib/s)]	2.55051E-07
Take-off to [m]	500
Take-off to [ft]	1640.5
W_2/W_0	0.9996
W_f/W_0	0.0004
W_f [kg]	0.25
W_f [Ib]	0.56
Tank capacity (gal)	0.099
Tank capacity (liters)	0.38

2- Take-off to 300 AGL+ 200km cruise	
W_1/W_0	0.98
W_2/W_1	1
C [Ib/hp.h]	0.505
C [Ib*s/(ft.Ib/s)]	2.55051E-07
Rang [km]	200
Rang [ft]	656200
η	0.81
Cl/CD	50
$\ln(w_2/w_3)$	0.004
(W_3/W_2)	0.996
W_4/W_3	1
W_5/W_4	1
W_5/W_0	0.98
W_f/W_0	0.02
W_f [kg]	14.66
W_f [Ib]	32.31
Tank capacity (gal)	5.73
Tank capacity (litr)	21.69

APPENDIX B: ENGINE SPECIFICATIONS.

B.1 SOLO 2625-01 Technical Data and Operating Limitations

III. Technical data:

1.Type definition:	Type definition according to Parts list 20 00 625 01 from January 1st, 1998
2.Description:	Two cylinder in line two stroke-engine, watercooled, Breakerless twin spark ignition, Pully for belt transmission, exhaust adapted to the aircraft.
	Displacement: 625 ccm
	Bore/stroke: 76 mm / 69 mm
	Compression ratio: 9.5:1
	Reduction: According to the relation between engine/propeller pully-diameter
3.Equipment:	According to specifications specified in the parts-list
4.Mass (dry):	appr. 23 kg (without exhaust)
5.Power:	Take-off and cont. power 39 kW at 6 250 rpm
6.Fuel:	according to the limitations in the manual

IV. Operating limitations:

1.Temperature limits:

1.1. Cylinder head temperature:	Coolant temperatuere max. 115 °C

2.Permissable rpms:

2.1.Idle:	appr. 2 300 rpm
2.2.Take off & max. cont. rpm:	6 250 rpm
2.3.Max. rpm:	7 000 rpm

3.Pressure limitations:

3.1.Fuel pressure:	Fuel-pump-pressure min. 0.2 bar, max 0.4 bar

Fuel consumption:	**21,5 l/h**
Carburetor:	**1 Mikuni**
Ignition;	**Ducati, Bosch W5 AC**
Alternator;	**12 V 150 W**
Lubricant;	**1:50 Autosuper-2-stroke eng. oil**

B.2 SOLO 2625-01 Engine Detail design drawing

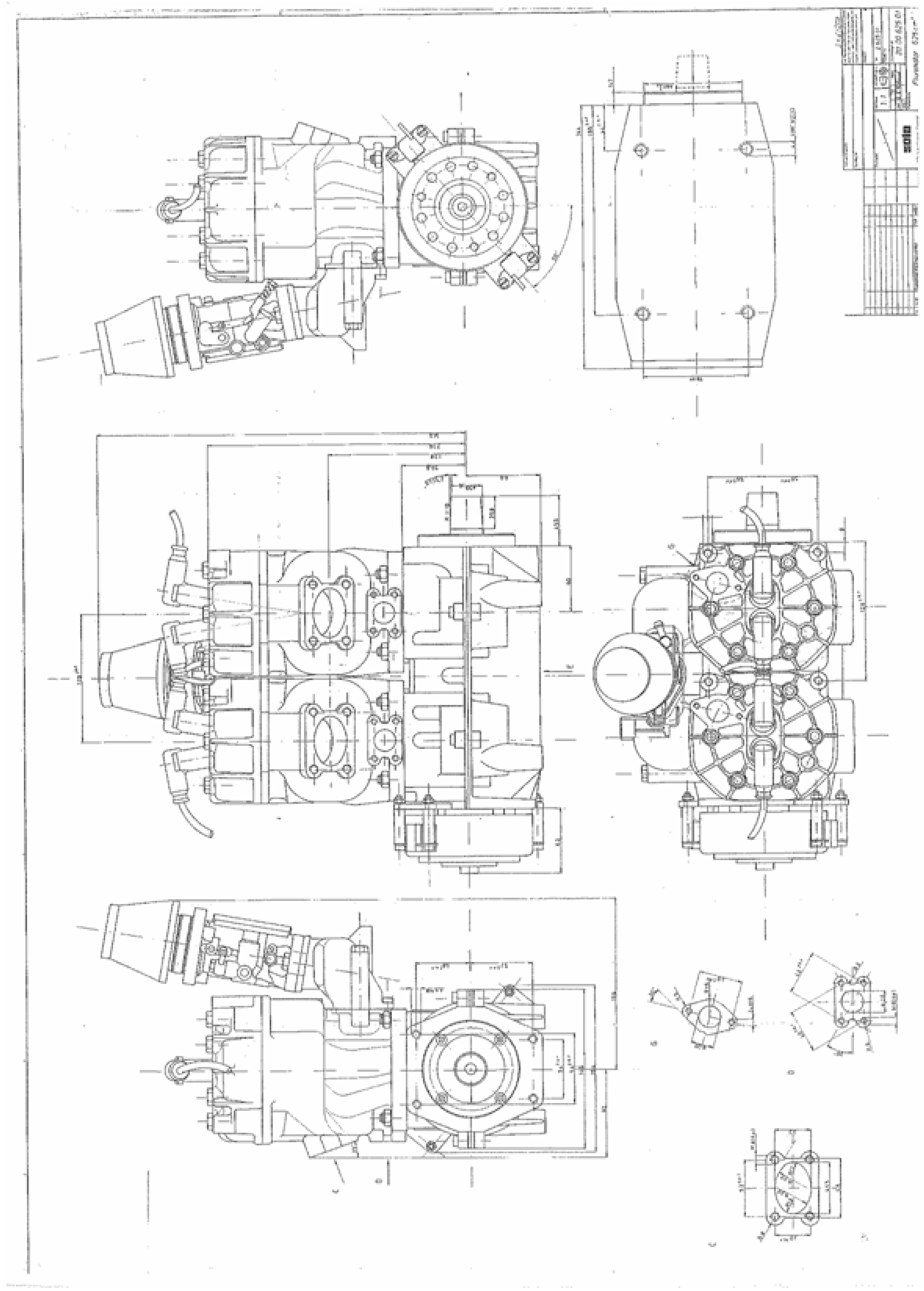

APPENDIX C: PROPELLER DESIGN OUTPUTS

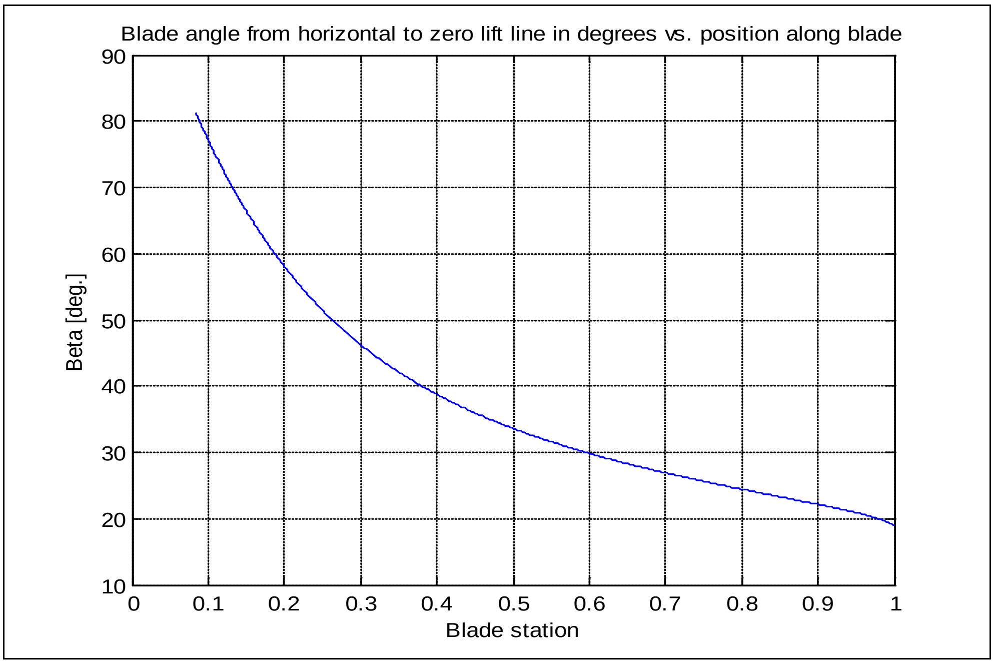

Figure C.1: Blade angle vs. position along blade.

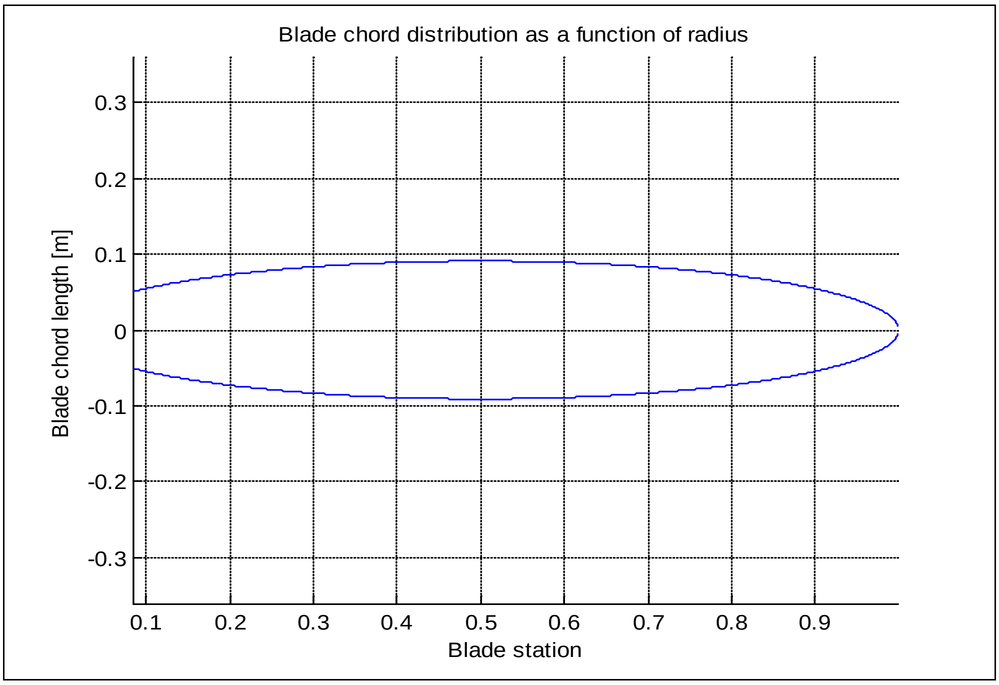

Figure C.2: Blade chord length vs. blade station.

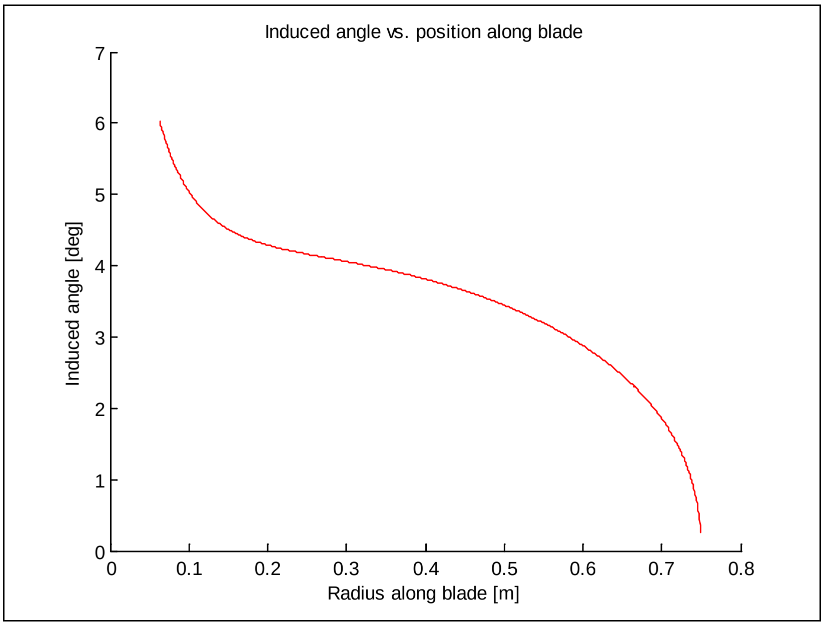

Figure C.3: Induced angle vs. radius along blade.

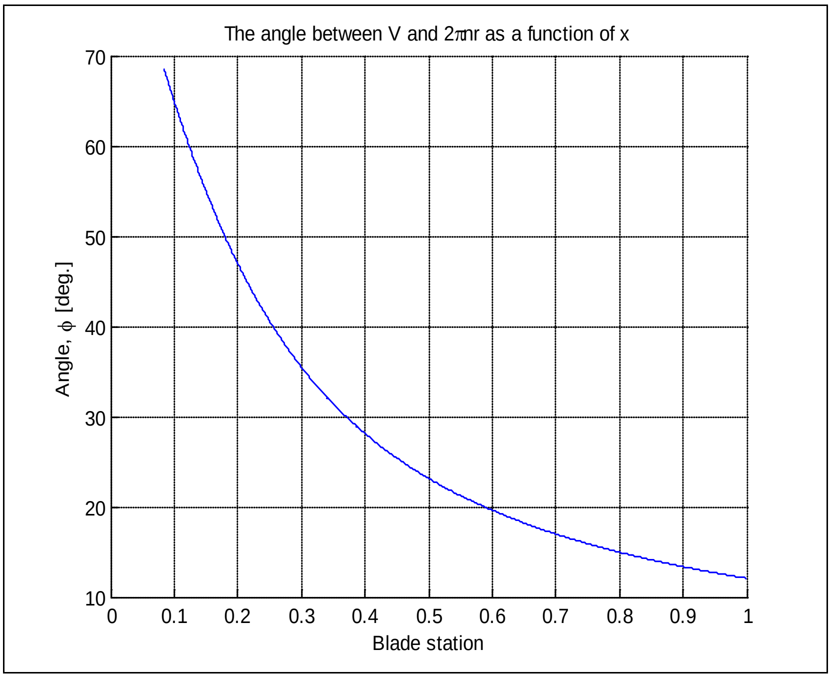

Figure C.4: Helix angle vs. blade station.

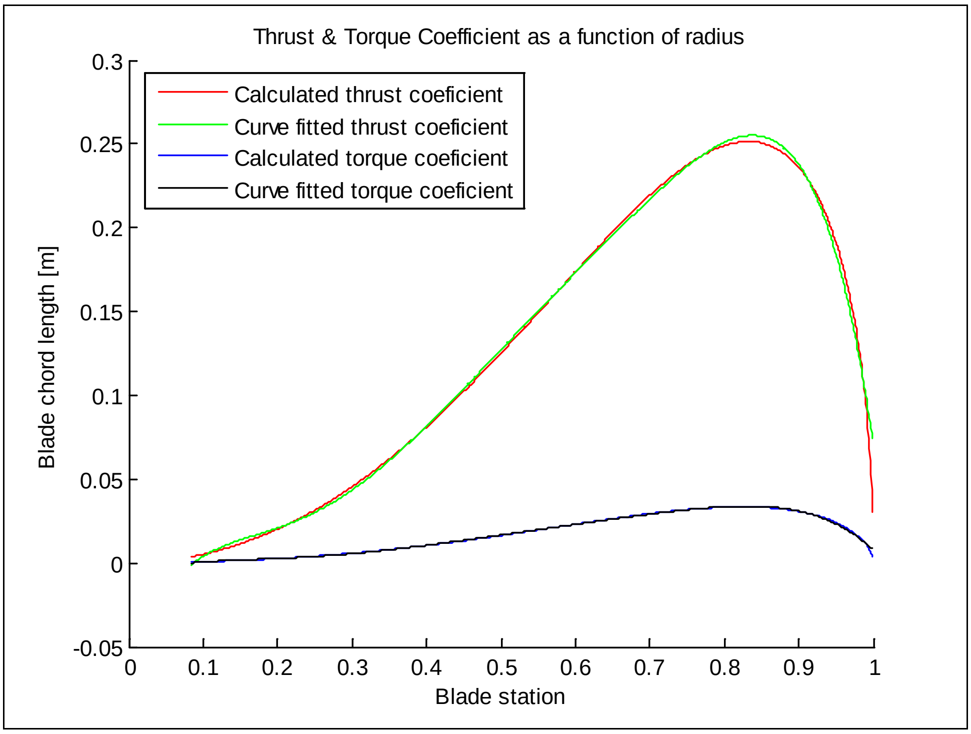

Figure C.5: Thrust and torque coefficient vs. blade station.

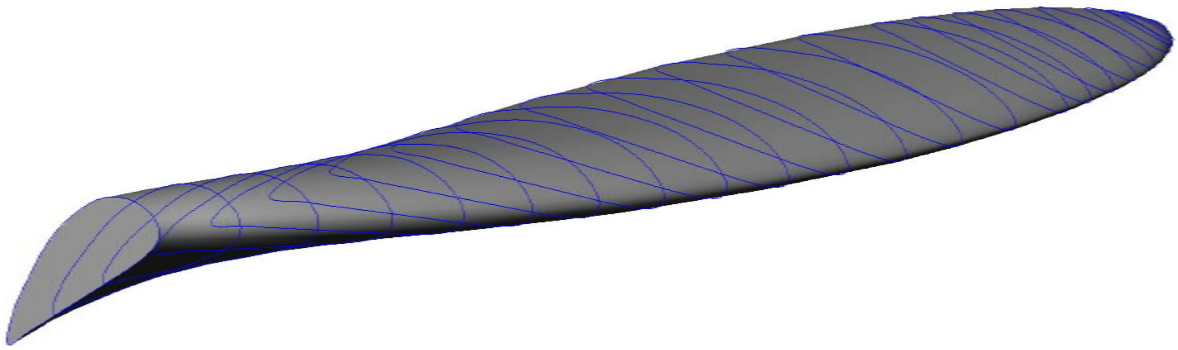

Figure C.6: Solid model of propeller blade.

APPENDIX D: LUG CALCULATION CHARTS (Young, 1990)

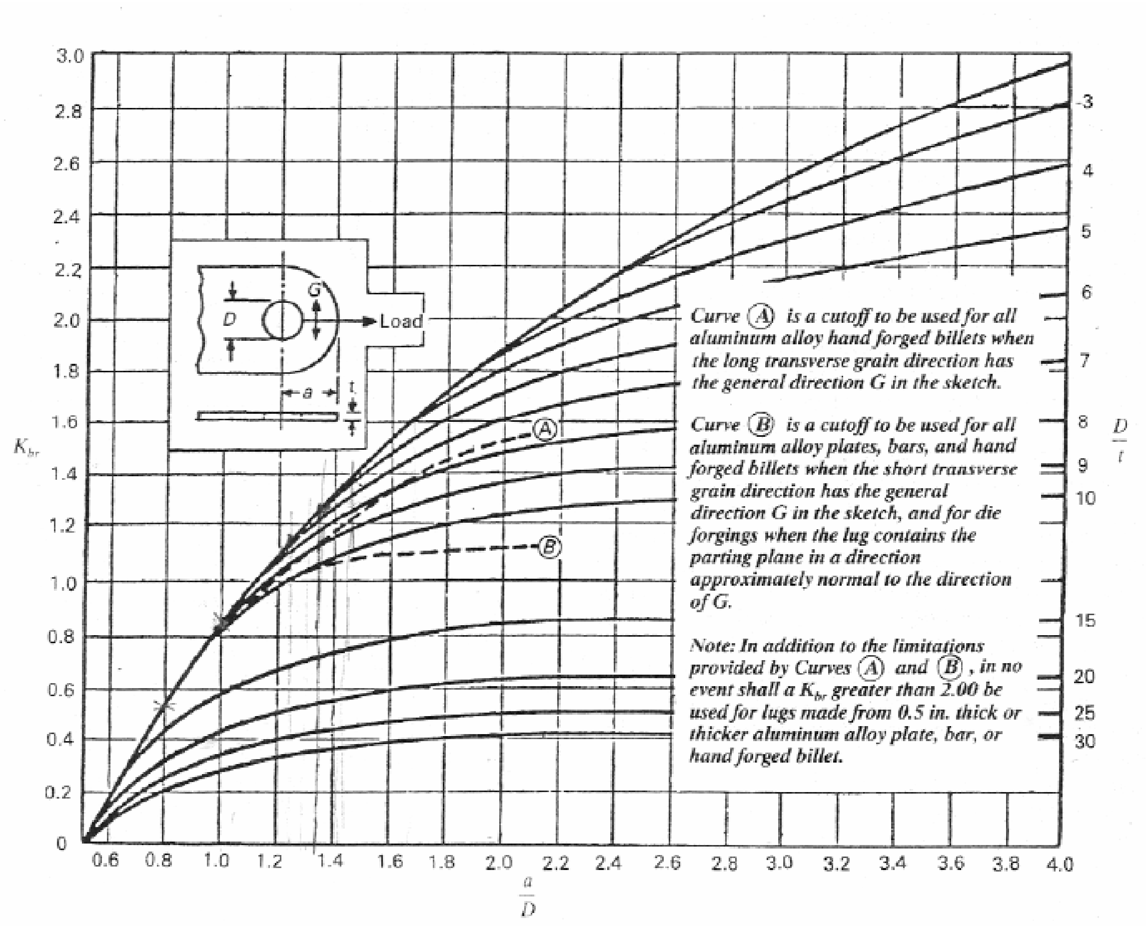

Figure D.1: Shear-bearing efficiency factor, K_{br}

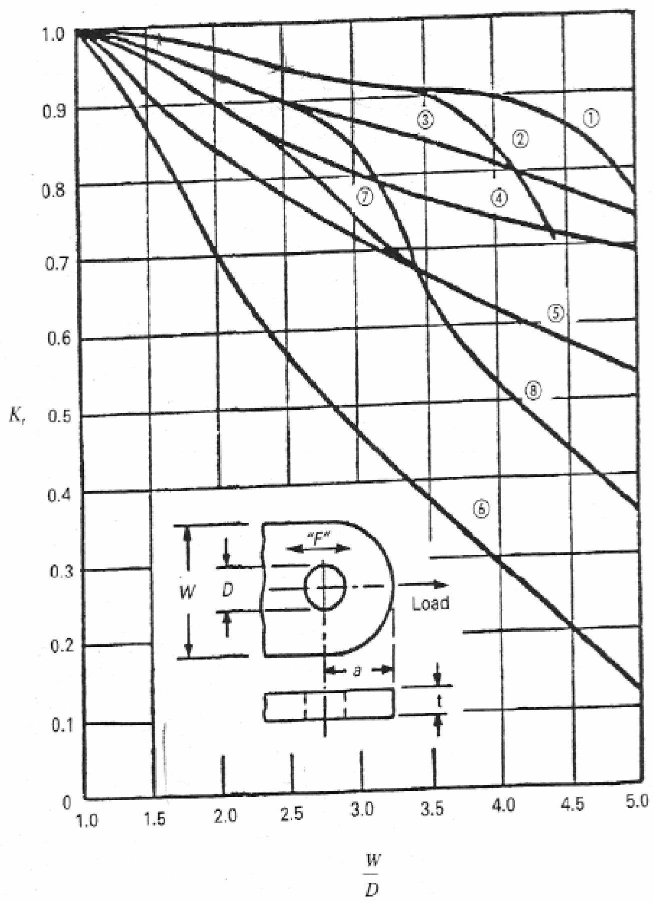

Legend L, LT and ST indicate grain in direction F in sketch:
Aluminum designation:
14S-2014
24S-2024
75S-7075

Curve ①
4130 steel
14S-T6 and 75S.T6 plate ≤ 0.5 in (L, LT)
75S-T6 bar and extrusion (L)
14S-T6 hand forged billet ≤ 144 sq in (L)
14S-T6 and 75S-T6 die forgings (L)

Curve ②
14S-T6 and 75S-T6 plate > 0.5 in , ≤ 1in
75S-T6 extrusion (LT, ST)
75S-T6 hand forged billet ≤ 36 sq in (L)
14S-T6 hand forged billet > 144 sq in (L)
14S-T6 hand forged billet ≤ 36 sq in (LT)
14S-T6 and 75S-T6 die forgings (LT)

Curve ③
24S-T6 plate (L, LT)
24S-T4 and 24S-T42 extrusion (L, LT)

Curve ④
24S-T4 plate (L, LT)
24S-T3 plate (L, LT)
14S-T6 and 75S-T6 plate > 1 in (L, LT)
24S-T4 bar (L, LT)
75S-T6 hand forged billet > 36 sq in (L)
75S-T6 hand forged billet ≤ 16 sq in (LT)

Curve ⑤
75S-T6 hand forged billet > 16 sq in (LT)
14S-T6 hand forged billet > 36 sq in (LT)

Curve ⑥
Aluminum alloy plate, bar, hand forged billet, and die forging (ST)
75S-T6 bar (LT)

Curve ⑦
18-8 stainless steel, annealed

Curve ⑧
18-8 stainless steel, full hard. Note: for $\frac{1}{4}$, $\frac{1}{2}$ and $\frac{3}{4}$ hard, interpolate between Curves ⑦ and ⑧.

Figure D.2: Efficiency factor for tension, K_t

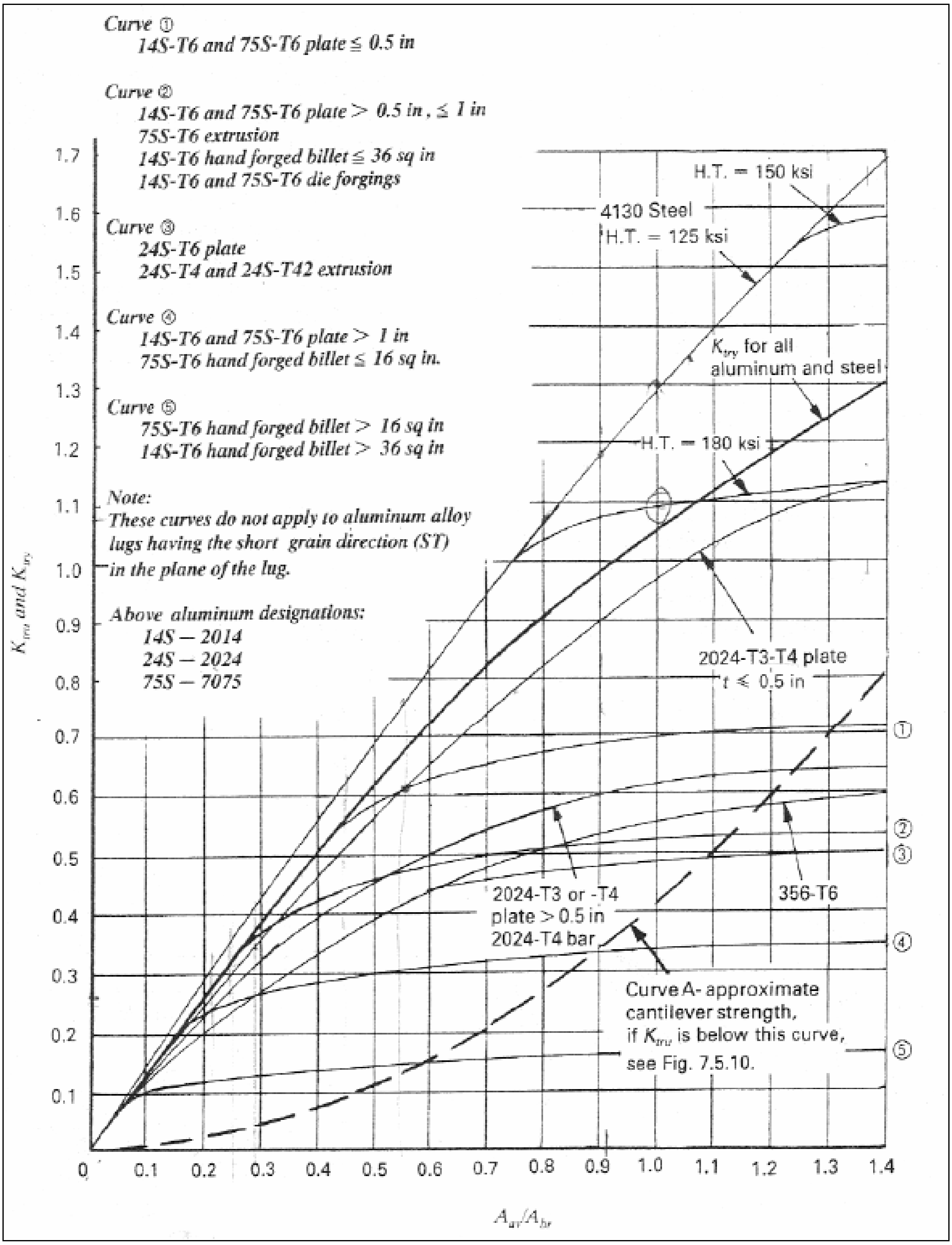

Figure D.3: Efficiency factor for transverse load, K_{tru}

APPENDIX E: TECHNICAL DATA DRIVE ACTUATOR 85199

Load Capacity

1000 lbs. (dynamic)
3000 lbs. (static)
Note: 1000 lb. load rating can be extended in certain applications.

Stroke

2, 3, 4, 5, 6, 7, 8, 9, 10, 11, 12, 15, 18 and 24 inches are stock units; however any stroke may be specified from 1.000 to 30.000 inches with no limitation on interim dimensions.

Stroke Speed

AC Motors:

Gear Ratio	10:1	20:1	40:1
115, 220 VAC 1700 RPM	.82/.60*	.41/.34	.21/.19
115, 220 VAC 3400 RPM	1.64/1.14*	.82/.65	.41/.36

DC Motors:

Gear Ratio	10:1	20:1	40:1
12, 24 VDC (PM) 3000 RPM	1.36/.91	.68/.58	.34/.30
12, 24 VDC (PM) 6000 RPM	2.72/.92*	1.36/.90	.68/.53
115 VDC (PM) 6000 RPM	2.72/.70*	1.36/.68	.68/.38

Note: Stroke speeds are in./sec. with no load speed shown first and 1000 lb. load speed shown second except 10:1 units marked with an asterisk where stroke speed is at 750 lbs.

Gear Ratios

10:1, 20:1, 40:1 are standard ratios.

Motors

AC Motors:

1) 115 VAC 60/50 Hz., Permanent Split Capacitor Induction, 3.3 diameter, 1700 RPM, intermittent duty cycle (25%), 3 wire, enclosed construction, automatic reset thermal overload protector, UL, CSA recognized, 1.8 amps no load, 1.9 amps at 1000 lbs. with 20:1 ratio, 30 MFD electrolytic capacitor supplied.
2) 115 VAC 60/50 Hz., Permanent Split Capacitor Induction, 3.3 diameter, 3400 RPM, intermittent duty cycle (25%), 3 wire, enclosed construction, automatic reset thermal overload protector, UL, CSA recognized, 3.5 amps no load, 4.6 amps at 1000 lbs. with 20:1 ratio, 60 MFD electrolytic capacitor supplied.
3) 220 VAC 60/50 Hz., Permanent Split Capacitor Induction, 3.3 diameter, 1700 RPM, intermittent duty cycle (25%), 3 wire, enclosed contruction, automatic reset thermal overload protector, UL, CSA recognized, 1.2 amps no load, 1.3 amps at 1000 lbs. with 20:1 ratio, 10 MFD oil filled capacitor supplied.
4) 220 VAC 60/50 Hz., Permanent Split Capacitor Induction, 3.3 diameter, 3400 RPM, intermittent duty cycle (25%), 3 wire, enclosed construction, automatic reset thermal overload protector, UL, CSA recognized, 1.8 amps no load, 2.5 amps at 1000 lbs. with 20:1 ratio, 17 MFD polypropylene capacitor supplied.
5) 115 VAC 60/50 Hz., Permanent Split Capacitor Induction, 3.8 diameter, 1700 RPM, continuous duty, 3 wire, enclosed construction, automatic reset thermal overload protector, UL, CSA recognized, .6 amps no load, .8 amps at 150 lbs. with 20:1 ratio, 10 MFD oil filled capacitor supplied.

Motors

DC Motors:

1) 12 VDC Permanent Magnet Brush, 3.0 diameter, 3000 RPM (no load), intermittent duty cycle (60%), 2 wire, enclosed construction, 2 amps no load, 20 amps at 1000 lbs. with 20:1 ratio.
2) 12 VDC Permanent Magnet Brush, 2.5 diameter, 6000 RPM (no load), intermittent duty cycle (60%), 2 wire, enclosed construction, 6 amps no load, 36 amps at 1000 lbs. with 20:1 ratio.
3) 24 VDC Permanent Magnet Brush, 3.0 diameter, 3000 RPM (no load), intermittent duty cycle (60%), 2 wire, enclosed construction, 1 amp no load, 10 amps at 1000 lbs. with 20:1 ratio.
4) 24 VDC Permanent Magnet Brush, 2.5 diameter, 6000 RPM (no load), intermittent duty cycle (60%), 2 wire, enclosed construction, 3 amps no load, 18 amps at 1000 lbs. with 20:1 ratio.
5) 115 VDC Permanent Magnet Brush, 2.5 diameter, 6000 RPM (no load on rectified 115 VAC), intermittent duty cycle (60%), 2 wire, enclosed construction, 1.1 amps no load, 3.5 amps at 1000 lbs. with 20:1 ratio.

Ball Drive

Epicyclic Ball Screw 85039 with integral freewheeling at ends of stroke.

Screw OD: .979

Screw root dia.: .843

Advancement/rev.: .281

Centerline pin dimension: 2.343 + stroke

Nut OD: 1.625

Nut mounting: 1 9/16-18 thread.

Materials: heat treated alloy steel with bearing races Rockwell 56C.

Efficiency: 90%

Gear Reducer	Single stage worm gear type with 6302 ball bearing to accommodate ball screw thrust. Housing: die cast aluminum 380 alloy. Bearings: worm shaft and Ball Drive shaft both supported on sleeve bearing and ball bearing.	Worm and gear materials: heat treated steel. Motor coupling: 60 durometer neoprene with two heat treated steel inserts. Lubrication: permanently lubricated with SP500 synthetic grease.
Mounting Dimensions	85199: minimum retracted centerline mounting dimension is 5.750 plus stroke. For example: a 3.500 stroke unit will measure 9.250 (5.750 + 3.500) in the retracted position and 12.750 (9.250 + 3.500) in the extended position. A retracted dimension can be specified greater than the minimum. For example: a 3.500 stroke unit could be 12.000 in the retracted position and 15.500 (12.000 + 3.500) in the extended position. Design options add to the minimum retracted dimension: Support bushing: 1.250 Rod end: 2.500 Adjustable stop: 1.250	85200: minimum retracted centerline gearbox mounting hole to nut shoulder is 5.000. For example: a 3.500 stroke unit will measure 5.000 in the retracted position and 8.500 (5.000 + 3.500) in the extended position. A retracted dimension can be specified greater than the minimum. Design options add to the minimum retracted dimension: Adjustable stop: 1.250 With the alternate nut, the minimum retracted centerline gearbox mounting hole to the centerline of the .379 holes is 5.300 (5.000 + .300). When the alternate nut is reversed, this minimum dimension will be 3.193. Note: Above dimensions are for Type A mount. For Type B and C mounts .210 must be added (85200 units only).
Weight	85199: 9.1 lbs. (6 in. stroke with AC motor) 8.4 lbs. (6 in. stroke with DC motor – 3.0 dia. PM)	85200: 8.2 lbs. (6 in. stroke with AC motor) 7.5 lbs. (6 in. stroke with DC motor – 3.0 dia. PM)

Wiring

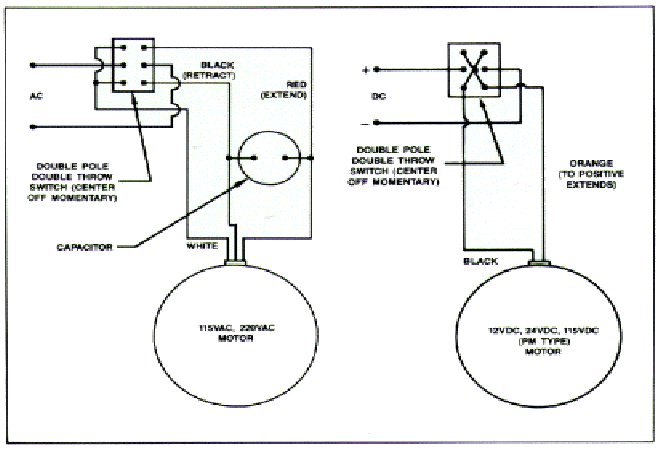

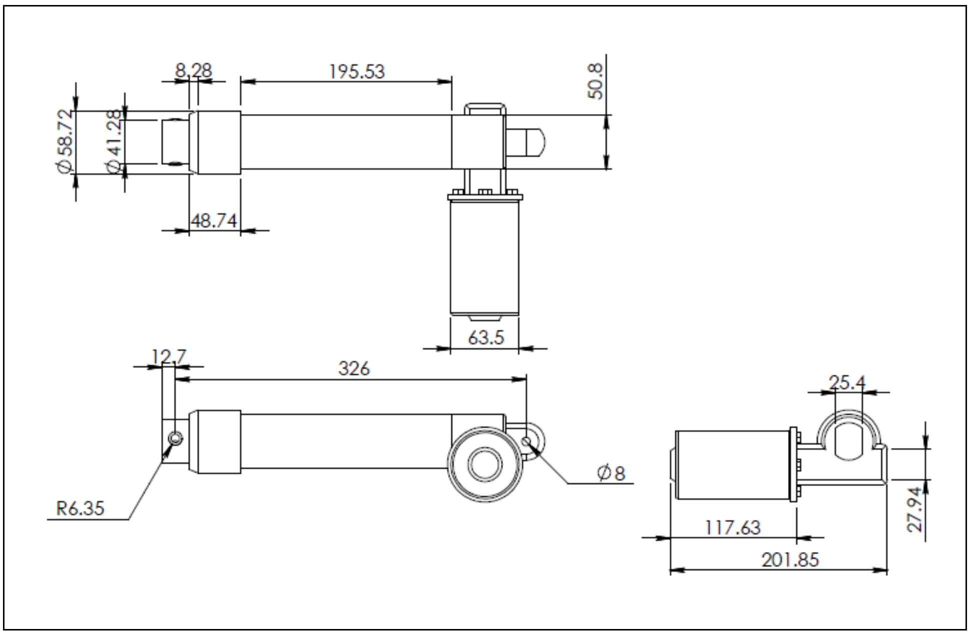

Figure E.1: Ball Drive Actuator 85199 drawing.

APPENDIX F: DETAIL DESIGN DRAWING

The detail design drawings of the self-launching system are given in the following drawings.

ITEM NO.	PART NUMBER	manual explode/QTY.
1	Propeller pylon	1
2	water cooling	1
3	linkAB	1
4	Link BCD	1
5	exhuaste muffler	1
6	joint of actu	2
7	Frame	1
8	exhaust manifold	1
9	solo262501	1
10	stand	1
11	connection bar	1
12	t_pulley guide	2
13	Actuator	1
14	Connection bar rear	1
15	Frame attachment lug	1

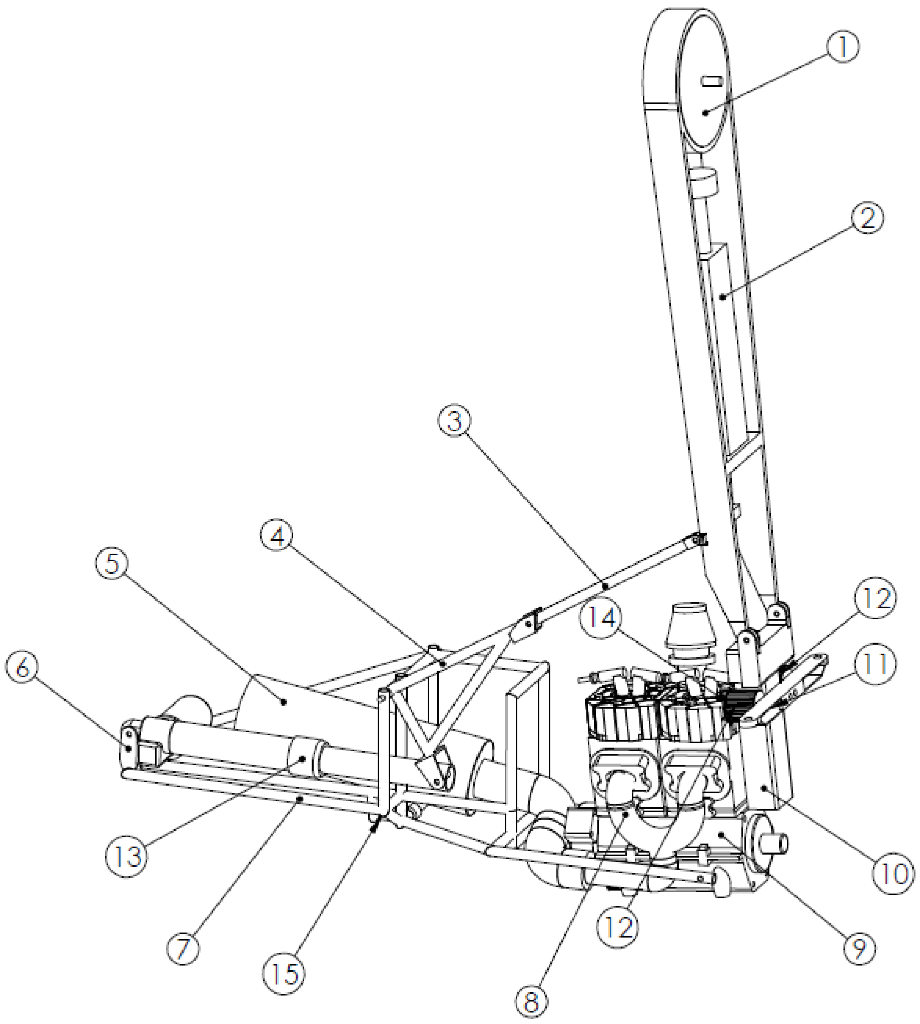

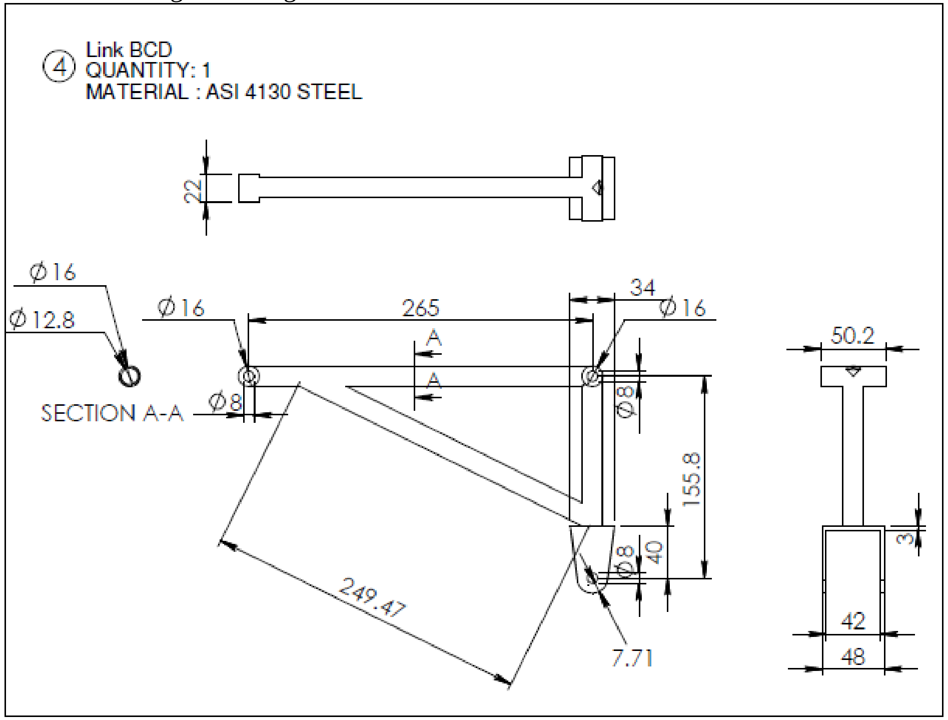
4
Link BCD
QUANTITY: 1
MATERIAL : ASI 4130 STEEL
22
Ø16
Ø12.8
SECTION A-A
Ø16
265
34
Ø16
A
A
Ø8
Ø8
155.8
Ø8
40
249.47
7.71
50.2
3
42
48

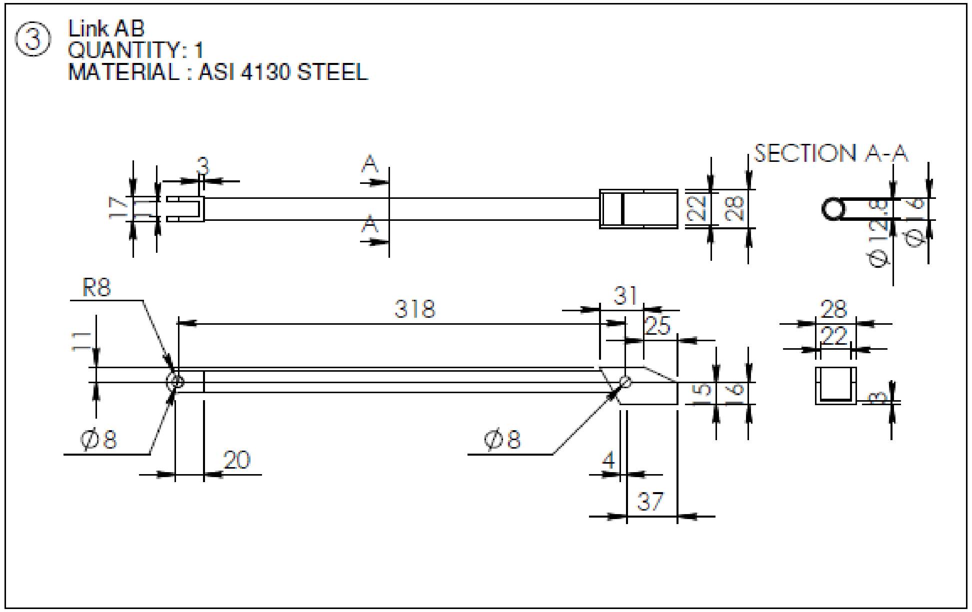
3
Link AB
QUANTITY: 1
MATERIAL : ASI 4130 STEEL
SECTION A-A
3
A
A
17
22
28
Ø12.8
Ø16
R8
318
31
25
28
22
11
Ø8
Ø8
20
4
37
5
16
3

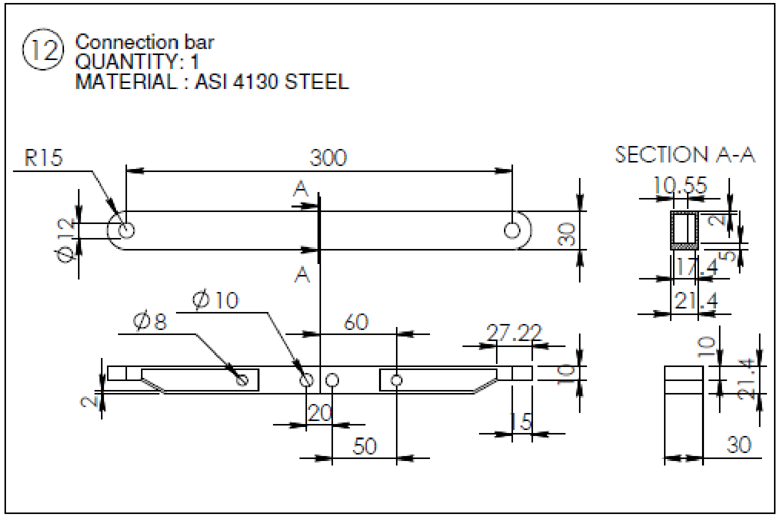
12
Connection bar
QUANTITY: 1
MATERIAL : ASI 4130 STEEL
R15
300
A
A
Ø12
30
SECTION A-A
10.55
2
5
17.4
21.4
Ø10
Ø8
60
27.22
2
10
20
15
50
10
21.4
30
30

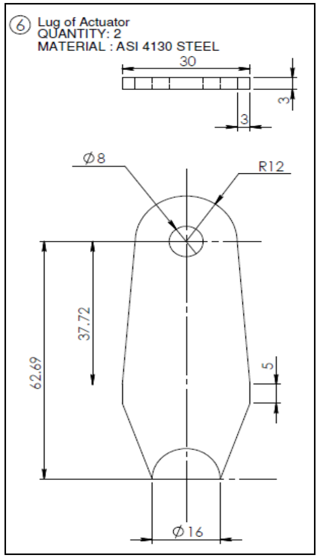
6
Lug of Actuator
QUANTITY: 2
MATERIAL : ASI 4130 STEEL
30
3
3
Ø8
R12
37.72
62.69
5
Ø16

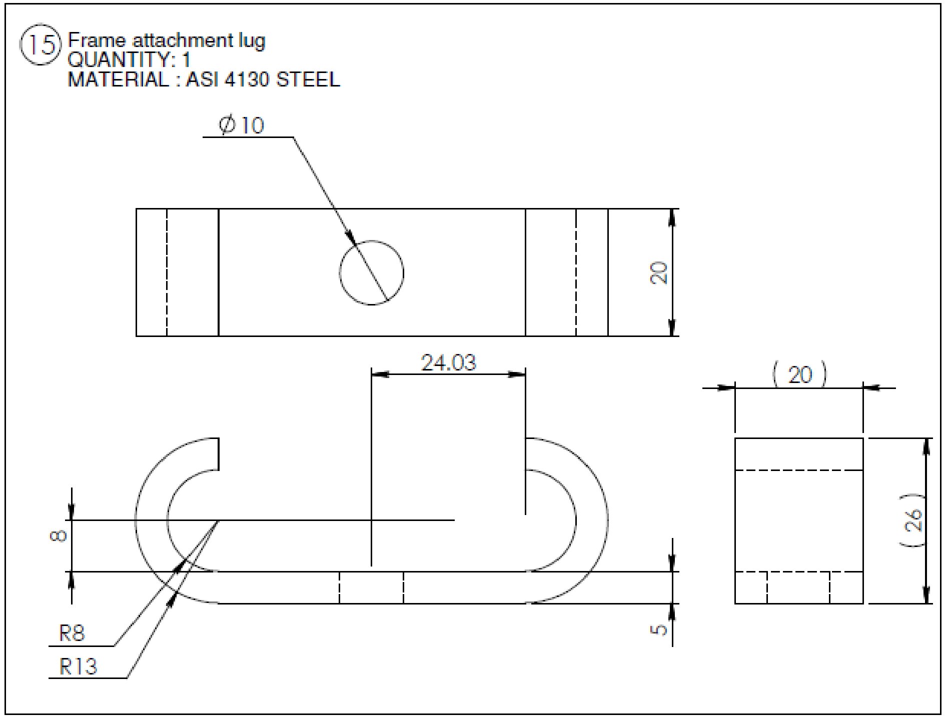
15
Frame attachment lug
QUANTITY: 1
MATERIAL : ASI 4130 STEEL
Ø10
20
24.03
(20)
8
(26)
5
R8
R13

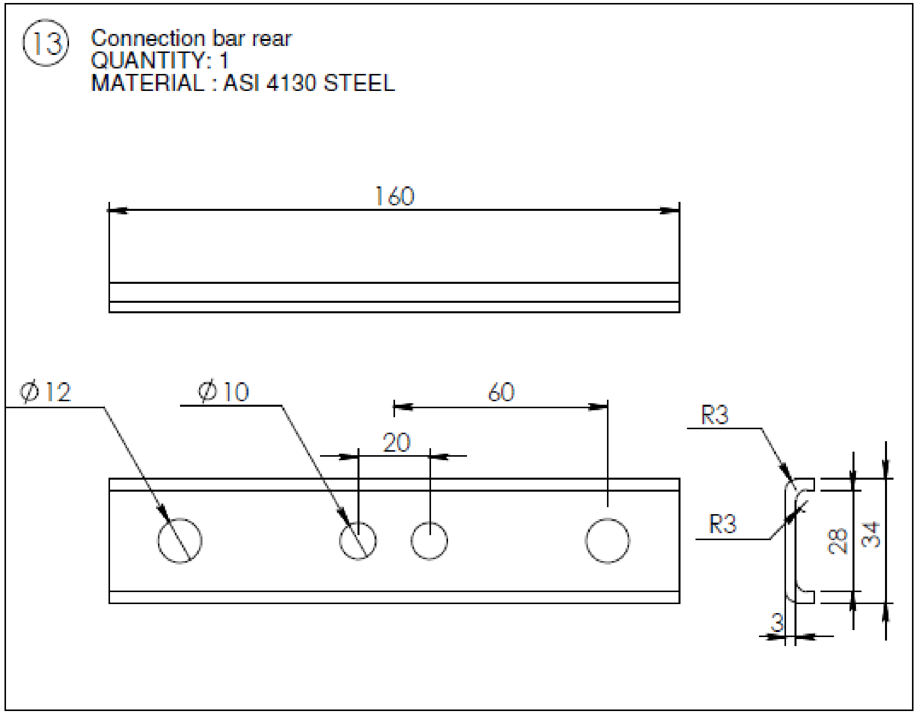
13
Connection bar rear
QUANTITY: 1
MATERIAL : ASI 4130 STEEL
160
Ø12
Ø10
60
20
R3
R3
28
34
3

(1) Propeller pylon
QUANTITY: 1
MATERIAL : Carbon Fiber

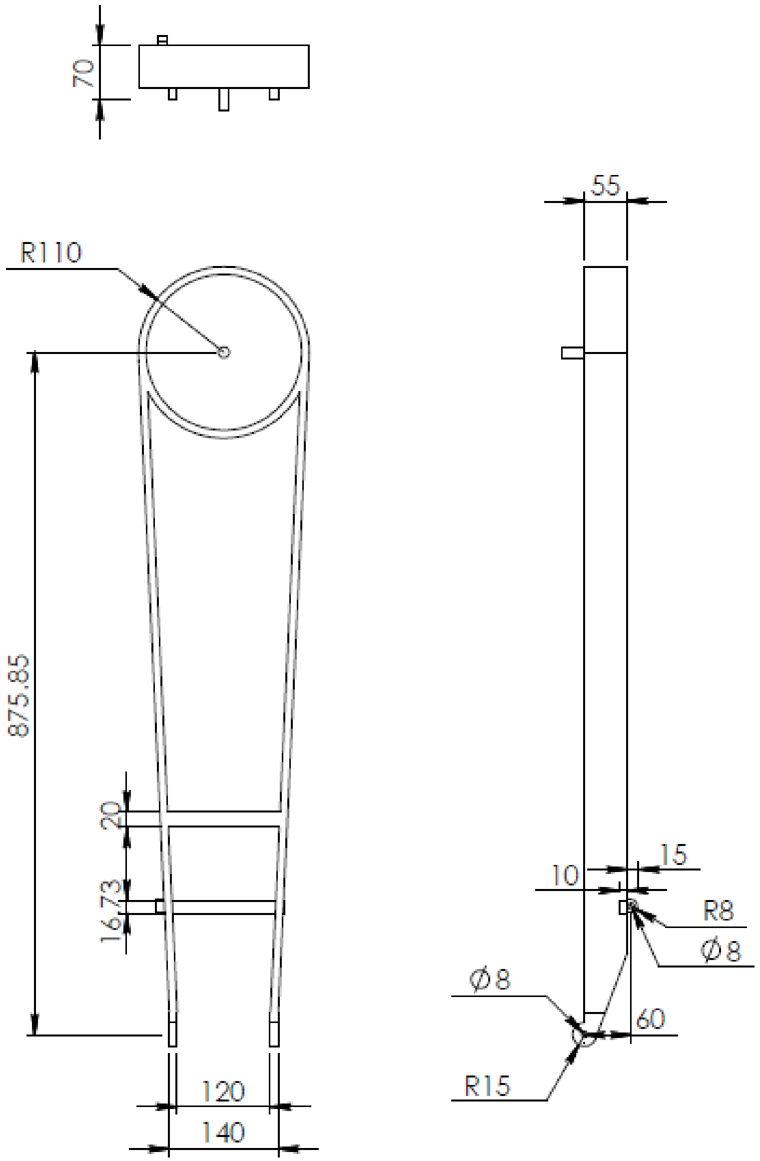

(12) Puelly Guied
QUANTITY: 2

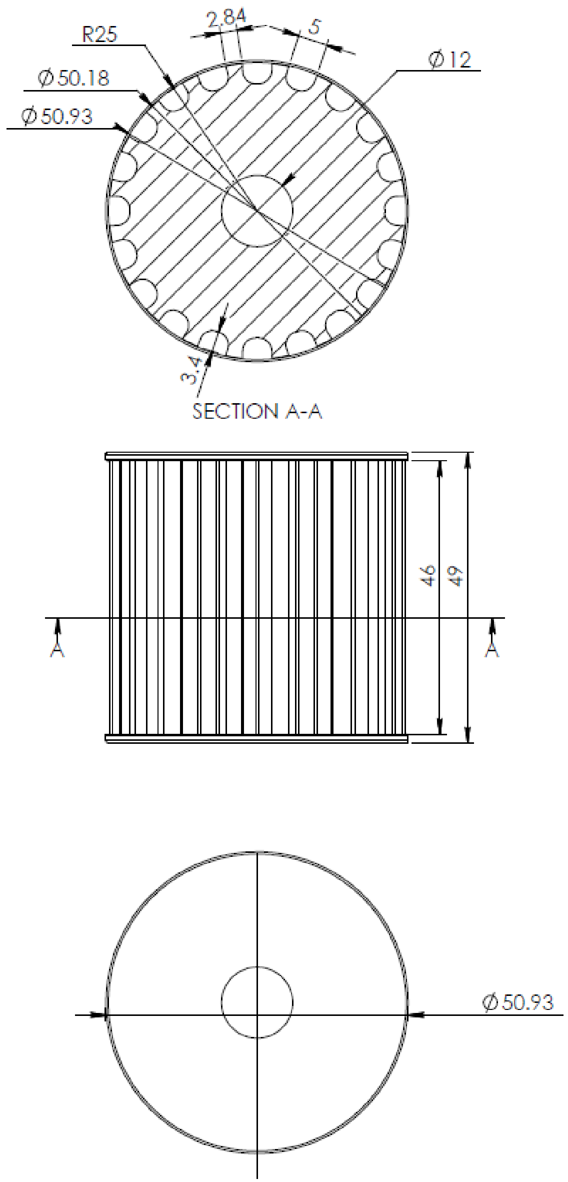

(7) Frame
QUANTITY: 1
MATERIAL : ASI 4130 STEEL

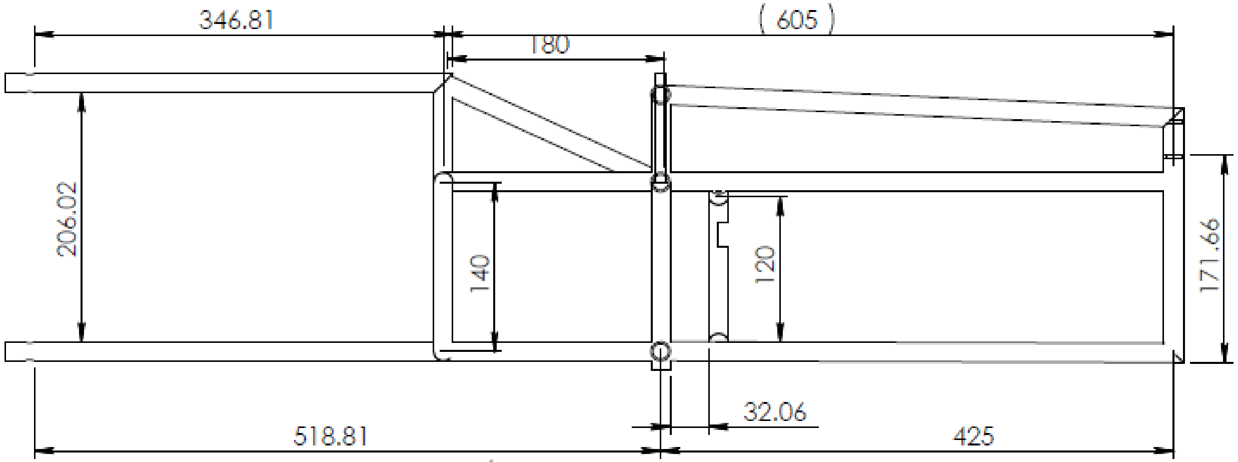

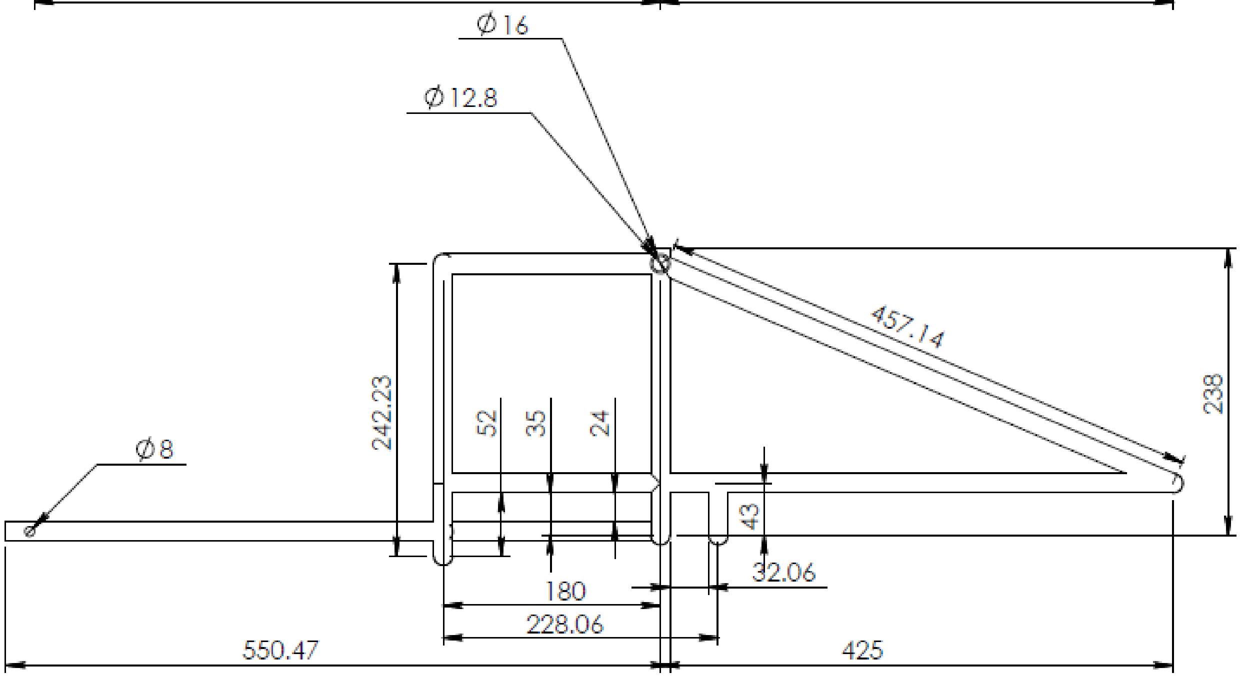

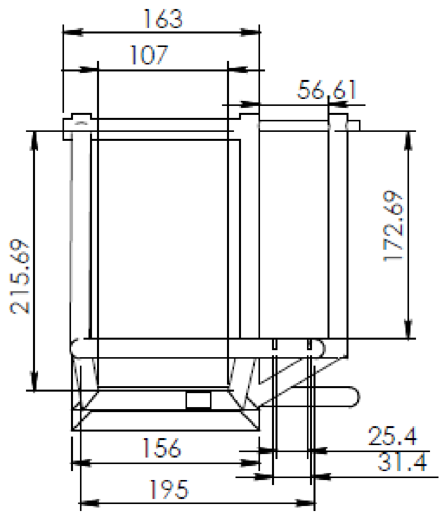

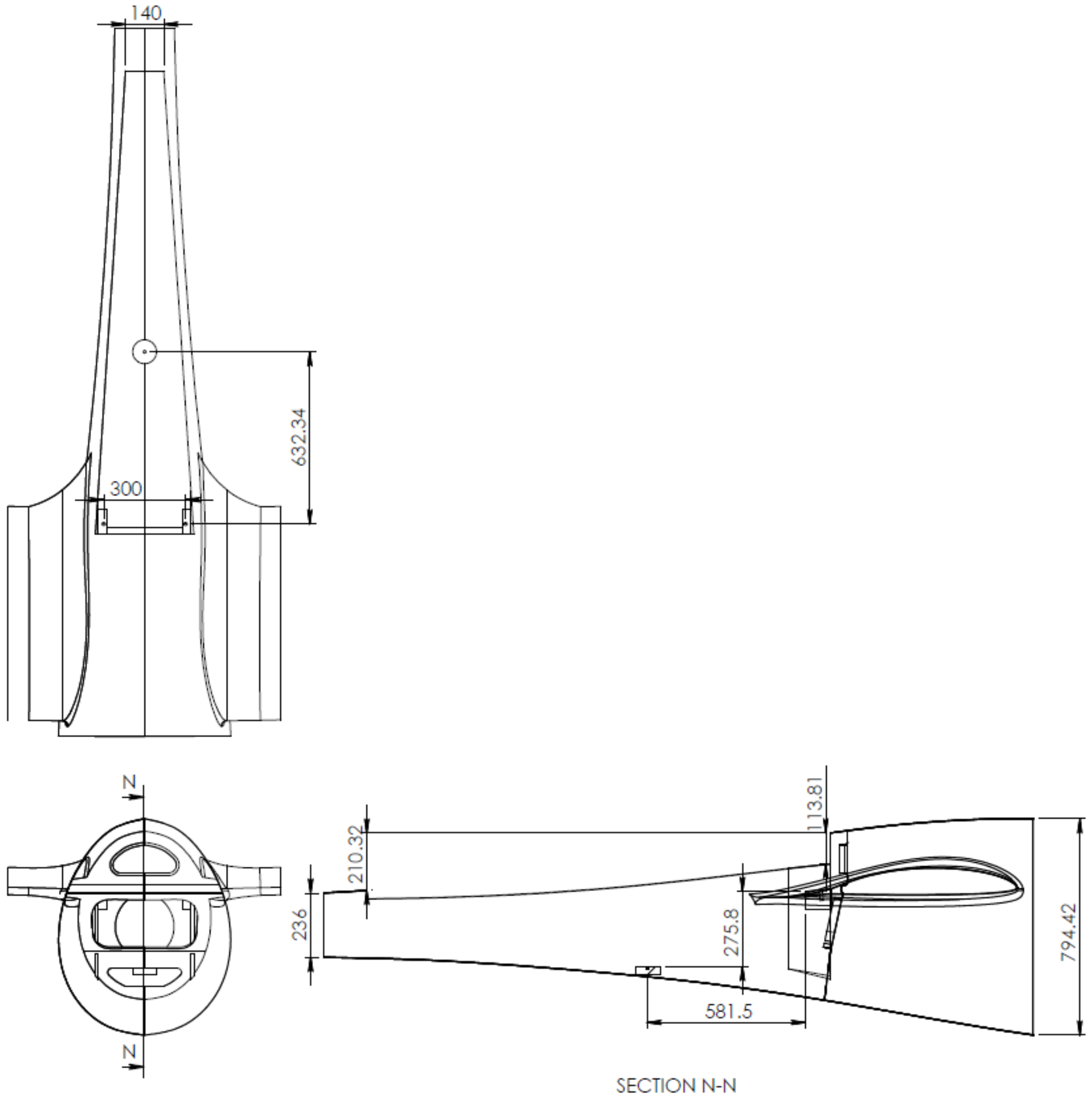
140
632.34
300
N
N
113.81
210.32
236
275.8
581.5
794.42
SECTION N-N
SCALE 1 : 20